Modelling the Shear Behavior of Short Columns under Single Curvature

Master of Sustainable Constructions

Under

natural hazards and catastrophic events

(SUSCOS)

Author: Gamil Gamal Al-yousefi

Supervisor: Prof. Boyan Mihaylov

University of Liège

European Commission
ERASMUS MUNDUS

January, 2018

ABSTRACT

Short concrete columns are the structural members dominated with nonlinear strains distribution (D region), and they are characterized with small shear span to depth ratios. Since short columns fail in brittle shear pattern, they can not be modelled using the plane -sections-remain-plane hypothesis (beam theory). Therefore, this thesis introduces an effective and simple approach to model such members by applying the modified 3PKT theory which is originally based on a three-degree-of-freedom kinematic model for the deformation patterns in walls. This research also focuses on verifying the ability of non-linear finite element software (VecTor2) to capture the responses behaviour of short columns and compare the FEA results with both experimental and 3PKT results.

Several experimental studies on short reinforcement concrete columns have been filtered to only three series of experimental studies to be placed as a test database which is applicable for the scope of the project. The series specimens are having either rectangular or square sections and their experimental test setup is a single beam configuration with aspect ratios smaller than approximately 3.0. Then, the specimens have been modeled using the two tools (3PKT-VecTor2). The results showed that both approaches successfully predicted the shear behavior of the specimens. The resulted peak load experimental to predicted ratios of VecTor2 and 3PKT approaches have a mean value of 0.87 and 0.98 with a coefficient of variation of 7.58% and 6.78 % respectively.

Author keywords: Short concrete columns; Shear behaviour; Kinematic model; Nonlinear strains distribution

ACKNOWLEDGEMENTS

It is a great pleasure to address those people who helped me throughout this project to enhance my knowledge and practical skills. My deepest and most heartfelt gratitude goes to my supervisor Professor Boyan Mihaylov for his continuous guidance and support that have enabled me to approach work positively, and make even the impossible seem possible.

I wish to express my special thanks to my beloved parents, family and my friends who gave me spirit, support and encouragement to complete this project. Warm thanks also go to my office colleagues Jian Liu, Nikola Tatar and Renaud Franssen. They always answered my questions and created such a friendly environment.

Many thanks to my sponsorship (SUSCOS) who gave me this chance to pursue my study in this prestigious Master course, and I would like to thank all the coordinators and professors from all the partner universities and in particular Professor František Wald, Professor Jean-Pierre Jaspart, Professor Jean-François Demonceau and Professor Jean-Marc Franssen for all the effort and dedication which makes SUSCOS such a unique learning experience.

Finally, thanks to all my classmates for their help and support. I would also like to thank everyone who has contributed whether directly or indirectly to this project. This project would have been impossible without your guidance, advice and support.
Thank you…

LIST OF FIGURES

LIST OF TABLES

LIST OF SYMBOLS

N = The axial load (kN)

a = The column height from the base to the applies lateral load (mm)

h = Depth of the cross section (mm)

b = Width of the cross section (mm)

d = Effective depth of section from the compression edge of the section to the centroid of As (mm)

d_b = The diameter of the main longitudinal bars (mm)

ρ_v % = Ratio of the transverse reinforcements

ρ_l% = Ratio of the main longitudinal reinforcements

f_{yl} = The yield strength of main longitudinal reinforcement(MPa)

f_{ul} = The ultimate strength of main longitudinal reinforcement(MPa)

f_{yv} = The yield strength of transverse reinforcement(MPa)

f_{uv} =The ultimate strength of transverse reinforcement(MPa)

E_s = The modulus of elasticity of longitudinal reinforcement (MPa)

f_c = Concrete cylinder strength (MPa)

V = Shear force and lateral load (kN)

V_{exp} = Experimental peak shear force and lateral load (kN)

V_{FEM} = Predicted peak shear force and lateral load (kN) using FEM modelling

V_{3PKT} = Predicted peak shear force and lateral load (kN) using 3PKT modelling

δs = Crack slip

γs = Crack slip shear strain

vci = Local shear stresses

ε_x = Average horizontal strain

ε_2 = Principal compressive strain

f_2 = Principal compressive stress

F_{CLZ} = Compression force in the concrete of CLZ

F_{cn}; F_{ct} = Normal and tangential contact forces at the bottom of critical diagonal crack

F_{ci} = Aggregate interlock force

F_d = Dowel action force

F_s = Force in the stirrups

F_{sc} = Force in longitudinal reinforcement in CLZ

F_t = Force in longitudinal tension reinforcement As

f_b = Stresses in compression zone in base section

f_t = Stresses along longitudinal tension reinforcement

f_c' = Concrete cylinder strength

$f_{c,CLZ}$ = Average compressive stress in CLZ

jd = Lever arm between F_b and $F_{t,max}$

l_{b1e} = Characteristic length of CLZ

l_t = Cracked length along longitudinal reinforcement

l_k = Length of transition zone between fan and rigid block

v_{ci} = Aggregate interlock shear stress

$w;\Delta_{ci}$ = Crack width and crack slip

α = Angle of wall diagonal with respect to the vertical axis

α_1 = Angle of critical crack;

α_Δ = Angle of displacement at CLZ

α_F = Angle of force F_{CLZ}

Δ = Applied lateral displacement

Δ_c = Horizontal displacement at CLZ

Δ_{cx} = Vertical displacement at CLZ

Δ_i = Deformations of springs

Δ_{i0} = Displacements of ends of springs attached to the fan (offset displacements)

ε_b = Strains across base section

ε_{CLZ} = Average strain in CLZ

ε_t = Strains along longitudinal tension reinforcement;

$\varepsilon_{t(min)(max)}$ = Minimum (maximum) strain along longitudinal tension reinforcement;

$\varepsilon_{t,avg}$ = Average strain along longitudinal tension reinforcement

ε_y = Yield strain of longitudinal reinforcement

ε_u = Breaking strain of longitudinal reinforcement

ε_{uv} = Breaking strain of transverse reinforcement

ε_v = Strain in transverse reinforcement

θ = Rotation of rigid block

θ_b = Angle of force Fb with respect to the vertical axis

TABLE OF CONTENTS

1. INTRODUCTION

1.1. GENERAL OVERVIEW

Columns are the members that mainly carry the compression loads and sometimes bending either about one axis or both axes of the cross section (Nilson et al, 1997). Columns support vertical loads from the floor and roof slabs and then transfer these loads to the footings. The columns can be classified as short and long columns based on slenderness ratio and strain distribution (B and D regions). B-region is defined as the portion of the member where beam theory (Bernoulli's hypothesis) is valid and their internal state of stresses can be derived directly from the sectional forces and moments. Referring to the Bernoulli's hypothesis the design of B region is based on the assumption that the strain changes linearly (plane sections remain plane). On the other hand, D-region stands for discontinuity or details which has a non-linear strain distribution (Schlaich et al., 1987). D-region are caused by a sudden change in geometry or loading conditions. Saint Venant's Principal is used to determine the dimensioning of both B and D regions which suggests that one-member depth away from the source of any disturbance induced in a structural component due to either geometrical irregularities or loading condition is the length of D-region as it is elaborated in Figure 1.1.

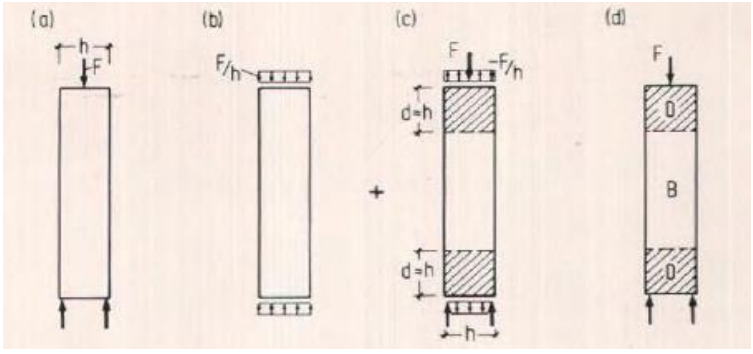

Column with point loads

Figure 1.1 Saint Venant's principle for D regions (Schlaich et al., 1987): a) real structure; b) loads and reactions applied in accordance with Bernoulli hypothesis c) self-equilibrating state of stress d) real structure with B- and D- regions

The short columns have a shear- span- to- depth ratio equal or less than 3.0(small slenderness) in which nonlinear strains dominate the behavior (D region). Meanwhile the long or slender columns have a shear- span- to- depth ratio of more than 3.0 with both D and B regions as shown in Figure 1.2. The short columns can be found in many applications such as in structures that built in a sloping

ground or with technical floor (mezzanine) floor (Alqatamin, A., et al., 2009) as it can be shown in Figure 1.3.

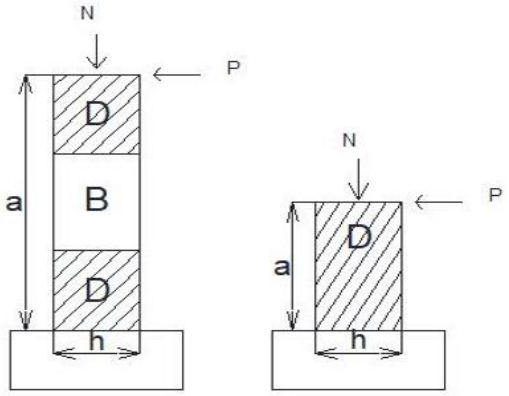

a) Long column b) Short column

Figure 1.2 Column classification based on D-B regions

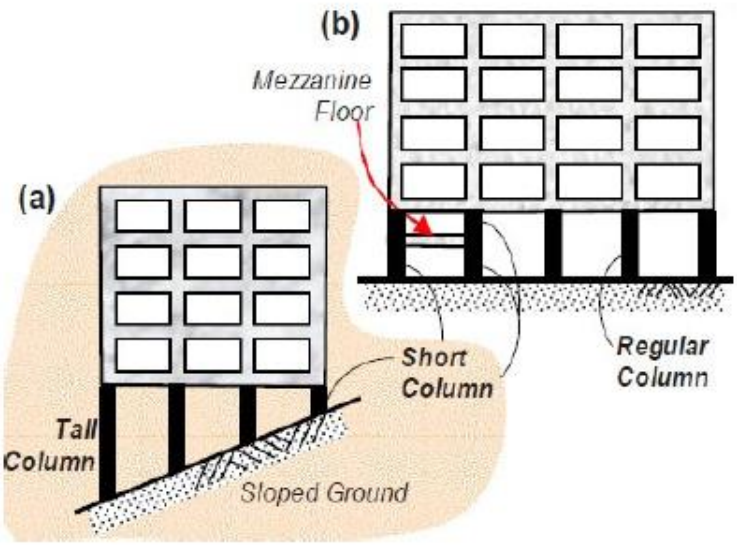

Figure 1.3 Structures with short columns due to: a) Sloped ground b) Mezzanine floor (Alqatamin and Talpos, 2009)

The behaviour of the short columns controls the response of the whole structure during earthquake, as they are the first members to fail. Short columns are governed by brittle shear failures due to their high stiffness with low ductility (Li et al., 2014). Such members are subjected to relatively large lateral loads with small lateral displacements which cause their brittle shear failure. As short columns fail in a brittle shear mode, their force and deformation capacity decrease dramatically.

It has been reported that reinforced concrete short columns experience a large number of brittle shear failures during destructive earthquakes in the earthquake countries (Yoshimura et al.,2004).As

evident from Figure 1.4, Chi-Chi earthquake that hit central of Taiwan on September 21, 1999 and Kobe earthquake that occurred on January 17, 1995 in Japan both caused large damage for the infrastructure, and it was clearly observed that reinforced concrete rectangular columns in buildings were subjected to high shear forces which resulted in shear and flexural shear failures.

Shear failure (1999 Chi-Chi, Taiwan)

Flexural shear failure (1995 Kobe, Japan)

Figure 1.4 Example of the short column failures (Yoshimura et al.,2004)

The strength of materials and the geometry of the cross section are the two parameters that govern the short column strength which fails by yielding of reinforcements or crushing of concrete, while slender column fails due to reducing its strength by either lateral deflections or buckling (Nilson, 1997).

The old standards were used to design and construct many existing buildings, which are inadequate to resist major earthquakes. Therefore, number of researches have been done to develop new techniques and standards to further improve the seismic resistance of the structures (Aboutaha ,1994).

Inelastic deformations are developed in the reinforced concrete frame structures when subjected to strong earthquakes. Generally, the energy induced by earthquakes is dissipated thought plastic hinges in the beams; nevertheless, they are formed in the columns especially in the first story during a strong ground motion. Hence, it is necessary to enhance the seismic resistance of the columns to maintain their design strength during a strong event of earthquake (Saatcioglu and Ozcebe ,1989).

During previous earthquakes, it was obvious that the column failures was caused by high shear stress, lack of concrete confinement and bidirectional load effects. In 1967, Venezuela earthquake caused a failure of the Macuto-Sheraton Hotel short columns due to high shear stress reversal. Most of the column failures were clearly observed after the 1985 Mexico City earthquake. A good example of failures due to bidirectional loading effects was the column of the Imperial country services building damaged during the 1979 Imperial Valley earthquake (Saatcioglu and Ozcebe ,1989).

As many structures were built without considering the current capacity design requirements, it is a necessary step to asses the seismic resistance of the existing structures in order to measure the need of retrofitting process to increase their lateral resistance and ductility. The methods for predicting member's behavior should be such a simple, fast and computationally inexpensive approaches.

The plane -sections-remain-plane hypothesis is not applicable to short columns as they are D-regions, therefore short columns behavior can not be modelled based on the conventional beam theory. There are some methods that can be used for modelling members, one of them is strut-and-tie-based models. However, because strut-and-tie models are inherently conservative, they can result in very large amounts of shear reinforcement (stirrups) with difficulties in construction. The other approaches that can be used as well are empirical approach and fiber element models but they are based on many degrees of freedom, which consume a large amount of time for modelling and computation. Therefore, an alternative approach that is simple, fast and effective to model and predict the behavior of short columns is required. This project will focus on an existing three-parameter kinematic theory (3PKT) (Mihaylov et al., 2016) which was developed for wall structures to be applied on short reinforced concrete columns. The 3PKT approach is used to capture the complete responses of the members that fail either in shear or flexural shear in such an efficient time. The members will be modelled as well using a nonlinear finite element approach to capture the shear behaviour of such members and compare the results with the 3PKT approach.

1.2. RESEARCH OBJECTIVES

This thesis is an extension of the project "Three-Parameter Kinematic Theory for Shear-Dominated Reinforced Concrete Walls" (Mihaylov et al., 2016). The 3PKT was originally developed to predict the response of shear critical walls loaded horizontally and vertically at the top of the wall, and capture the pre-peak and post-peak behavior of the walls. However, the main goal of this project is to apply

the existing three-parameter kinematic theory (3PKT) with the necessary modifications to predict the behaviour of short reinforced concrete columns. Moreover, this project will validate the ability of a nonlinear finite element approach based on the disturbed stress field model (DSFM) to capture the shear behaviour of short columns and compare the results with the 3PKT approach.

Experimental studies on short columns will be collected to form a test database. Only specimens have the following characteristics will be considered:

- The specimens have rectangular or square sections
- The failure of a specimen is either in shear or in flexural- shear
- The shear-span-to-depth ratio is equal or smaller than 3.0 ($a/h \leq 3.0$)
- The column is subjected to single curvature

Finally, the analysis will be done using an existing 3PKT code in which the modifications can be made in order to improve the predictions of the model and compare the results with both finite elements and experimental results.

1.3. THESIS OUTLINE

This thesis contains five chapters plus references and appendixes.
Chapter 1 provides a brief background about short columns. It also explains that short columns are D-region (discontinuity, disturbance) in which can not be modelled based on Bernoulli's hypothesis. Then the objectives of the thesis have been stated.
Chapter 2 describes tests of short columns by including specimens' details, test setup and main column properties. The main experimental results of each test series have been as well included.
Chapter 3 provides a concise background about the nonlinear finite element program based on the DSFM (VecTor2) which has been used in this thesis. A specimen is selected to be modeled using VecTor 2 to show with details how columns have been modeled and then the post-processing of the result was performed using the program Augustus. Finally, each test series have been modeled and their FEM results are compared with the experimental results.
Chapter 4 describes three-parameter kinematic theory for shear-dominated walls and explains that the theory extended to cover short columns modelling. The specimens are modeled using modified 3PKT

and then the results are compared with the experimental failure loads and FEM predictions simultaneously.

Chapter 5 summarizes the results obtained from FEM and 3PKT with a comparison to the observed results.

2. TESTS OF SHORT COLUMNS

In this project, three sets of short columns specimens were considered as they match the requirements and the scope of the project.

2.1. TEST SERIES BY ABOUTAHA (1994)

This set was taken from the thesis entitled "seismic retrofit of non-ductile reinforced concrete columns using rectangular steel jackets" (Aboutaha ,1994). Four specimens out of total eleven specimens were considered (SC1-SC3-SC4-SC9) as these specimen within the scope of the project. Ready mix concrete was used for all the column sets. Deformed reinforcing bars of grade 60 were used for all longitudinal bars while grade 40 deformed reinforcing bars were used for all transverse reinforcements of the columns. The direction of loading, transverse reinforcement ratio and the concrete strength were the main variable parameters of the experiment.

Test setup and main column properties

The figure below shows the test setup of Aboutaha's series. The footing of the columns was large enough with anchorage to provide a fix end. The tip of a column was subjected to a lateral load using either a 890 kN or a 2224 kN actuator. For this set of experiment, there was no axial load while the lateral displacements were increased in steps of 0.5% drift ratios.

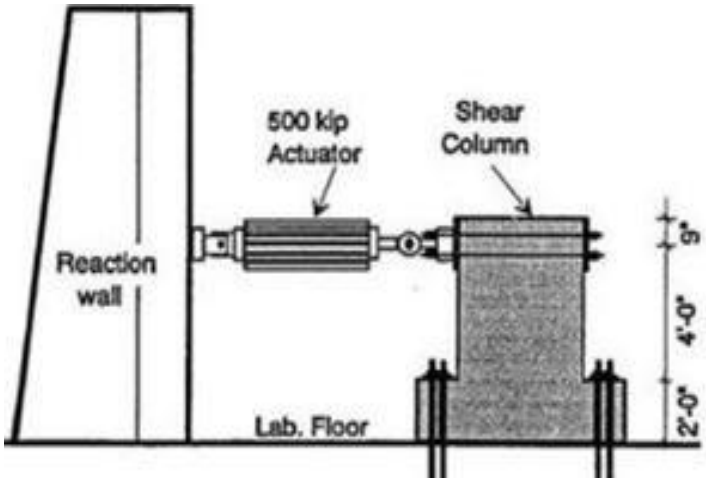

Figure 2.1 Test setup program (Aboutaha ,1994) (1 inch =25.4 mm,1 Kip =4.45 kN,1 foot =304 mm)

Three specimens were loaded in the weak direction (SC1,SC2,SC3) with a cross section of 915 X 457 mm and shear span to depth ratio of 2.67 while SC9 was loaded in the strong direction and its shear span to depth ratio was 1.33. The specimens were reinforced longitudinally with a total 16 bars of 25 mm diameter and transversally reinforced with 10 mm diameter at every 406 mm in the region of wide spacing and 100 mm in the region of close spacing. The yield strength of the main longitudinal bars was 434 MPa while the yield strength of the transverse reinforcement was 400 MPa. As it can be seen in the Figure 2.2 that the ratio of transverse reinforcement parallel to the load direction is the highest in specimens (SC1,SC4) and lowest in SC9 specimen.

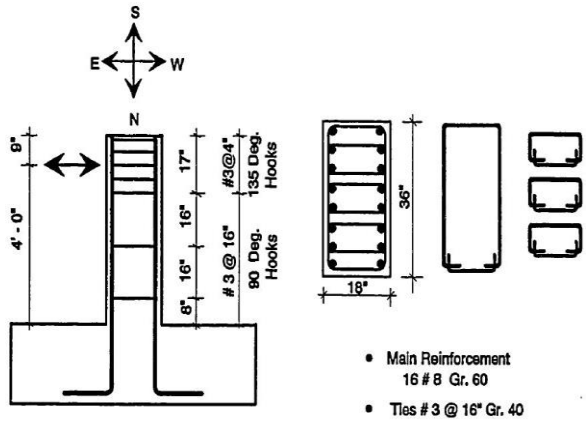

a) SC1 specimen

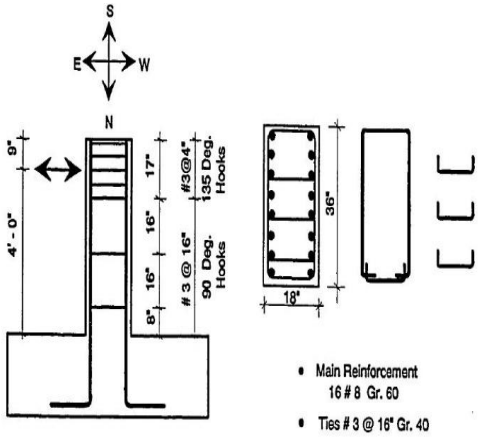

b) SC3 specimen

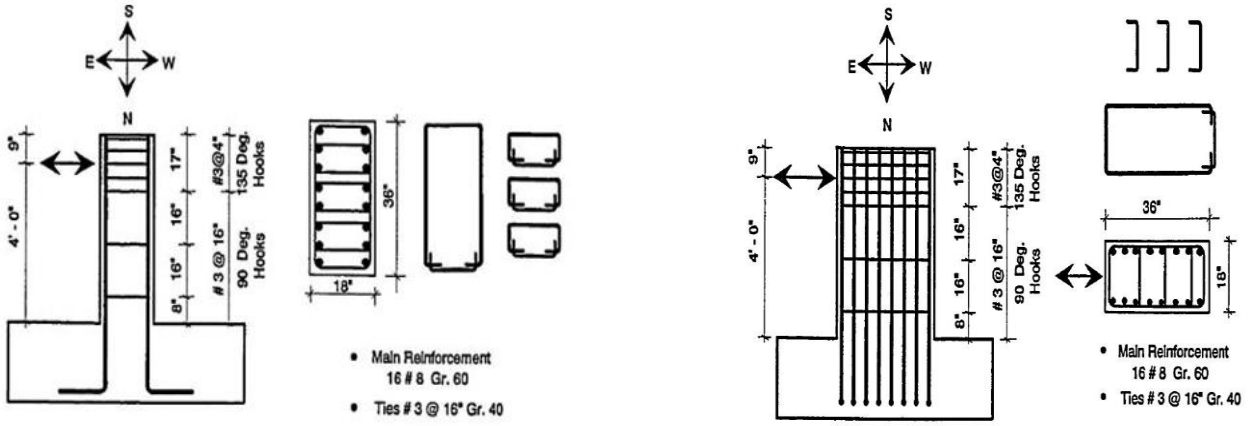

c) SC4 specimen d) SC9 specimen

Figure 2.2 Columns details (Aboutaha ,1994) (1 inch =25.4 mm, Kip =4.45 kN ,1 foot =304 mm,#3 bar diameter=9.525 mm, #8 bar diameter =25.4 mm).

Main experimental results

Generally, Aboutaha ,1994 concluded that the specimens had several diagonal cracks in the concrete compression zone at the bottom of a column. Figure 2.3 shows the failure mode of SC9 specimen as an example. Then, a major diagonal crack over the full height of each specimen was formed which widely opened with dramatic loss in strength and stiffness. Due to higher transverse reinforcement ratio in both SC1 and SC4, they experienced higher lateral strength and lower rate of stiffness degradation (Figure 2.4). SC9 specimen showed limited energy dissipation and displacement ductility as the peripheral ties were the only transverse reinforcements which resist the shear.

Figure 2.3 SC9 crack pattern at the end of the test (Aboutaha ,1994)

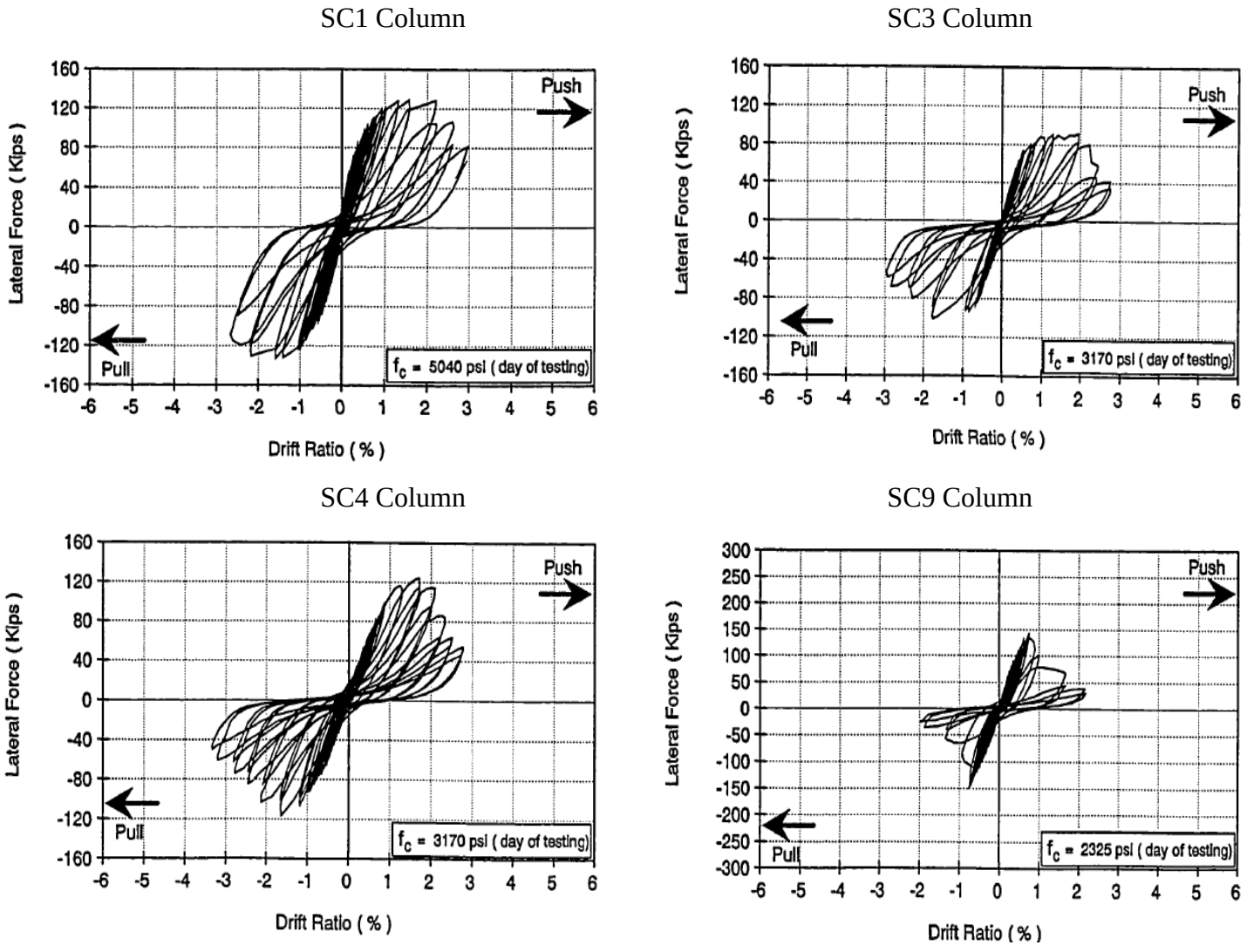

Figure 2.4 Hysteretic responses of Aboutaha series (1994) (Kips=4.45 kN)

2.2. TEST SERIES BY TANAKA AND PARK (1990)

This set consists of four specimens starting by No.5 to No.8. The variable parameters of this set are the type of the transverse reinforcement, anchorage details and the level of the axial compressive load applied. The concrete used was normal weight with maximum aggregate of 20 mm.

Test setup and main column properties

Constant axial compressive load was applied to each specimen by the 10 mN servo-controlled hydraulic jack in DARTEC testing machine. At the same time ,500 kN or 1000 kN double acting hydraulic jacks was applied as the cyclic lateral loading. Figure 2.5 shows the loading arrangement of the test specimens.

One unit of one elastic cycle has been imposed by lateral load and displacement history to a nominal displacement ductility factor μN ±0.75 while two units of elastic cycles imposed for μN = ± 2, ±4, etc, where the μN is the ratio between the measure of lateral displacement at the jack to the lateral displacement at first yield. The potentiometer used to measure the horizontal displacement whilst a load cell measured the horizontal load. Different locations on the hoops, cross ties and longitudinal reinforcement with a potential plastic hinges zones attached by electrical resistance strain gauges with 5 mm gauge length.

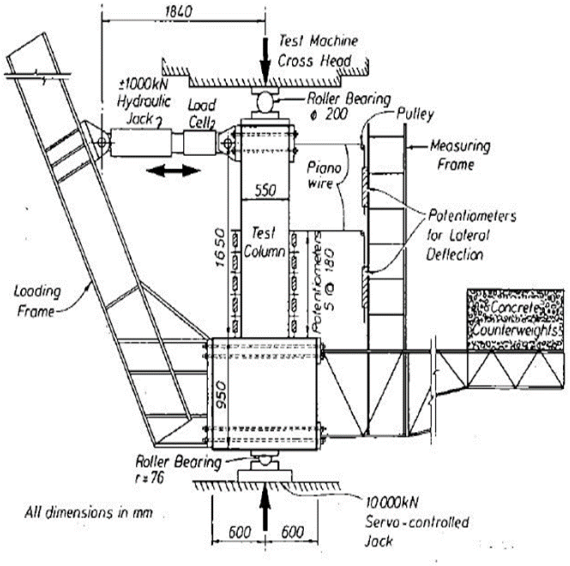

Figure 2.5 Loading arrangement (Tanaka and Park ,1990)

Figure 2.6 Shows the details of the specimens. They had a height of 1650.0 mm and 550 mm square cross section with the shear span to depth ratio of 3.0. All columns were reinforced longitudinally with 12 bars of 20 mm diameter while they were transversally reinforced with 12 mm diameter bar at every 110 mm and 220 mm in close and wide spacing zones respectively for both unit 5 and unit 6.

On the other hand, the transverse bars were placed at every 90 mm and 180 mm in close and wide spacing respectively for unit 7 and unit 8. Unit 5 and 7 were supplied with J bar crossties with 90° hook at one end and 135° hook at the other end alternating from side to side along the column length. Unit 6 and unit 8 used the tension splice of bar U overlapped crossties (Figure 2.6). The yield strength of the main longitudinal bars was 511 MPa while the yield strength of the transverse reinforcement was 325 MPa. The ratio of transverse reinforcement parallel to the load direction was the same for both specimens.

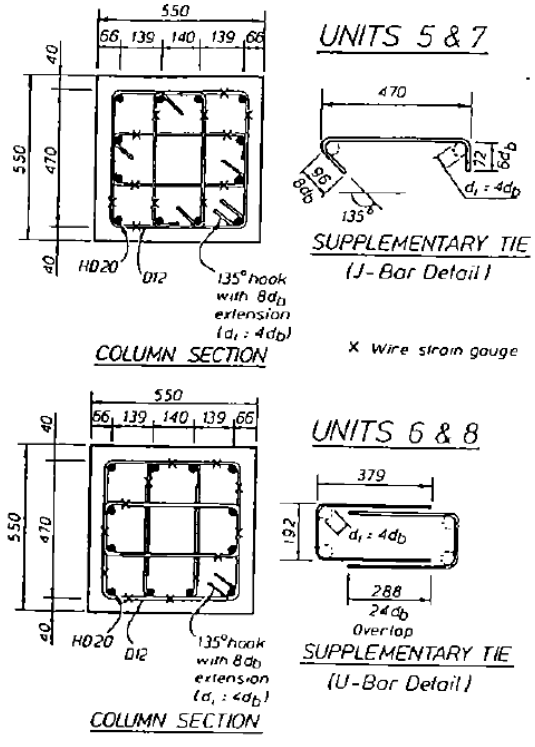

a) transverse sections

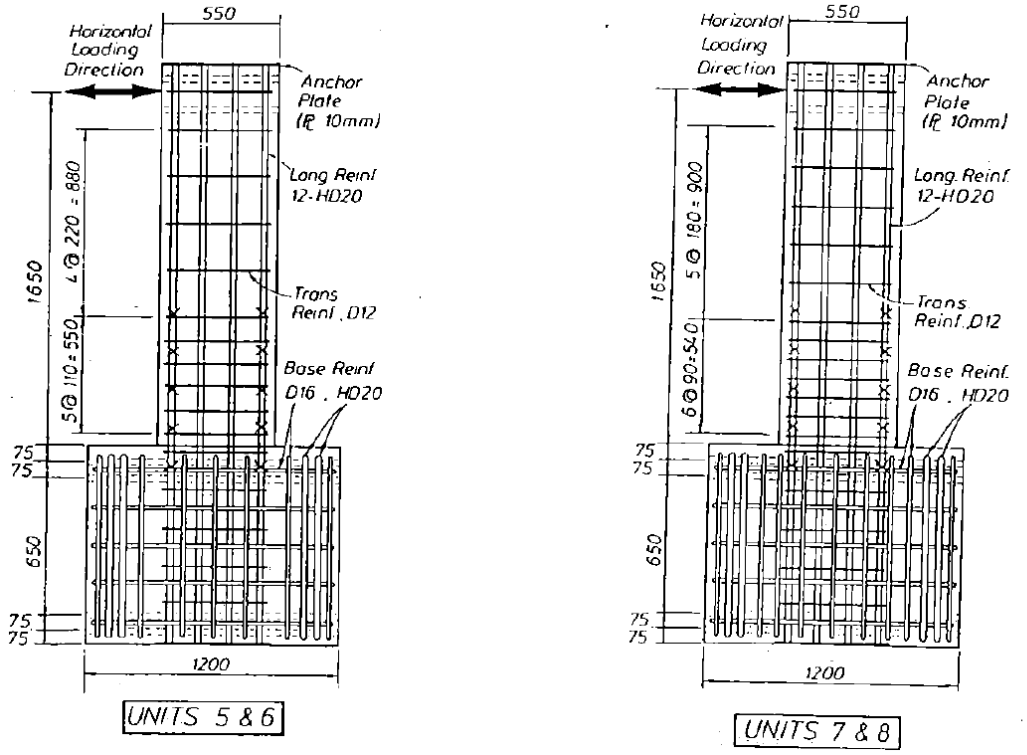

b) longitudinal sections

Figure 2.6 Details of the specimens (Tanaka and Park ,1990)

Main experimental results

Only Unit 5 and Unit 6 will be considered in this project because unit 7 and unit 8 are not applicable for the 3PKT as their axial load ratios were more than 0.2. Figure 2.7 shows inclined flexural shear crack predominated in both columns with a good stable behavior and energy dissipation till the final stage of the testing. It was observed that since the cracks did not penetrate along the splices, hence the bond conditions of splices were then maintained. Figure 2.8 shows an example of the crack pattern of unit 5. Concrete Crushing with buckling of longitudinal compression reinforcement observed during the final stage of the test.

Specimen No.5 Specimen No.6

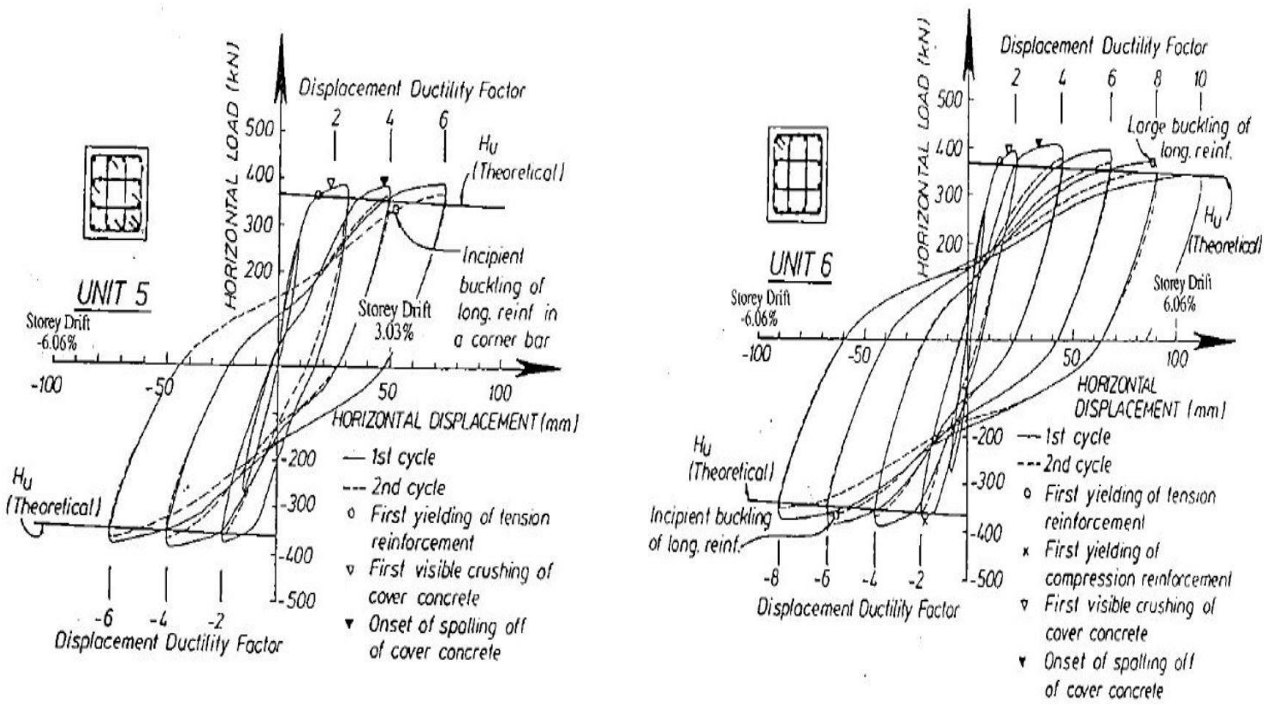

Figure 2.7 Specimens hysteretic responses (Tanaka and Park, 1990)

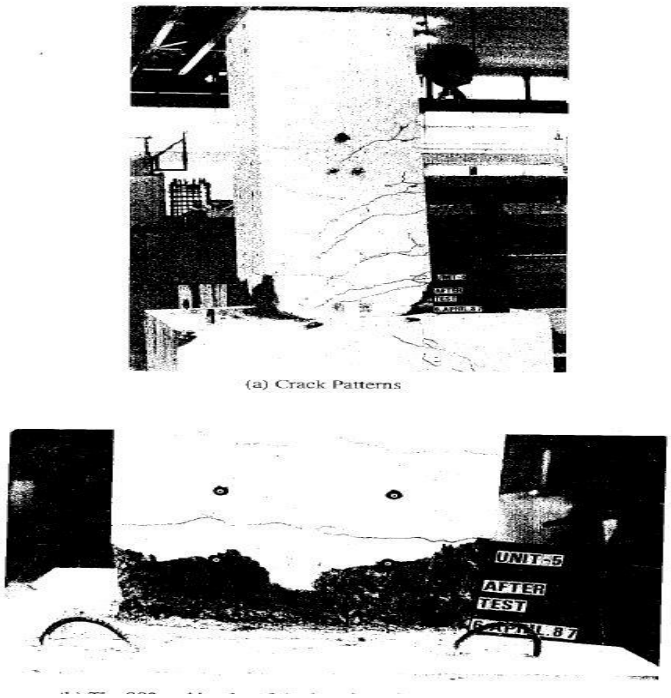

Figure 2.8 Crack pattern of unit 5 specimen after failure (Tanaka and Park, 1990)

2.3. TEST SERIES BY WIGHT AND SOZEN (1973)

This series contains a total number of ten specimens of concrete columns which experienced a shear failure. These specimens were tested under loading reversals to deflections large than the yield deflection. The variable parameters of the testing program were as following: the axial loading, the ratio of the transverse reinforcement and the required deflection ductility for each cycle.

Test setup and main column properties

The test programme was conducted in a horizontal position of each specimen as it is elaborated in figure 2.9. The axial load was applied through a pair of external cables by a servoram which was attached to one of the end of the specimen (Wight and Sozen,1973). The central joint was kept motionless by a pair of hydraulic jacks. Hence, the deflection of a specimen column was at the same time in opposite directions of each double ended of the specimen with frequent stops to record applied shear, deflection, rotation at the joint, and strains in the reinforcing steel. Twenty minutes was needed to complete each cycle of load reversals. The dimension of each specimens was 152 x 305 mm (6 x12 in) with a double ended test configuration of a length equal to 876 mm as Figure 2.9 shows.

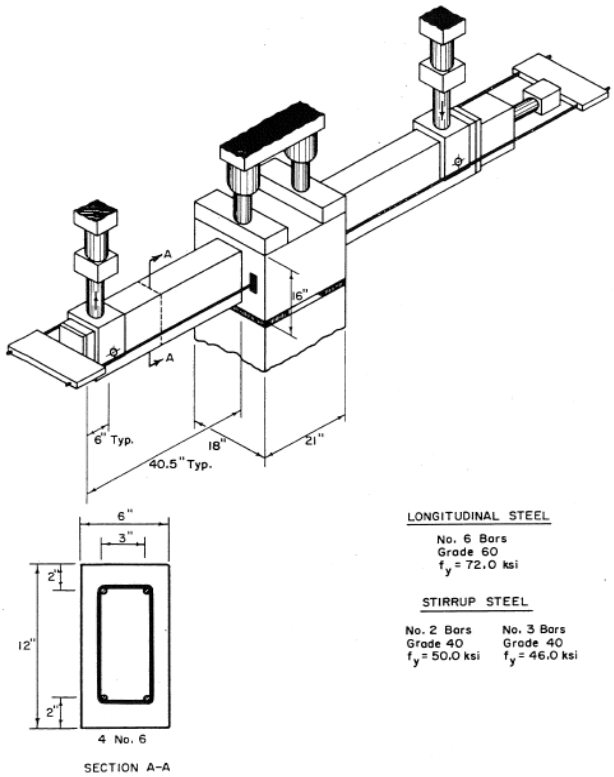

Figure 2.9 Test setup and column section properties (Wight and Sozen, 1973) (1 inch =25.4 mm, Kip =4.45 kN, 1 ksi=6.9 MPa, 1 foot =304.8, #6 bar diameter=19 mm, #2 bar diameter = 6.35 mm, #3 bar diameter = 9.52 mm)

Each specimen was having a total number of 4 longitudinal deformed reinforcement bars with 19 mm diameter while the transverse reinforcements were with 6.3 mm diameter bar at various spacing along the length of each column. Generally, bars' yield strength was 496 MPa and 345 MPa for both longitudinal and transverse bars respectively.

Main experimental results

Inclined cracks along the height of a column were formed including yielding of the transverse reinforcement and spalling of the shell concrete. Due to the cycles of inelastic load reversals, the specimens could experience full flexural yield capacity and then inelastic deflection. Vertical cracks were observed in the specimens with zero axial load. Figure 2.10 shows the development of the crack pattern of the specimens while Figure 2.11 depicts the final crack pattern of an example specimen after completing the test. It can be said that as the ratio of transverse reinforcement increased, the length of the inelastic deformation region was decreased.

The specimens with lower axial load experienced a more rapid declined in shear displacement response as it can be seen clearly in the comparison between the specimen No. 40.033(west) with axial load of 177.93 kN and the specimen No. 25.033(East) with 111.21 kN axial load (Figure 2.12). As a result of the load reversals, inclined cracks were formed, splitting and spalling deflection cracks created in the compressed concrete and splitting cracks formed along the tension reinforcement. The concrete core was the only part to resist the shear after one complete cycle.

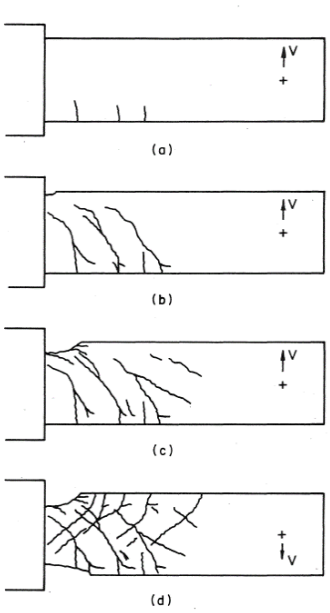

Figure 2.10 Crack pattern development (Wight and Sozen, 1973)

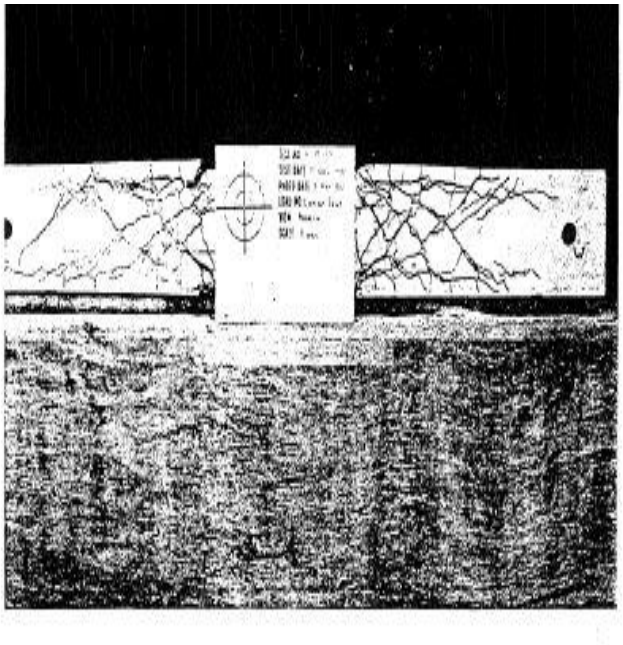

Figure 2.11 Specimen 40.033 after failure (Wight and Sozen, 1973)

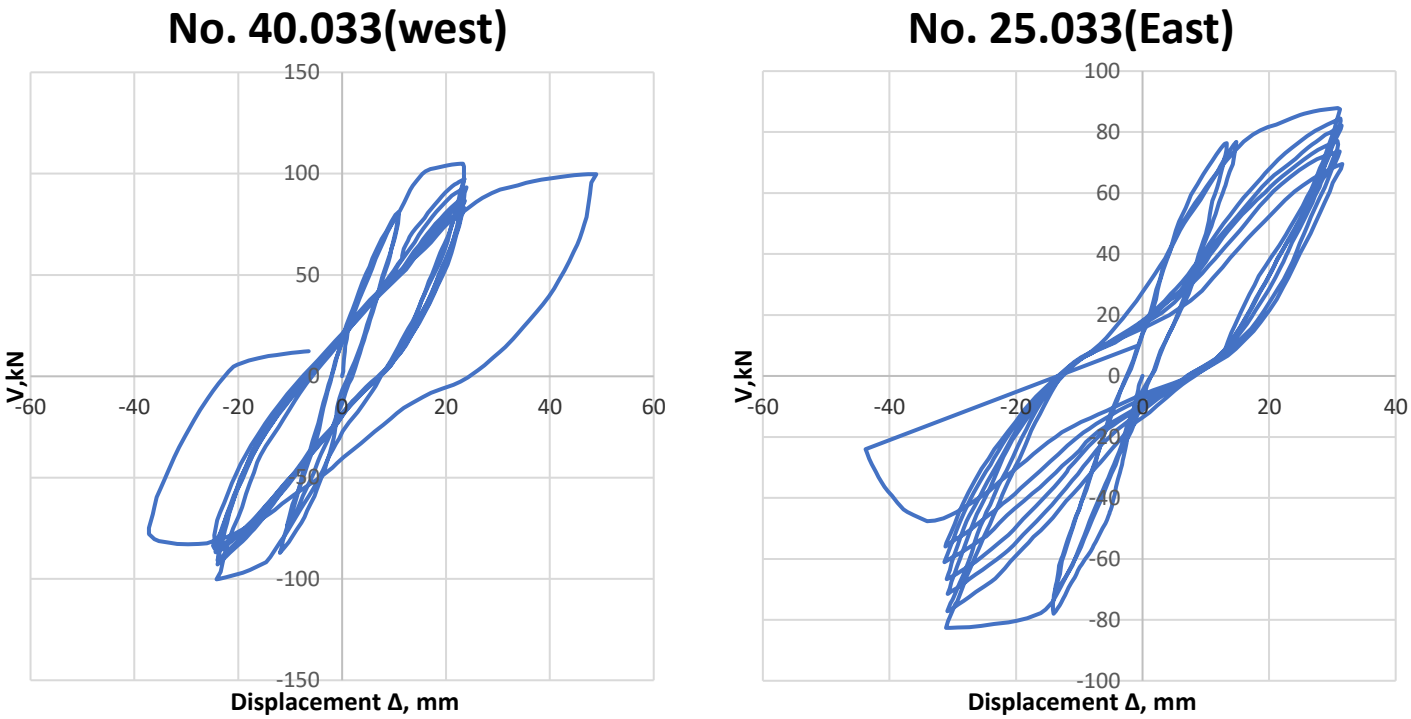

Figure 2.12 Specimens hysteretic responses (Wight and Sozen, 1973)

2.4. TESTS DATABASE

This section summarizes the properties of all specimens that have been discussed in the previous sections (Table 2.1). Below are the definitions of the terms in Table 2.1:

N: The axial load (kN).

a: The column height from the base to the applies lateral load (mm).

h: Depth of the cross section (mm).

b: Width of the cross section (mm).

d: Effective depth of section from the compression edge of the section to the centroid of As (mm).

d_b: The diameter of the main longitudinal bars (mm).

ρ_v %: Ratio of transverse reinforcements.

ρ_l %: Ratio of the main longitudinal reinforcements.

S: Shear failure.

FS: Flexural shear failure.

f_{yl}: The yield strength of main longitudinal reinforcement(MPa).

f_{ul}: The ultimate strength of main longitudinal reinforcement(MPa).

f_{yv}: The yield strength of transverse reinforcement(MPa).

f_{uv}: The ultimate strength of transverse reinforcement(MPa)

E_s: The modulus of elasticity of longitudinal reinforcement (MPa).

f_c: Concrete cylinder strength (MPa).

$V_{exp,max}$: Experimental maximum shear force (kN).

Table 2.1 Database of short column tests

			Geometry					Reinforcement and concrete									Experiment	
Test ID	**Reference**	**N (kN)**	**a (mm)**	**b(mm)**	**h(mm)**	**a/h**	**d(mm)**	**d_b(mm)**	**ρ_l%**	**ρ_v (%)**	**f_{yl}(MPa)**	**f_{ul}(MPa)**	**f_{yv}(MPa)**	**f_{uv}(MPa)**	**f_c(MPa)**	**N/bhf$_C$**	**$V_{exp,max}$(kN)**	**Failure**
SC1	Aboutaha (1994)	0	1220	915	457	2.67	397	25	1.878	0.1691	434	689	400	460	34.7	0	622	S
SC3	Aboutaha (1994)	0	1220	915	457	2.67	397	25	1.878	0.1057	434	689	400	460	21.9	0	459	S
SC4	Aboutaha (1994)	0	1220	915	457	2.67	397	25	1.878	0.1691	434	689	400	460	21.9	0	555	S
SC9	Aboutaha (1994)	0	1220	457	915	1.333	684	25	1.878	0.0847	434	689	400	460	16.5	0	675	FS
No. 5	Tanaka and Park (1990)	968	1650	550	550	3	437	20	1.246	0.748	511	675	325	429	32	0.1	383	FS
No. 6	Tanaka and Park (1990)	968	1650	550	550	3	437	20	1.246	0.748	511	675	325	429	32	0.1	410	FS
No. 40.033a(East)	Wight and Sozen (1973)	189	876	152	305	2.87	254	19	2.45	0.323	496	835	344	551	34.7	0.118	100	S
No. 40.033a(west)	Wight and Sozen (1973)	189	876	152	305	2.87	254	19	2.45	0.323	496	835	344	551	34.7	0.118	100	S
No. 40.048(East)	Wight and Sozen (1973)	177.9	876	152	305	2.87	254	19	2.45	0.461	496	835	344	551	26.1	0.147	102	S
No. 40.048(west)	Wight and Sozen (1973)	177.9	876	152	305	2.87	254	19	2.45	0.461	496	835	344	551	26.1	0.147	100	S
No. 00.048(East)	Wight and Sozen (1973)	0	876	152	305	2.87	254	19	2.45	0.461	496	835	344	551	25.9	0	85	S
No. 00.048(west)	Wight and Sozen (1973)	0	876	152	305	2.87	254	19	2.45	0.461	496	835	344	551	25.9	0	85	S
No. 40.033(East)	Wight and Sozen (1973)	177.9	876	152	305	2.87	254	19	2.45	0.323	496	835	344	551	33.6	0.114	95	S
No. 40.033(west)	Wight and Sozen (1973)	177.9	876	152	305	2.87	254	19	2.45	0.323	496	835	344	551	33.6	0.114	103	S
No. 25.033(East)	Wight and Sozen (1973)	111.2	876	152	305	2.87	254	19	2.45	0.323	496	835	344	551	33.6	0.071	90	S
No. 25.033(west)	Wight and Sozen (1973)	111.2	876	152	305	2.87	254	19	2.45	0.323	496	835	344	551	33.6	0.071	95	S
No. 00.033(East)	Wight and Sozen (1973)	0	876	152	305	2.87	254	19	2.45	0.323	496	835	344	551	32	0	82	S
No. 00.033(west)	Wight and Sozen (1973)	0	876	152	305	2.87	254	19	2.45	0.323	496	835	344	551	32	0	82	S
No. 40.067(East)	Wight and Sozen (1973)	177.9	876	152	305	2.87	254	19	2.45	0.646	496	835	344	551	33.4	0.115	95	S
No. 40.067(west)	Wight and Sozen (1973)	177.9	876	152	305	2.87	254	19	2.45	0.646	496	835	344	551	33.4	0.115	100	S
No. 00.067(East)	Wight and Sozen (1973)	0	876	152	305	2.87	254	19	2.45	0.646	496	835	344	551	31.8	0	87	S
No. 00.067(west)	Wight and Sozen (1973)	0	876	152	305	2.87	254	19	2.45	0.646	496	835	344	551	31.8	0	92	S
No. 40.092(East)	Wight and Sozen (1973)	177.9	876	152	305	2.87	254	19	2.45	0.918	496	835	317	482	33.5	0.115	116	S
No. 40.092(west)	Wight and Sozen (1973)	177.9	876	152	305	2.87	254	19	2.45	0.918	496	835	317	482	33.5	0.115	118	S
No. 00.0105(East)	Wight and Sozen (1973)	0	876	152	305	2.87	254	19	2.45	1.0491	496	835	317	482	33.4	0	105	S
No. 00.0105(west)	Wight and Sozen (1973)	0	876	152	305	2.87	254	19	2.45	1.0491	496	835	317	482	33.4	0	102	S

As it can be seen from the table above, the range of transverse reinforcement ratio (ρ_v %) was between 0.08% to 1.0% while the ratio of longitudinal reinforcement (ρ_l %) was from 1.25% to 2.45%, and the shear-span-to-depth ratio (a/h) was between 1.33 to 3.0. On the other hand, the concrete strength was between 17 MPa and 35 MPa, and the range of longitudinal and transverse reinforcements yield strength were from 434 to 511 MPa and from 317 MPa to 400 MPa respectively. Additionally, it was observed that the maximum and minimum shear forces were 675 kN and 82 kN respectively while the the axial load ratio (N/bhf_c) varied from 0 to 0.15.

3. FINITE ELEMENT MODELLING OF SHORT COLUMNS

3.1 INTRODUCTION

Each column has been modelled using a non-linear finite element program (VecTor2) which has been developed at the University of Toronto over the past 20 years. It is based on the Disturbed Stress Field Model (DSFM). Plane-stress modelling is used to study the behaviour of the member in the plane of loading under monotonic, cyclic and reversed cyclic loading. This program has a high numerical accuracy and a computational efficiency as it uses a fine mesh of low-powered elements. VecTor2 considers the post-cracking influences on concrete, such as compression softening, tension stiffening, hysteretic effects, dowel action of steel reinforcement, and the interaction between concrete and reinforcement by considering the bond mechanism. VecTor2 is facilitated by FormWorks as the pre-processor while Augustus is the the post-processor which is a software that provides graphical post-processing capabilities for the analysis results of VecTor2. This tool requires only the sectional, material and loading system details of the specimens to perform the analysis of reinforced concrete structures, however the other non-linear finite element modelling tools need the definition of the failure mechanism or are dependent on empirical values obtained through similar experimental tests. Hence, VecTor2 is a friendly program that captures different types of reinforced concrete structures responses under various loading conditions (Wong and Vecchio, 2002).

3.2 DISTURBED STRESS FIELD MODEL

Modified Compression Field Theory (MCFT) overestimates the shear stiffness and strength and assumes that the rotations of the principals' stress and strain fields are equal for some materials.

However, MCFT underestimates the shear stiffness and strength for elements that experience limited rotation of the principal stress and strain fields because the concrete compression response is excessively softened due to the principal tensile strains. Hence, the disturbed stress field model (DSFM) (Vecchio, 2000) improve the deficiencies of MCFT in predicting the response of certain structures and loading scenarios. DSFM includes the crack shear slip deformation. Below are a brief discussion of the compatibility, equilibrium and constitutive relationships of DSFM.

- **Compatibility Relationships**

The principal stress and strain axes do not remain coaxial as it is assumed by the MCFT. The strain field inclines at a larger rate than the stress field does. Figure 3.1 shows the deformation due to crack shear slip.

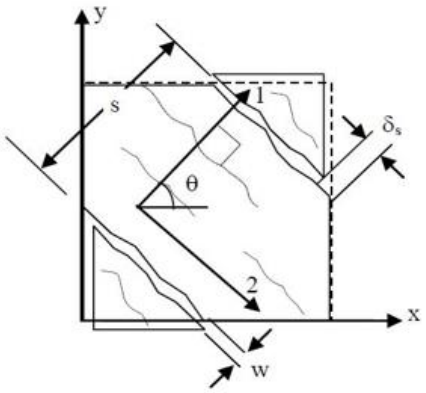

Figure 3.1 Deformation due to crack shear slip (Wong et al.,2013)

DSFM refers that the total strain ε_x, ε_y, and γ_{xy}, are the total net concrete strains ε_{cx}, ε_{cy}, and γ_{cxy} Adding to the shear slip strains ε_x^s, ε_y^s, and γ_{xy}^s as it shown below:

$$\varepsilon_x = \varepsilon_{cx} + \varepsilon_x^s$$

$$\varepsilon_y = \varepsilon_{cy} + \varepsilon_y^s$$

$$\gamma_{xy} = \gamma_{cxy} + \gamma_{xy}^s$$

- **Equilibrium Relationships**

DSFM and MCFT have the same average stress equilibrium relationship as it shows below:

$$\sigma_x = f_{cx} + \rho_{sx} f_{sx}$$

$$\sigma_y = f_{cy} + \rho_{sy} f_{sy}$$

$$\tau_{xy} = v_{cxy}$$

DSFM also incorporates the equilibrium relationships for local stresses at the crack.

- **Constitutive relationships**

The constitutive models for cracked concrete were improved. The reduction factor of softening concrete was added. Additionally, DSFM models the crack slip, δ_s, to find the the crack slip shear strain, γ_s by relating the crack slip to the local shear stresses, v_{ci}. More details on DSFM cane be found in "VecTor2 and FormWorks User's Manual". 2nd edition.

3.3 FEM OF COLUMN (NO.5)

Program VecTor2 was used for the modelling of the specimens in this project while the post-processing of the results was performed using program Augustus. VecTor2 utilizes the the compatibility, equilibrium, and constitutive relations of the Modified Compression Field Theory. Figure 3.2 shows the finite element model of column (NO.5) as an example (Tanaka and Park ,1990). The concrete was modelled as quadrilateral plane-stress elements. The transverse and longitudinal reinforcement bars were represented by smeared reinforcements with an angel of 0° and 90° from the horizontal axis, respectively. The nodes at the base of the model were restrained in both X and Y directions to represent the the block at the base. The axial load was applied vertically and distributed in each node along the top row. On the other hand, the displacement was introduced laterally in all the nodes along the first row at the top of the column to avoid local effects. The lateral displacement was increased monotonically to capture the entire column behavior including its post-peak response while the deformation of the base block was neglected for simplicity purposes.

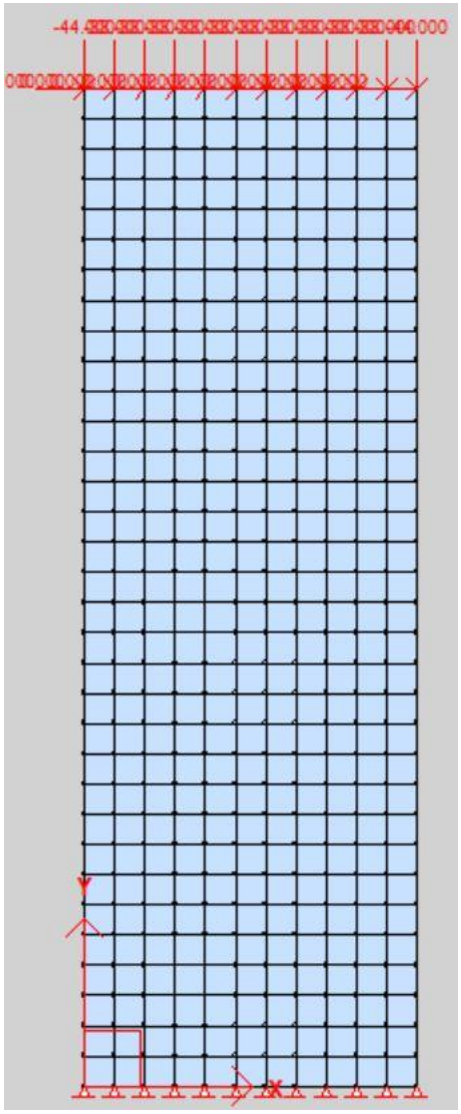

Figure 3.2 Finite element model of a short column (VecTor2 program)

Comparison with test results

The main results for the short column (NO.5) modelled by VecTor2 can be seen in Figures (3.3 -3.4). Figure 3.3 shows the measured and predicted load-deformation response of the specimen. FEM prediction agreed reasonably with the experimental response including a good post-peak prediction. However, the predicted response was stiffer than the measured one due to the fact that the block deformation was ignored in the modelling. Predicted crack and deformation pattern is shown in Figure 3.4. The flexural shear failure mode of the test specimen was captured very well including the yielding of tension reinforcement.

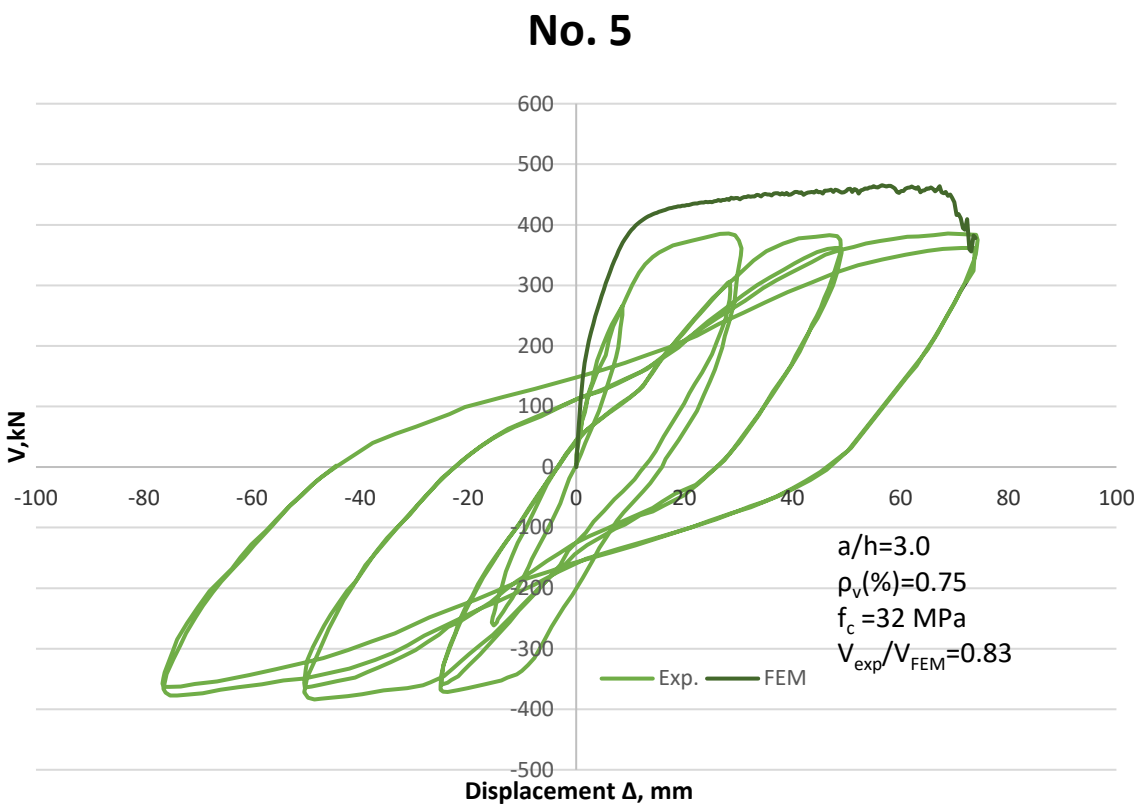

Figure 3.3 Measured and predicted load -deformation response of the short column NO.5 (Tanaka and Park ,1990)

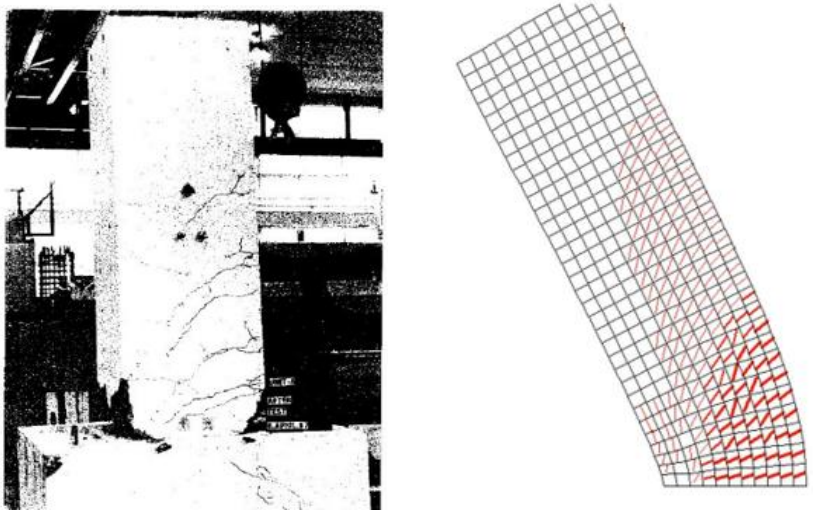

a) Experimental b) Analytical

Figure 3.4 Observed and predicted crack and deformation patterns of column NO.5 at failure (Tanaka and Park ,1990)

Stresses and deformations in the critical end sections

After it has been demonstrated that the FEM model can capture well the response of the test specimen, it is a good idea to use the simulation for further study on how the short columns resist the shear. The orientation and relative magnitude of the principal compressive stresses in the short column NO.5 has shown in Figure 3.5 where the green and the blue colours represent minimum and maximum values. It can be seen that the maximum stresses are located in the critical end section (left corner of the model), meanwhile the stresses were uniform with relatively low value in the other parts of the member. Figure 3.6 elaborates stresses distribution in the base section at failure of the member. It is clearly observed that the stresses mainly had been carried in the compression zone at the left corner of the model.

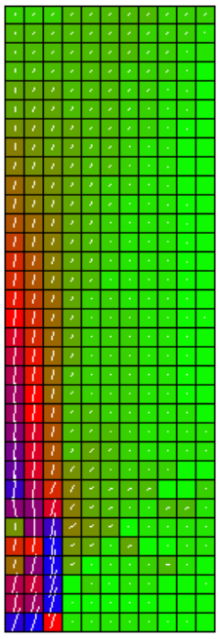

Figure 3.5 Principal compressive stresses in the concrete at failure

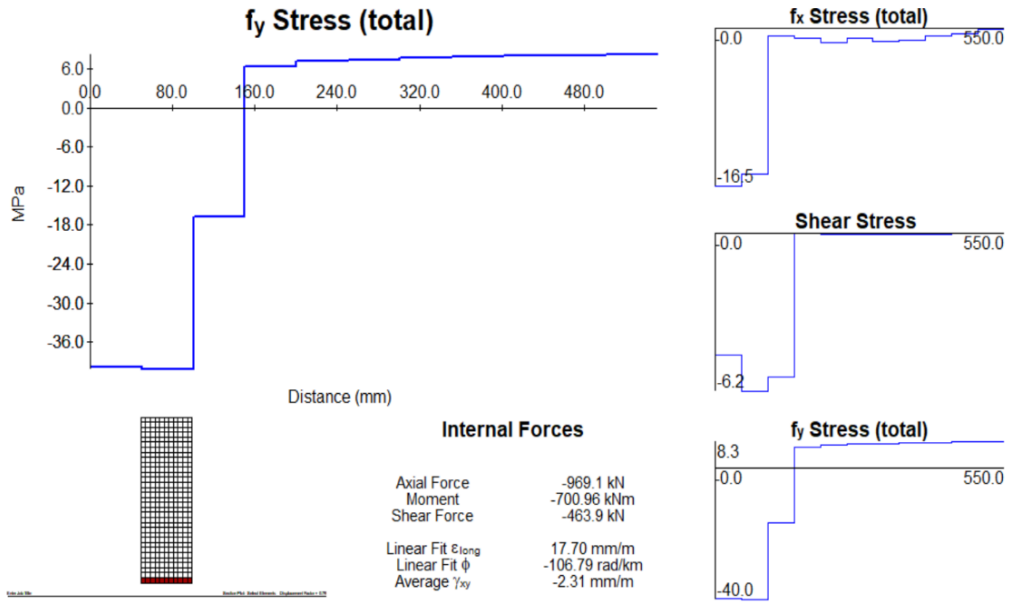

a) vertical stress

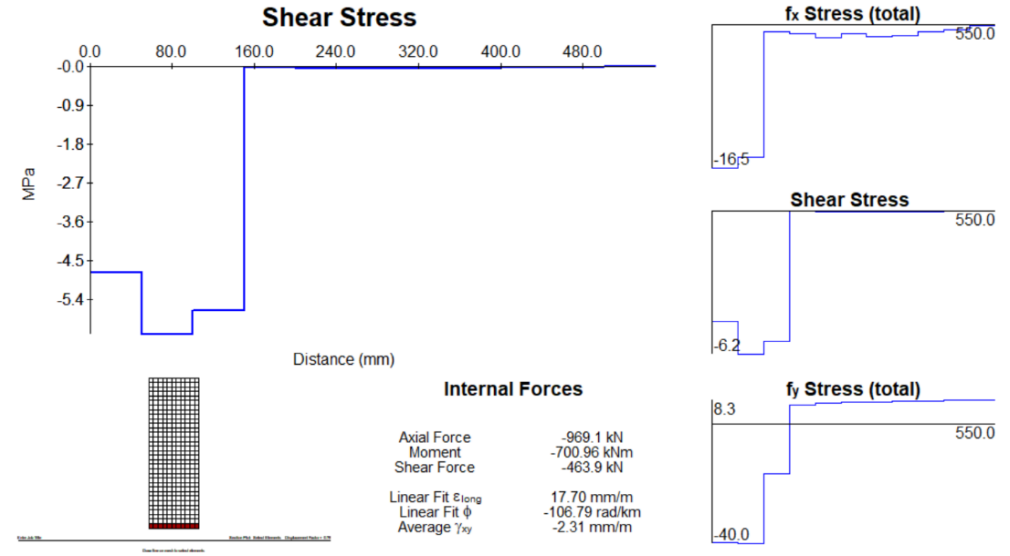

b) shear stress

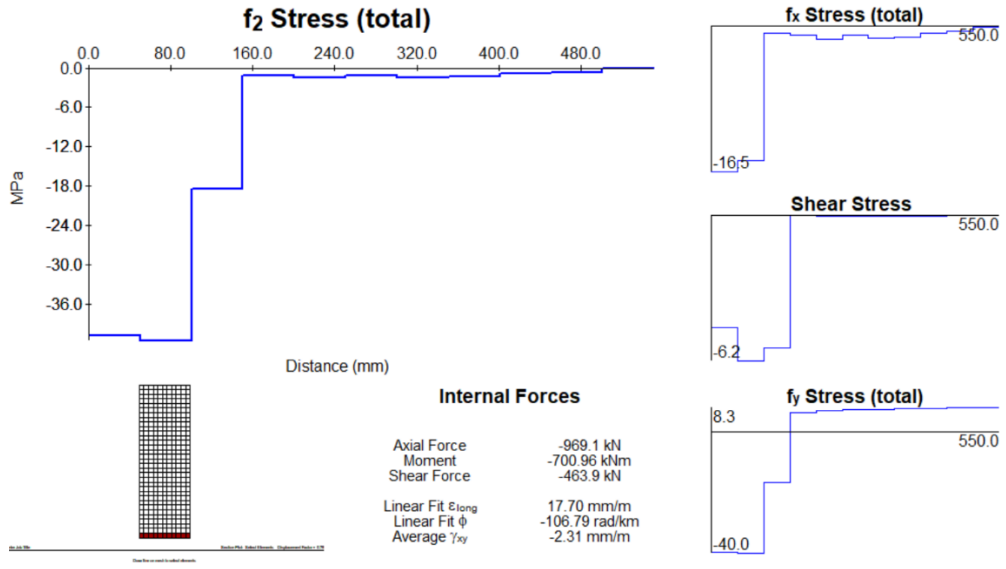

c) principal compressive stress

Figure 3.6 Stresses in the base section at failure a) vertical stress b) shear stress c) principal compressive stress (postprocessor Augustus)

Figure 3.7 shows the predicted strains of the short column NO.5 at shear failure. Figure 3.7 (a,b) depicts ε_x and ε_y which represent the horizontal and the vertical strains respectively, while Figure 3.7(c) shows the principal compressive strains (ε_2). FEM shows that ε_x and ε_y are non-linear distribution strains and do not follow the classical linear distribution strains as for the slender columns. It can be seen from Figure 3.7(b) that the vertical strain largely distributed at the portion far from the compression zone (right corner). Additionally, the ε_2 strains zone coincides with same zone of the principal compressive stresses.

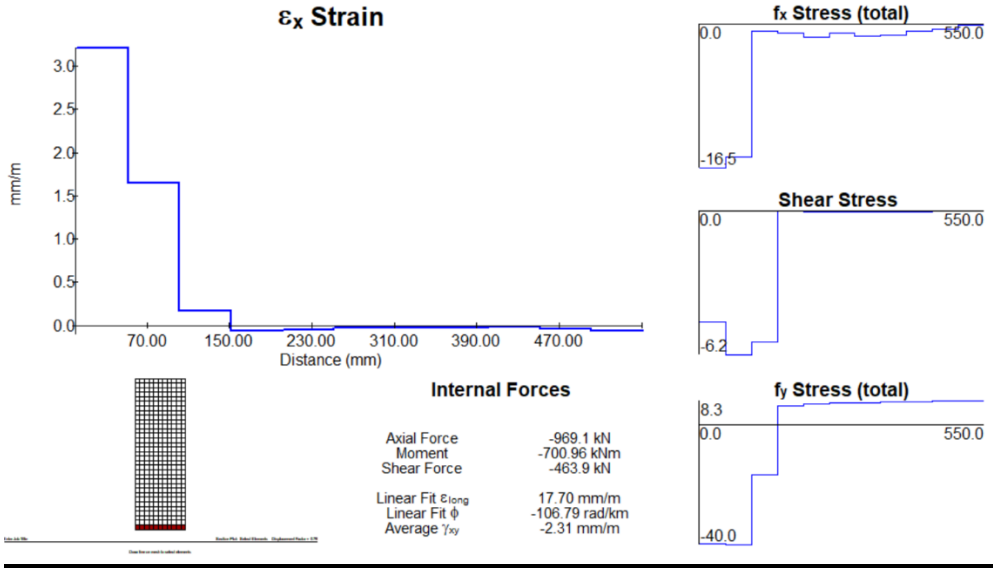

a) horizontal strain

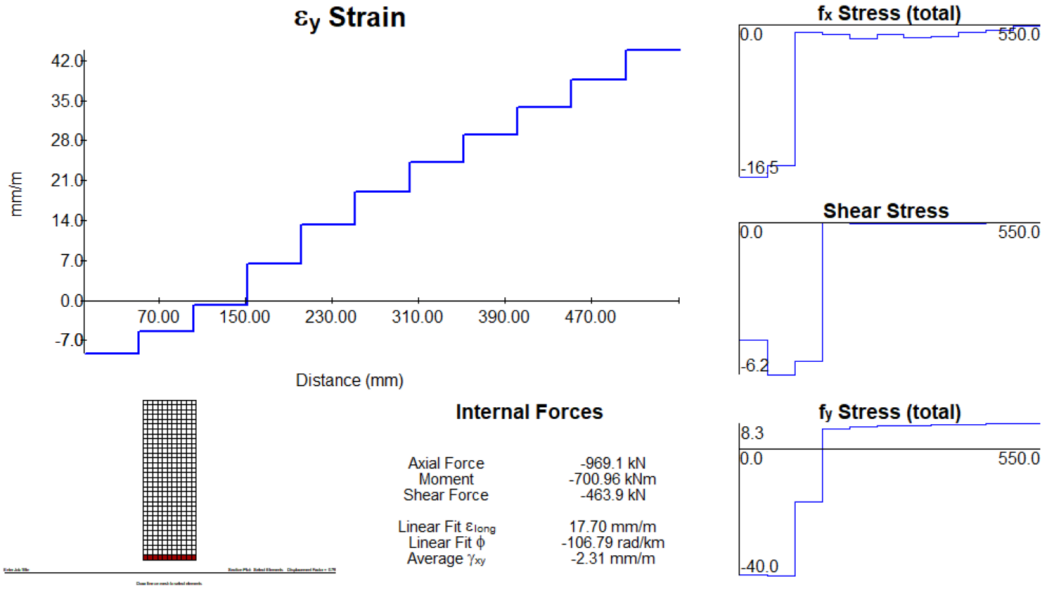

b) vertical strain

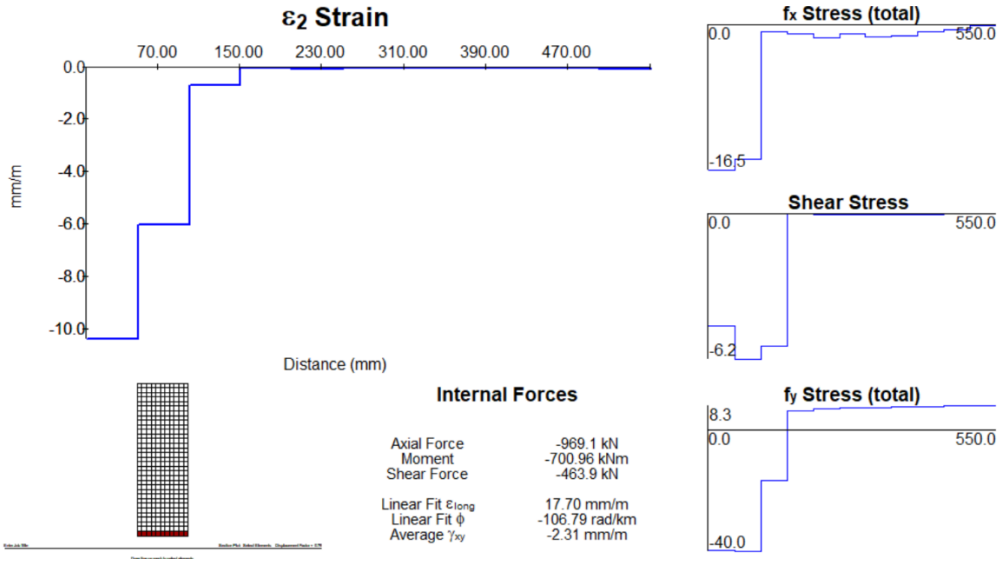

c) principal compressive strain

Figure 3.7 Predicted strains of the short column NO.5 at shear failure: a) horizontal strain b) vertical strain c) principal compressive strains (postprocessor Augustus)

3.4 TEST SERIES BY ABOUTAHA (1994)

In this section the comparison between experimental and predicted load-displacement responses of the specimens will be discussed. Figure 3.8 shows that the results of the predicted responses using VecTor2 are approximate reasonably well with the measured responses of the specimens. While the predicted initial stiffness is larger than the measured one due to neglecting the deformation of the base block, a good prediction of the maximum shear forces is obtained.

Another good observation from the results is that the FEM predicts well the failure load of the specimens. It can be seen that the column with smallest a/h and largest depth is stiffer and stronger than other columns having the largest a/h and the smallest depth. Additionally, it can be said that the smaller the a/h the smaller ductility and displacement capacity. The other significant variable was the ratio of shear reinforcement varied between 0.085% in the deepest column to 0.169% in the shallowest one. Specimen SC9 with the least shear reinforcement ratio was successfully predicted to remain elastic before it failed in a brittle shear failure while the other specimens with high shear reinforcement ratio experienced more plastic and ductile behavior as it is shown in Figure 3.8.

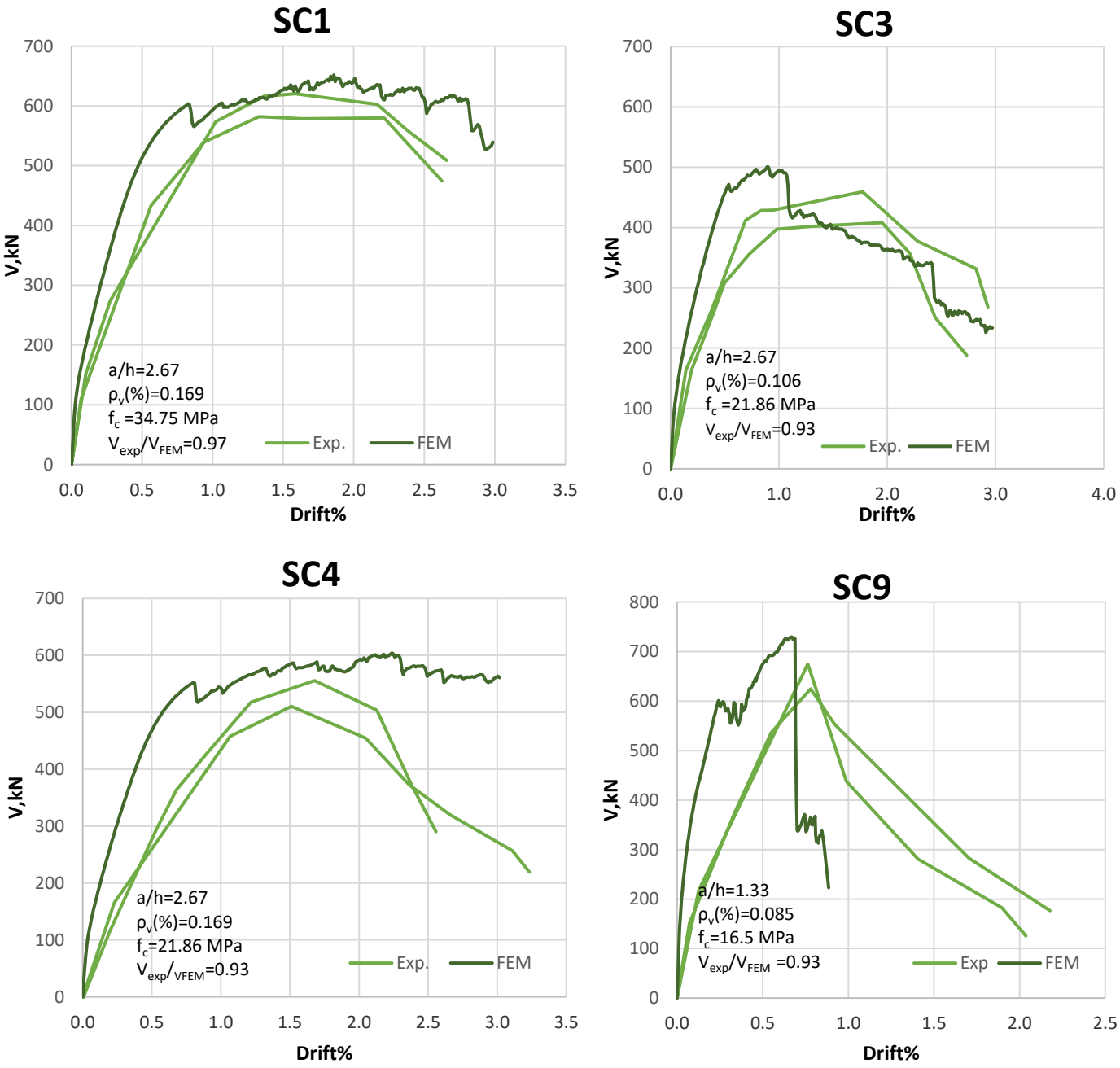

Figure 3.8 Comparison of VecTor2 predicted and measured load-deformation response—SC specimens

Failure modes

SC1 specimen

As it was reported by Aboutaha (1994), flexural crack formed at a load of 178 kN which were located at 279.4 mm from the footing top. Then, the number of flexural cracks increased over the 2/3 of the

column height. Diagonal flexural cracks formed obviously during the load cycles of 356 kN with a yielding of the main longitudinal and transverse reinforcements. The major shear cracks created over the full height of the column at the 534 kN. The major diagonal cracks were widely opened at the drift ratio 2.25 % with a significant degradation of strength and stiffness. Figure 3.9 shows the FEM prediction of the cracks formation at 178 kN ,356 kN, 534 kN and 2.25 % drift respectively from left to right.

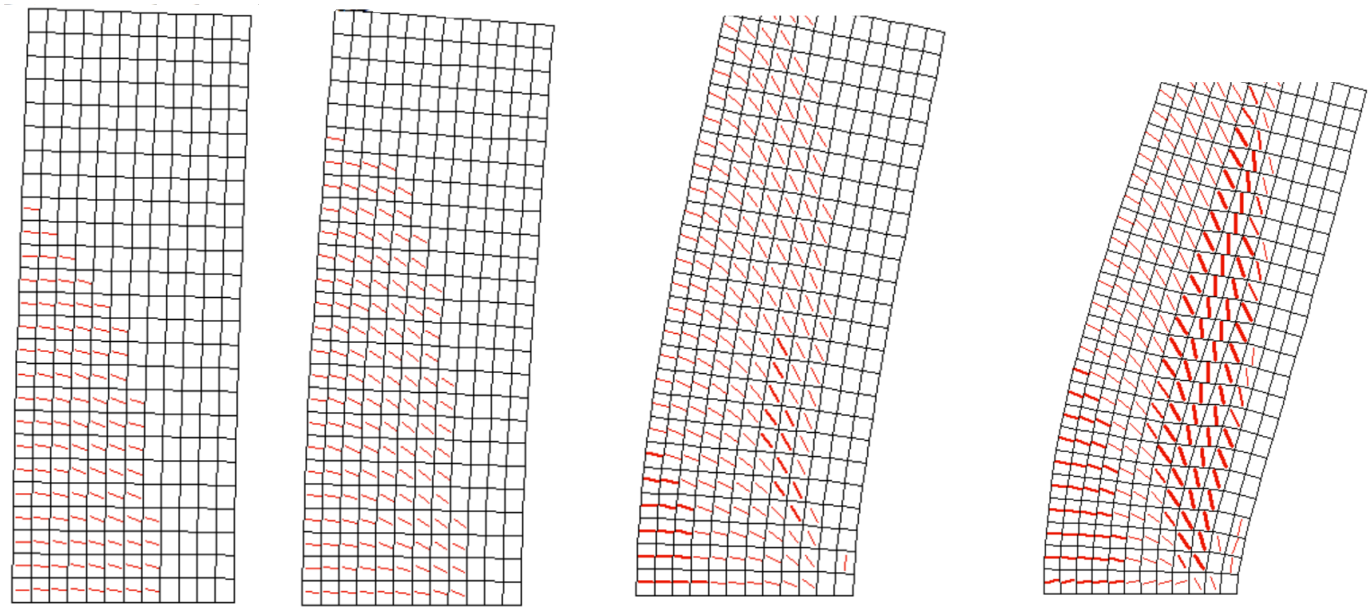

Figure 3.9 FEM prediction of SC1 cracks formation (postprocessor Augustus)

The formation of the flexural shear cracks along the column height in the observation study was well predicted by the VecTor2. Additionally, the major shear cracks were clearly formed with a wide opening in the drift ratio of 2.25 % just as the VecTor2 predicted.

SC3 specimen

Figure 3.10 compares the cracks formation of the experiment to the analytical results at loads 311 kN, 400 kN, and 2% drift ratio.

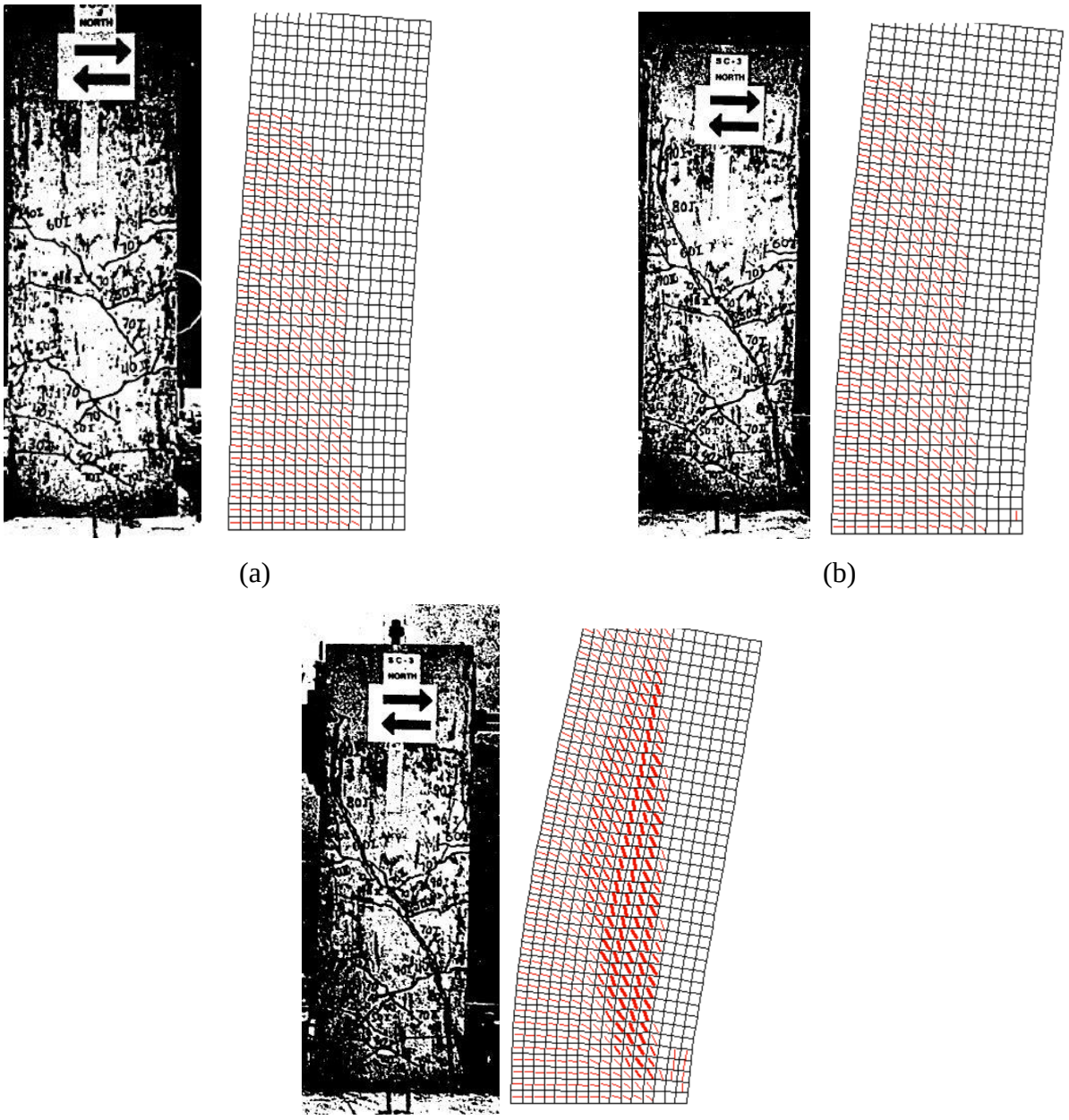

(a) (b)

(c)

Figure 3.10 Comparison of the crack patterns in SC3 obtained experimentally and analytically a) crack pattern during the cycle at 311 kN; b) crack pattern during the cycle at 400 kN c) crack pattern during the cycle at 2.0% drift ratio

The development of the failure mechanism and cracks pattern in the specimen SC3 were vey well captured by the VecTor2 analysis as it is depicted in Figure 3.10. The flexural cracks extended diagonally due to the shear load which increased starting from load cycle 311 kN to the load 356 kN and then 400 kN. The major diagonal cracks developed over 70 % of the column height. The transverse reinforcement was yielded at 400 kN while a large inelastic deformation was formed

during the cycle with a load higher than 400 kN. At a displacement of 2% to 2.5 % drift ratio a significant degradation of concrete strength at compression zone occurred along with a very wide opened diagonal crack.

SC4 specimen

A good match of the failure mechanism between the predicted and the observed behaviour of the specimen SC4 as it is shown below. The flexural cracks extended diagonally during the 311 kN due to the shear influence just like what the program predicted. As the load increased, the depth of the concrete in the compressive zone was slightly reduced. This is due to the fact that the flexural shear cracks were extended deeper into the concrete cross section. A considerable degradation in strength and stiffness of concrete was observed at 2% drift ratio with an extensive yielding of the reinforcements.

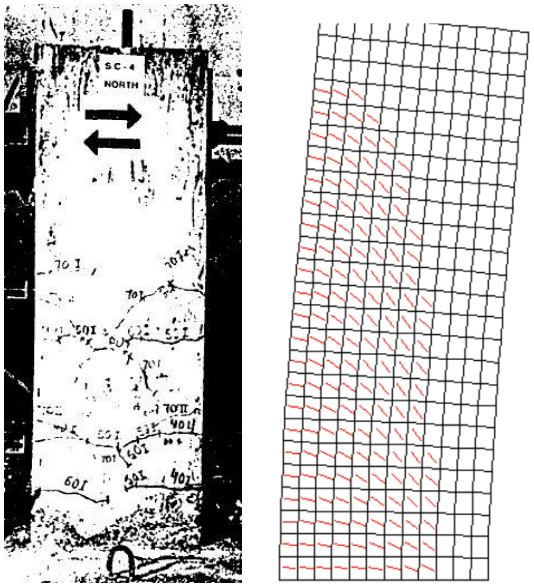

(a)

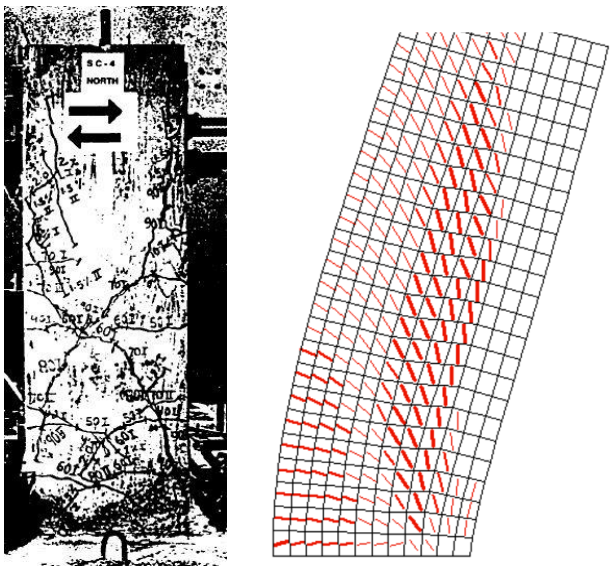

(b)

Figure 3.11 Comparison of the crack patterns in SC4 obtained experimentally and analytically a) Crack pattern during the cycle at 311 kN; b) Crack pattern during the cycle at 2.0% drift ratio.

SC9 specimen

The flexural shear failure mechanism of the column SC9 was successfully coincided with the analytical prediction as Figure 3.12 shows. The program predicted a compression shear failure at the bottom of the column with a several cracks which extended diagonally, Additionally, transverse reinforcement yielded and a dramatic loss of strength and stiffness occurred beyond the load 623 kN.

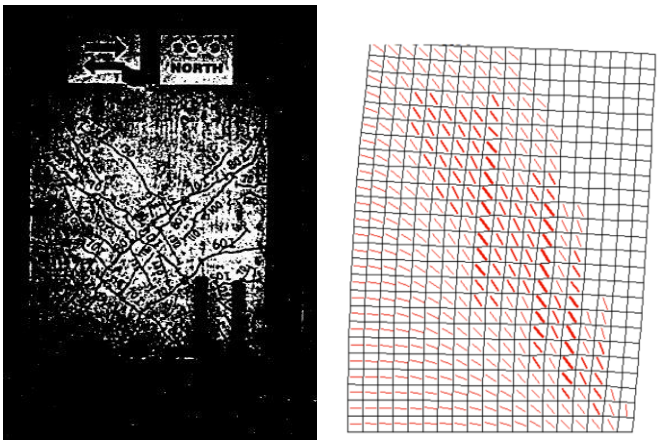

(a)

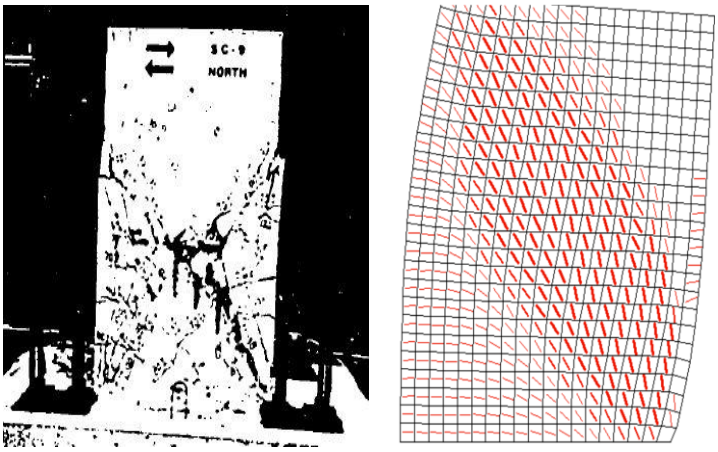

(b)

Figure 3.12 Comparison of the crack patterns in SC9 obtained experimentally and analytically: a) crack pattern during the cycle at 623 kN; b) crack pattern at failure

3.5 TEST SERIES BY TANAKA AND PARK (1990)

Figure 3.13 shows the comparison of the predicted and the measured load-deformation responses for No.5 and No.6 specimens. It can be seen that the prediction of the shear forces of the two specimens (No.5, No.6) were well captured including a good post-peak prediction. Nevertheless, the results revealed that the predicted stiffness is more than the measured one because the model neglected the deformation of the base block. The specimens experienced a good stability and ductility until the end of the test which was well captured as well.

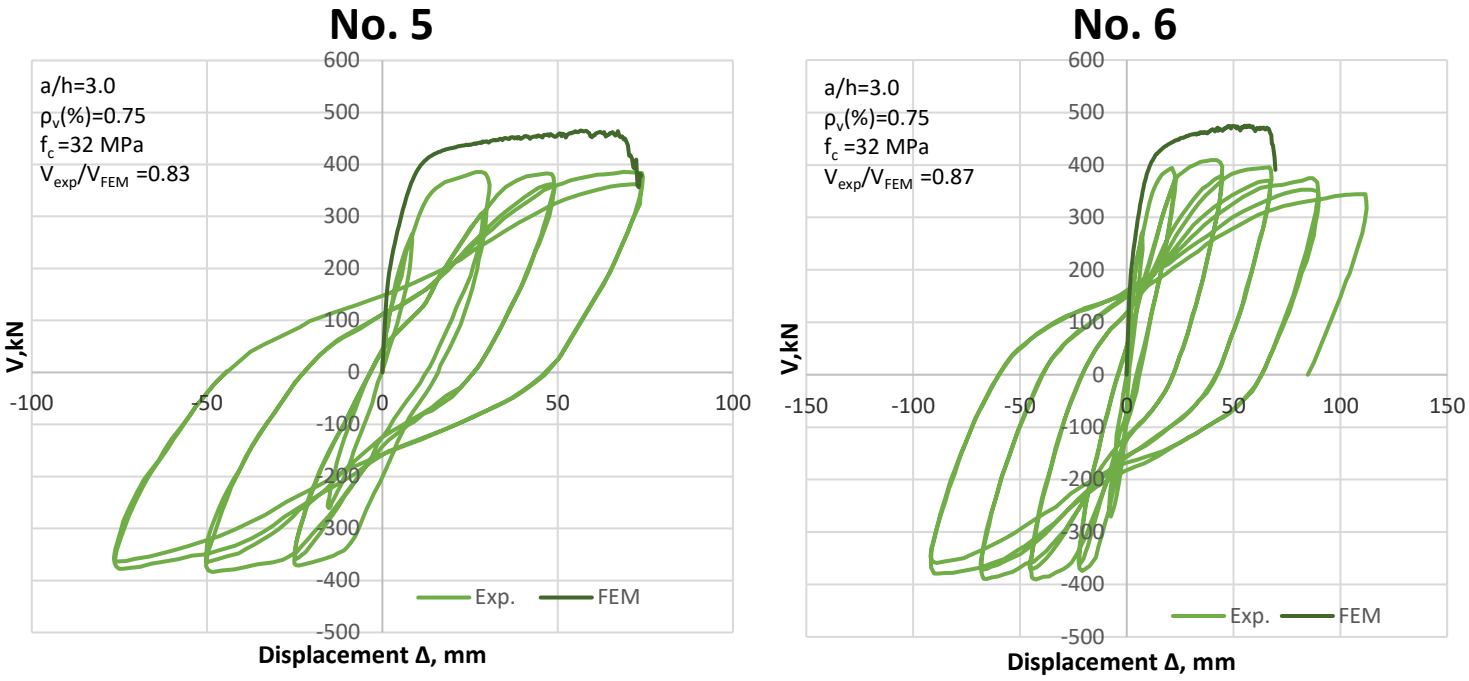

Figure 3.13 Comparison of VecTor2 predicted and measured load-deformation response—No.5, No.6 specimens

Failure modes

Crack pattern and failure mechanism of both specimens (No.5 and No.6) are shown in Figure 3.14. The failure started by the formation of flexural cracks which then extended diagonally as the load was increased. The flexural shear failure and cracks direction of both specimens were as the same as the experimental observation. The first yield of tension reinforcement and first visible crushing of concrete cover were observed at the first cycle during 25 mm displacement for both specimens.

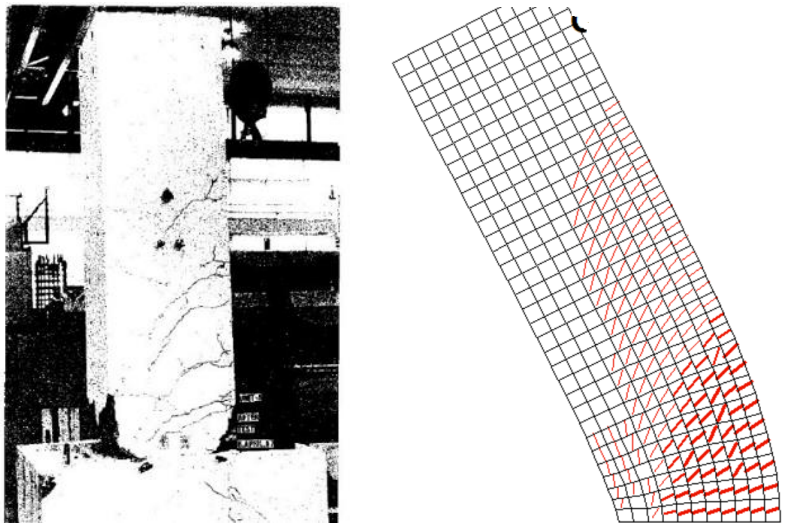

No. 5 specimen

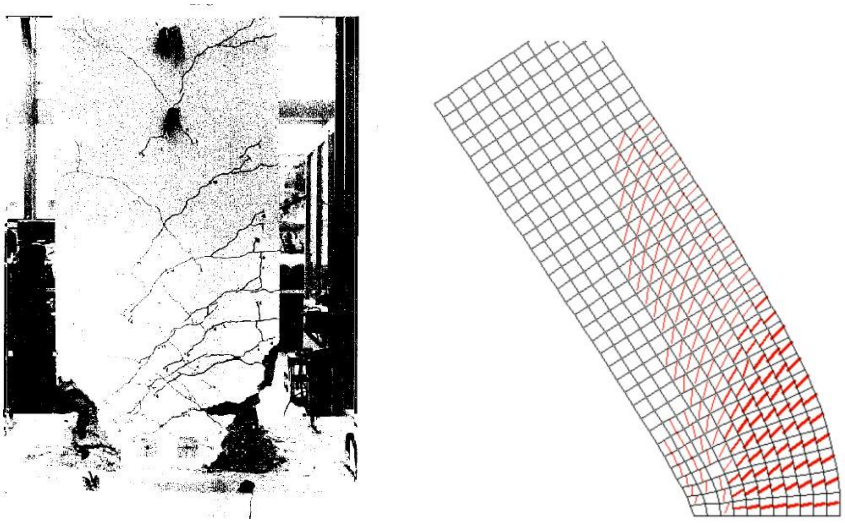

No. 6 specimen

Figure 3.14 Comparison of the crack patterns of (No.5, No.6) obtained experimentally and analytically

3.6 TEST SERIES BY WIGHT AND SOZEN (1973)

The failure of these specimens was due to the inclined cracks formation, spalling of shell concrete, yielding of the stirrups with abrasive motion along the cracks. The shear load versus the displacement result of the experimental specimens are given in a comparison to the analytical result in Figure 3.15,

which shows a similar behaviour. However, the models are stiffer than the experimental specimens as the deformation in the base was neglected. It can be observed that the decreasing of stiffness and strength rate was related to the axial load variations, the transverse reinforcement ratio and the ductility required per cycle. Increasing of both the axial load and the transverse reinforcement ratio slowed down the degradation of stiffness and strength with cycling while increasing the range of deflection per cycle resulted in higher rate of degradation of both stiffness and strength. The specimens without an axial load experienced more rapid decrease in strength and stiffness with each complete cycle of load reversals as it can be seen in the response of specimens (40.048 and 00.048) while specimens with axial load experienced higher yield and ultimate shear capacities. Noting that FEM could not converge and read the end of analytical analysis due to the fact of having much fluctuation at the end of graphs.

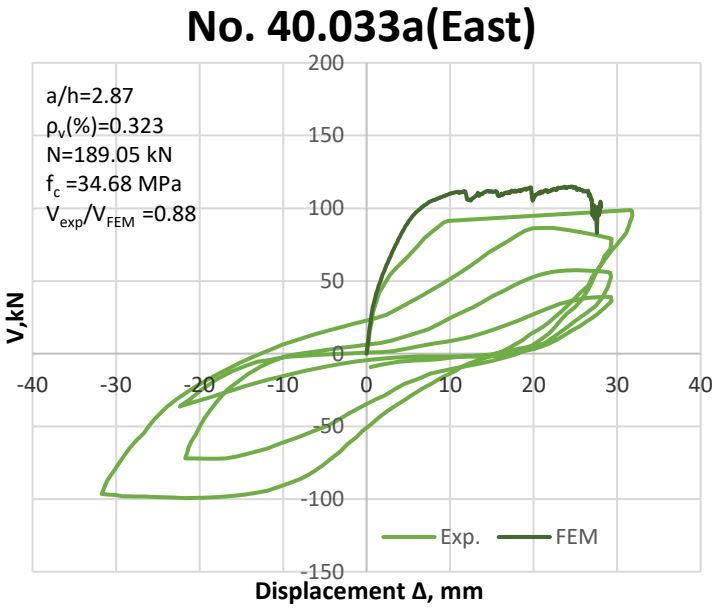

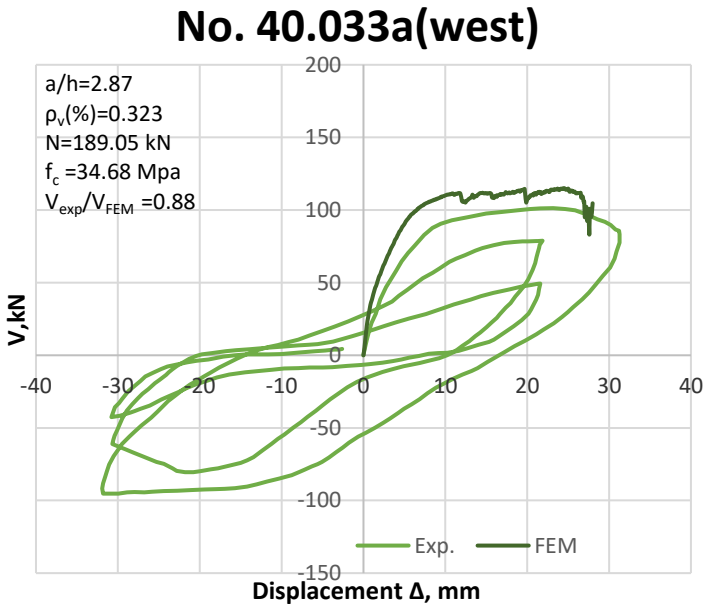

No. 40.048(East)

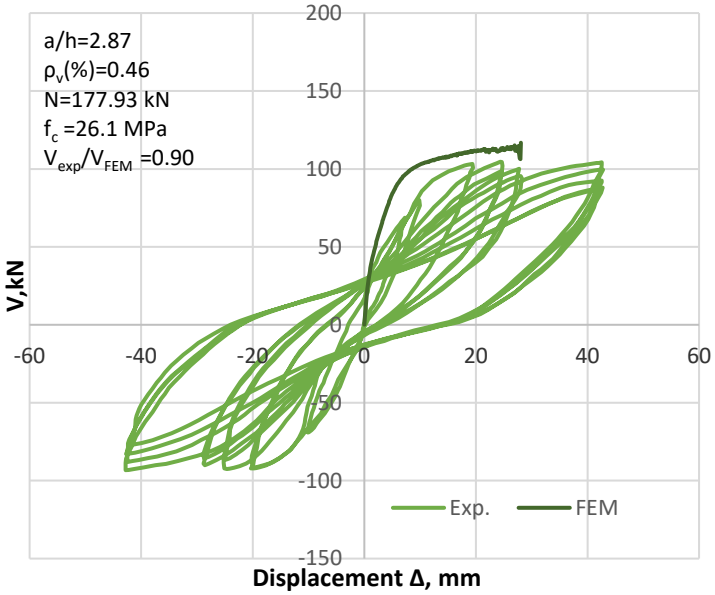

No. 40.048(west)

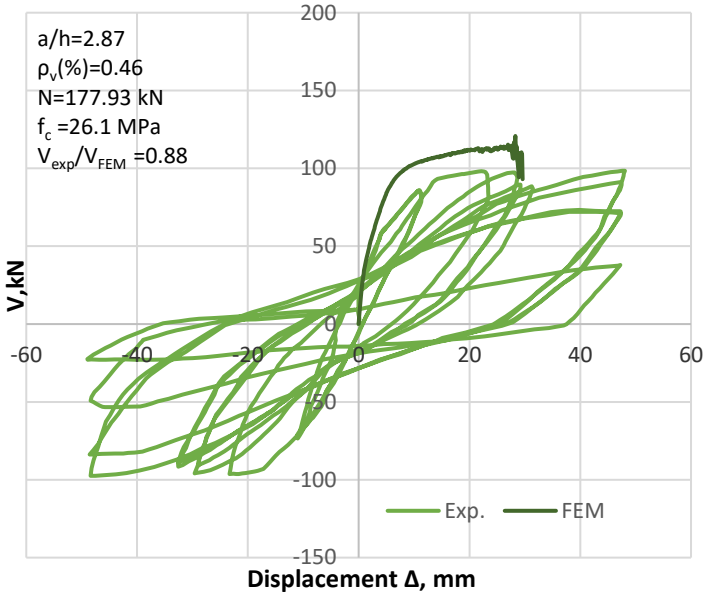

No. 00.048(East)

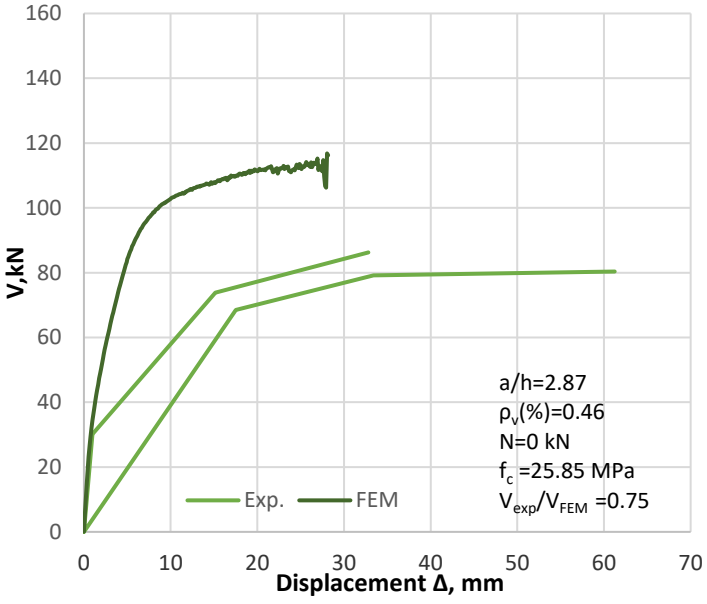

No. 00.048(west)

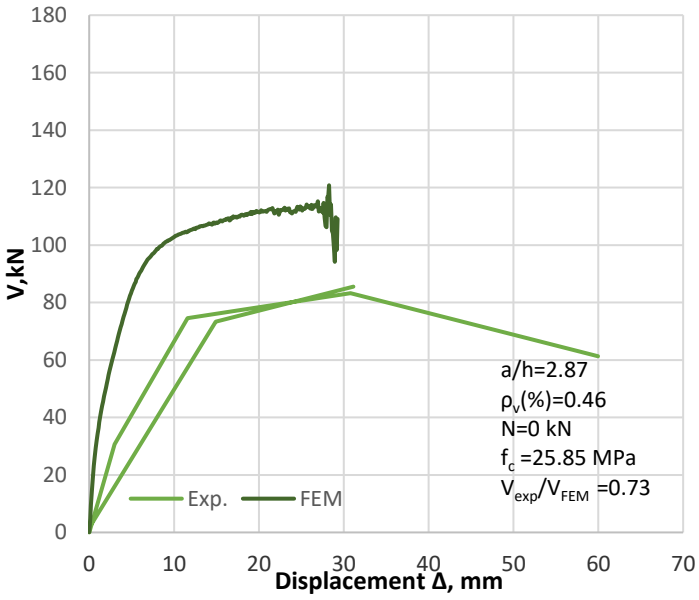

No. 40.033(East)

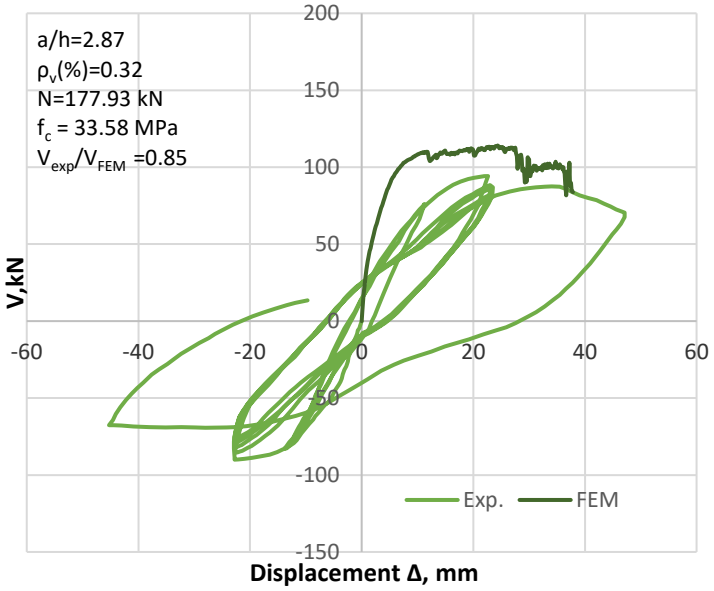

No. 40.033(west)

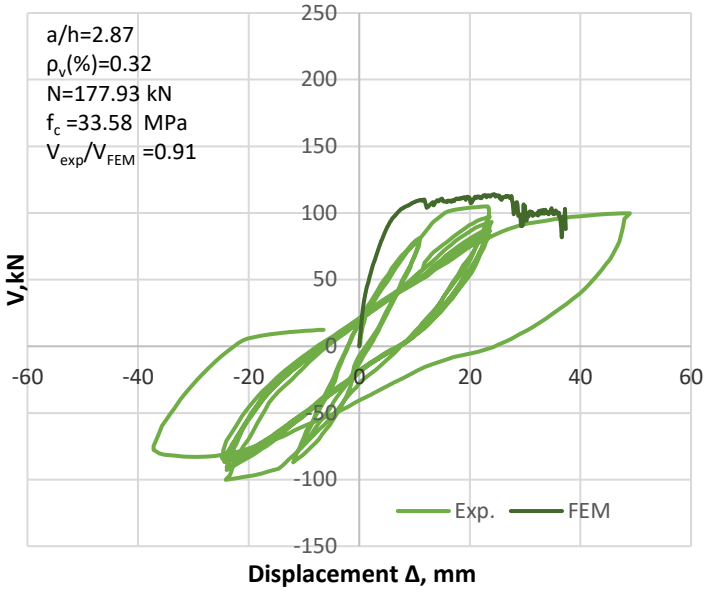

No. 25.033(East)

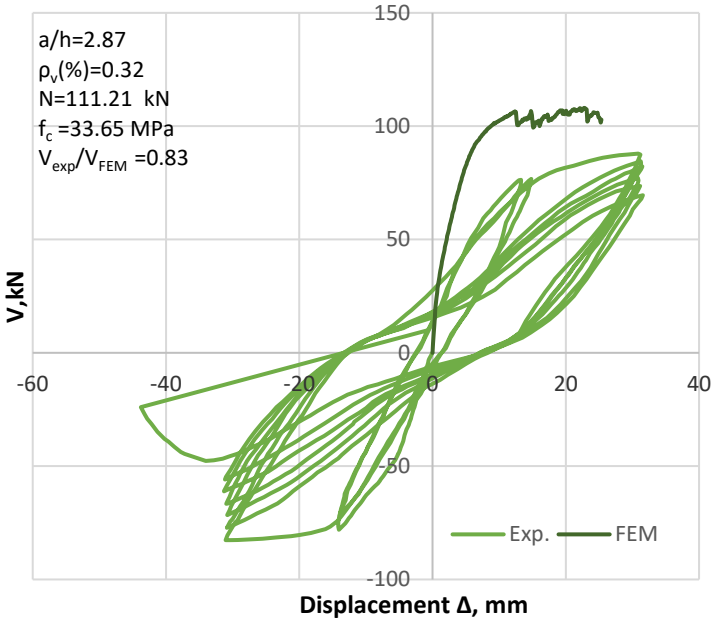

No. 25.033(west)

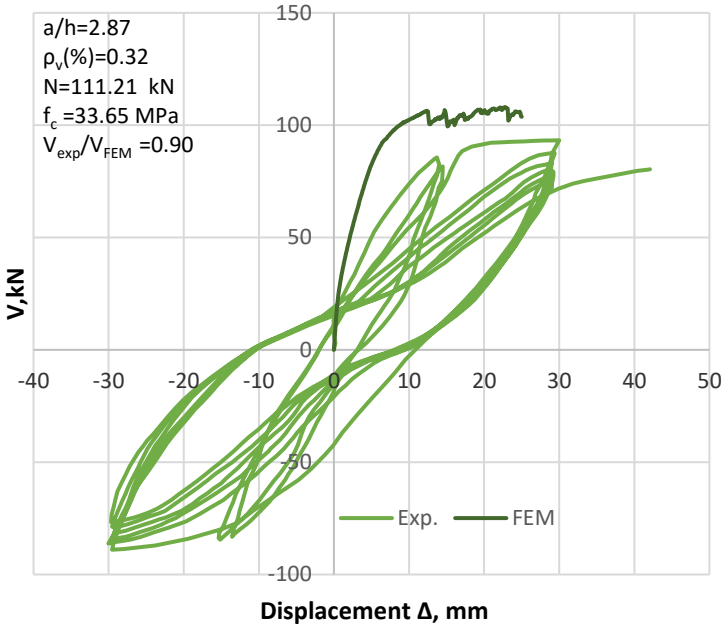

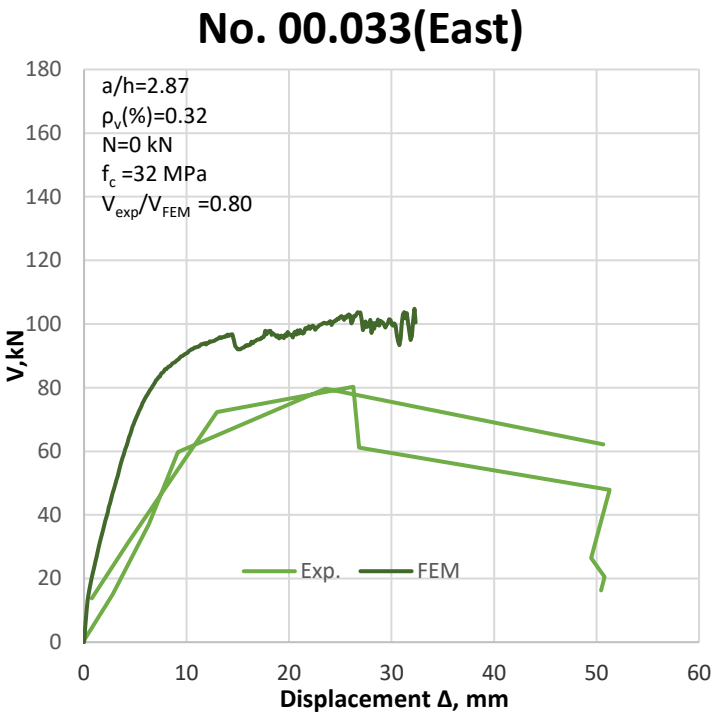
No. 00.033(East)
a/h=2.87
ρv(%)=0.32
N=0 kN
fc =32 MPa
Vexp/VFEM =0.80
V,kN
Displacement Δ, mm
Exp.
FEM

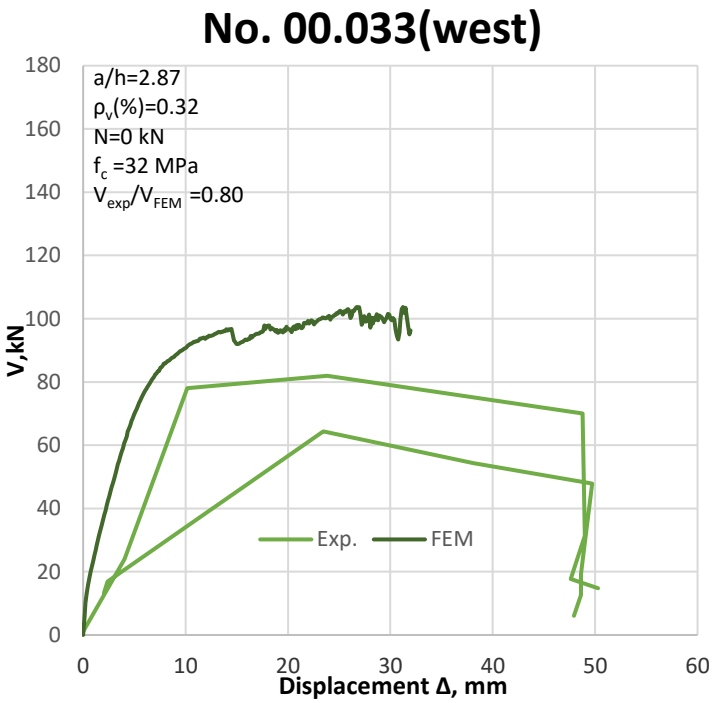
No. 00.033(west)
a/h=2.87
ρv(%)=0.32
N=0 kN
fc =32 MPa
Vexp/VFEM =0.80
V,kN
Displacement Δ, mm
Exp.
FEM

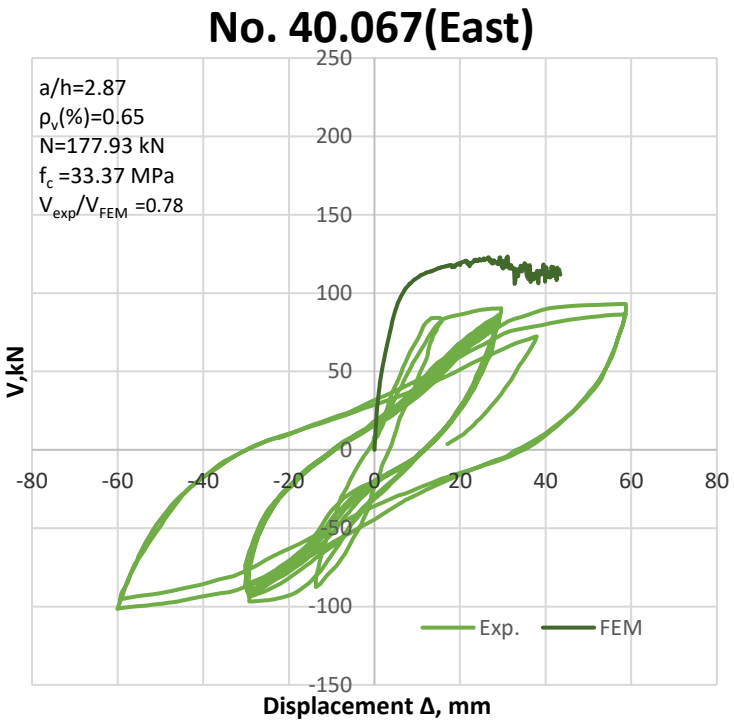
No. 40.067(East)
a/h=2.87
ρv(%)=0.65
N=177.93 kN
fc =33.37 MPa
Vexp/VFEM =0.78
V,kN
Displacement Δ, mm
Exp.
FEM

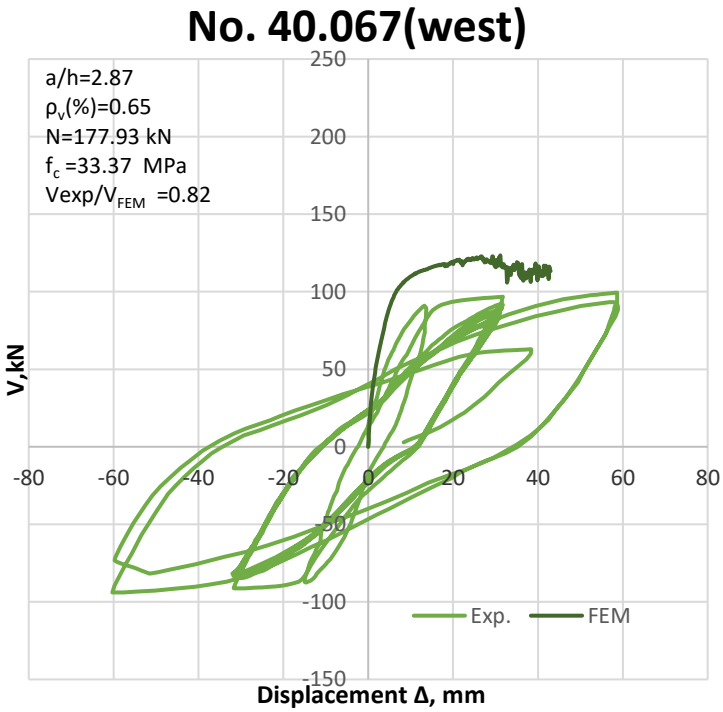
No. 40.067(west)
a/h=2.87
ρv(%)=0.65
N=177.93 kN
fc =33.37 MPa
Vexp/VFEM =0.82
V,kN
Displacement Δ, mm
Exp.
FEM

No. 00.067(East)

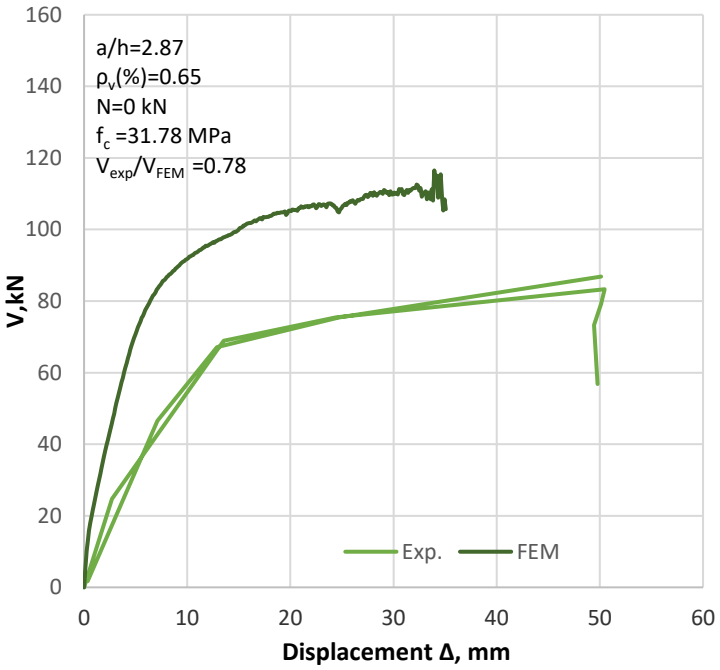

No. 00.067(west)

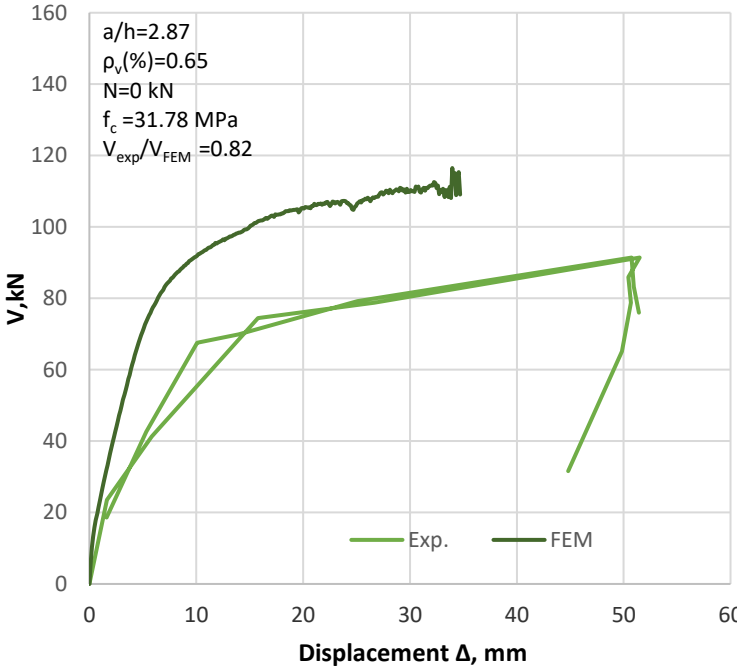

No. 40.092(East)

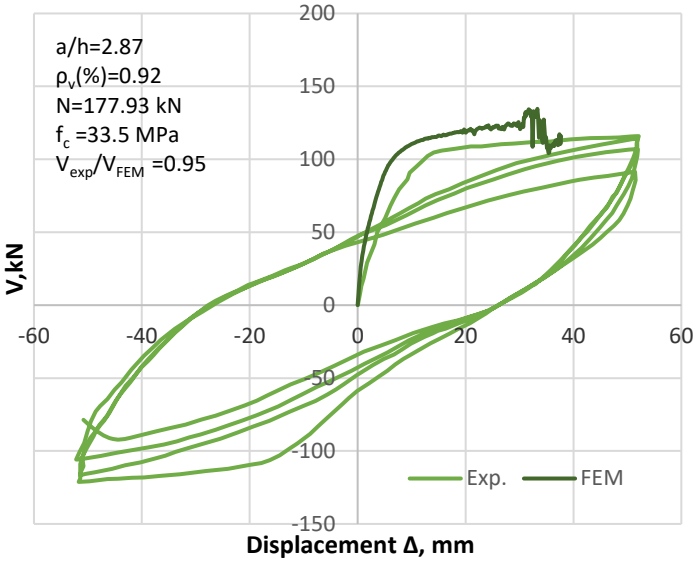

No. 40.092(west)

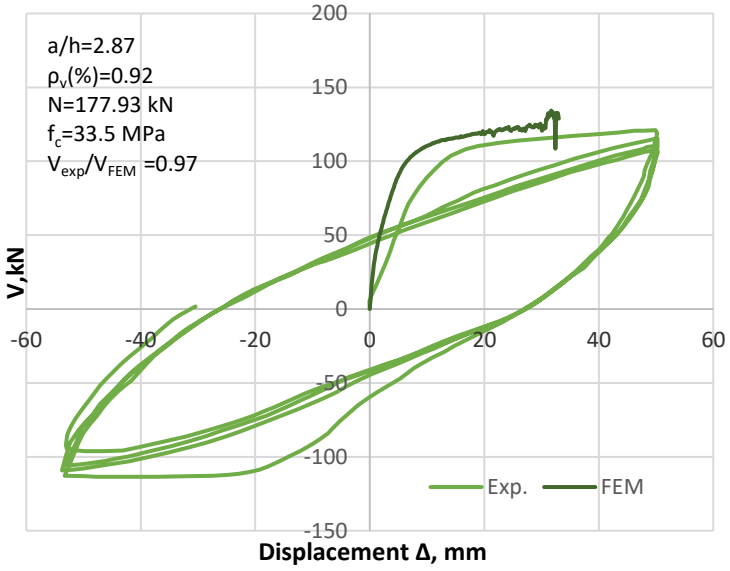

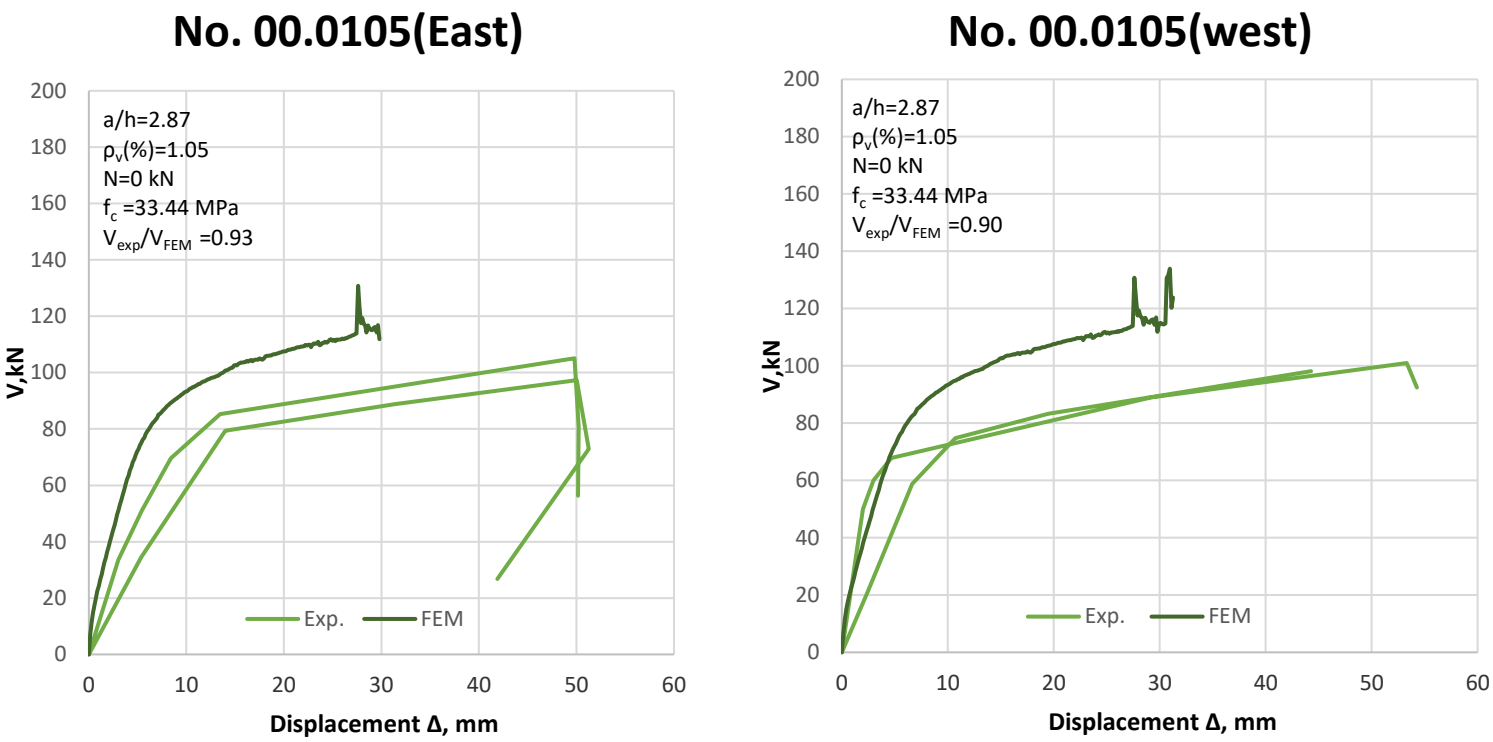

Figure 3.15 Comparison of VecTor2 predicted and measured load-deformation response of Wight and Sozen series

Failure modes

The inclined cracks formations and the failure mechanism of the experimental specimens were successfully matching with the analytical results of VecTor2. The shear transferred across the inclined crack which captured as well by the program. Beyond the crushing deflection, the stirrups carried more amount of shear due to the decrease of the shear capacity of compressed concrete and reducing the dowel forces by the formation of the splitting cracks along the tension reinforcement. While only the core resists the shear after one complete cycle during the reversal loads. High rate of deterioration of the concrete within the core due the displacement along the cracks. As it is reported experimentally, a stage of the test program was reached where the core concrete could not resist either by aggregate interlock or by providing a full capacity of the stirrups. Figure 3.16 compares the experimental and analytical failures for some specimens. Generally, it was observed that the crack pattern started by short vertical cracks near the central joint area, then inclined cracks extended more as the deflection and load increased, then the longitudinal cracks with splitting cracks along the tension reinforcement

were formed as the same as the analytical results. Figure 3.16 shows some specimens failure mechanism compared to the program prediction.

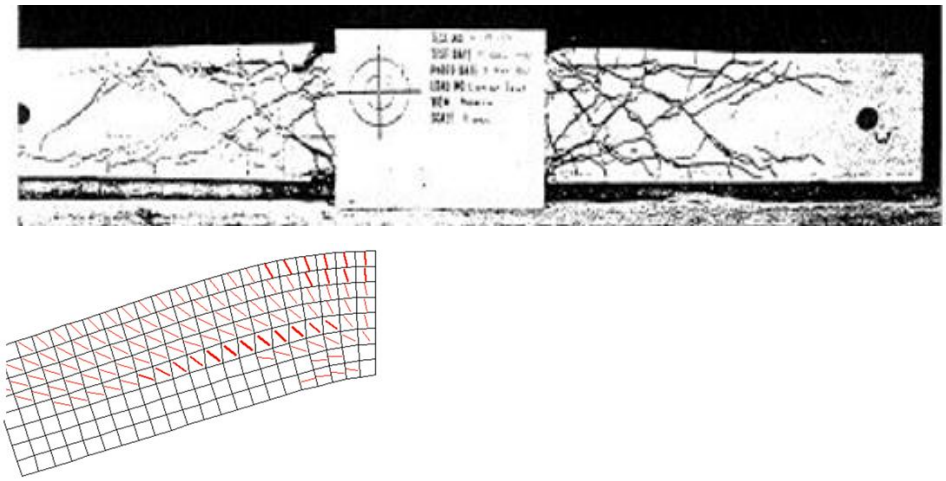

Specimen 40.033 failure

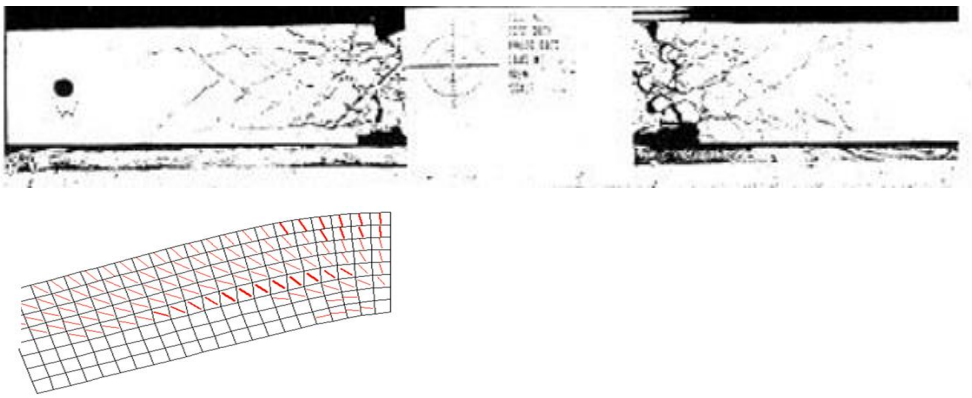

Specimen 40.067 failure

Figure 3.16 Comparison of the cracks formation obtained experimentally and analytically of some specimens (Wight and Sozen,1973)

3.7 SUMMARY OF FEM RESULTS

The VecTor2 analysis of the short columns specimens that have been described in the previous sections simulated reasonably well the load -deformation responses. The predicted peak shear values of all specimens were compared to the experimental values (Table 3.1). The mean value of the

measured to the observed shear forces ratio had a value of 0.866 and a coefficient of variation of 7.59%. Hence, the VecTor2 analysis was satisfactory to the measured analysis in terms of load-displacement response, the crack deformation and failure modes.

Table 3.1 Comparison of peak shear forces of all the specimens with FEM prediction

Test ID	a (mm)	b (mm)	h(mm)	a/h	ρ_l(%)	ρ_v (%)	f_c(MPa)	N/bhf$_c$	V_{exp}(kN)	V_{FEM}(kN)	V_{exp}/V_{FEM}
SC1	1220	915	457	2.67	1.878	0.1691	34.7	0	622	644	0.966
SC3	1220	915	457	2.67	1.878	0.1057	21.9	0	459	494	0.929
SC4	1220	915	457	2.67	1.878	0.1691	21.9	0	555	600	0.925
SC9	1220	457	915	1.333	1.878	0.085	16.5	0	675	728	0.927
No. 5	1650	550	550	3	1.246	0.748	32	0.1	383	465	0.824
No. 6	1650	550	550	3	1.246	0.748	32	0.1	410	472	0.869
No. 40.033a(East)	876	152	305	2.87	2.45	0.323	34.7	0.12	100	114	0.877
No. 40.033a(west)	876	152	305	2.87	2.45	0.323	34.7	0.12	100	114	0.877
No. 40.048(East)	876	152	305	2.87	2.45	0.461	26.1	0.15	102	113	0.903
No. 40.048(west)	876	152	305	2.87	2.45	0.461	26.1	0.15	100	113	0.885
No. 00.048(East)	876	152	305	2.87	2.45	0.461	25.9	0	85	114	0.746
No. 00.048(west)	876	152	305	2.87	2.45	0.461	25.9	0	85	112	0.759
No. 40.033(East)	876	152	305	2.87	2.45	0.323	33.6	0.11	95	112	0.848
No. 40.033(west)	876	152	305	2.87	2.45	0.323	33.6	0.11	103	113	0.912
No. 25.033(East)	876	152	305	2.87	2.45	0.323	33.6	0.07	90	108	0.833
No. 25.033(west)	876	152	305	2.87	2.45	0.323	33.6	0.07	95	105	0.905
No. 00.033(East)	876	152	305	2.87	2.45	0.323	32	0	82	103	0.796
No. 00.033(west)	876	152	305	2.87	2.45	0.323	32	0	82	103	0.796
No. 40.067(East)	876	152	305	2.87	2.45	0.646	33.4	0.12	95	122	0.779
No. 40.067(west)	876	152	305	2.87	2.45	0.646	33.4	0.12	100	122	0.82
No. 00.067(East)	876	152	305	2.87	2.45	0.646	31.8	0	87	112	0.777
No. 00.067(west)	876	152	305	2.87	2.45	0.646	31.8	0	92	112	0.821
No. 40.092(East)	876	152	305	2.87	2.45	0.918	33.5	0.11	116	122	0.951
No. 40.092(west)	876	152	305	2.87	2.45	0.918	33.5	0.11	118	122	0.967
No. 00.0105(East)	876	152	305	2.87	2.45	1.049	33.4	0	105	113	0.929
No. 00.0105(west)	876	152	305	2.87	2.45	1.049	33.4	0	102	113	0.903
										Average =	0.866
										SD =	0.0658
										COV =	7.59

4 KINEMATICS BASED MODELLING OF SHORT COLUMNS

4.1 INTRODUCTION

The column specimens that have been discussed previously, will here be modeled with a kinematic based approach. Short reinforced concrete columns behavior is very challenging to be predicted as it does not obey the classical plane-sections-remain-plane assumption and therefore cannot be modeled based on the beam theory. A three-parameter kinematic theory with modifications was introduced in this project to predict the behaviour of short columns. The idea was developed initially from measured deformed shapes of deep beams (Mihaylovet al. 2010). Then, it was extended to cover the wall structures, this theory is based on the idea that the deformation pattern of a cantilever member can be presented by a kinematic model with three DOFs as it is shown in Figure 4.1 (wall VK3, Bimschas 2010). The first DOF of the model is the average tensile strain in the flexural reinforcement ($\varepsilon_{t,avg}$) within the cracked zone [Figure 4.2(a)]. The second DOF of the kinematic model is the horizontal displacement Δ_c in the critical loading zone (CLZ) [Figure 4.2(b)]. Both Degrees of freedom $\varepsilon_{t,avg}$ and Δ_c are originated from the 2PKT for deep beams, while the downward displacement Δ_{cx} in the CLZ [Figure 4.2(c)] is introduced for the modelling of the walls. Δ_{cx} is related with rotation of the rigid block above the critical crack about point B. This project will use a modified 3PKT theory to model short columns (the code is attached in the appendix). The latter version of 3PKT was applied with neglecting both the web longitudinal reinforcement ratio and cross-sectional area of the ties in the edge zones perpendicular to the member plane (A_{st} in existing wall code) to simplify the modelling and to accurately predict the behaviour of the member.

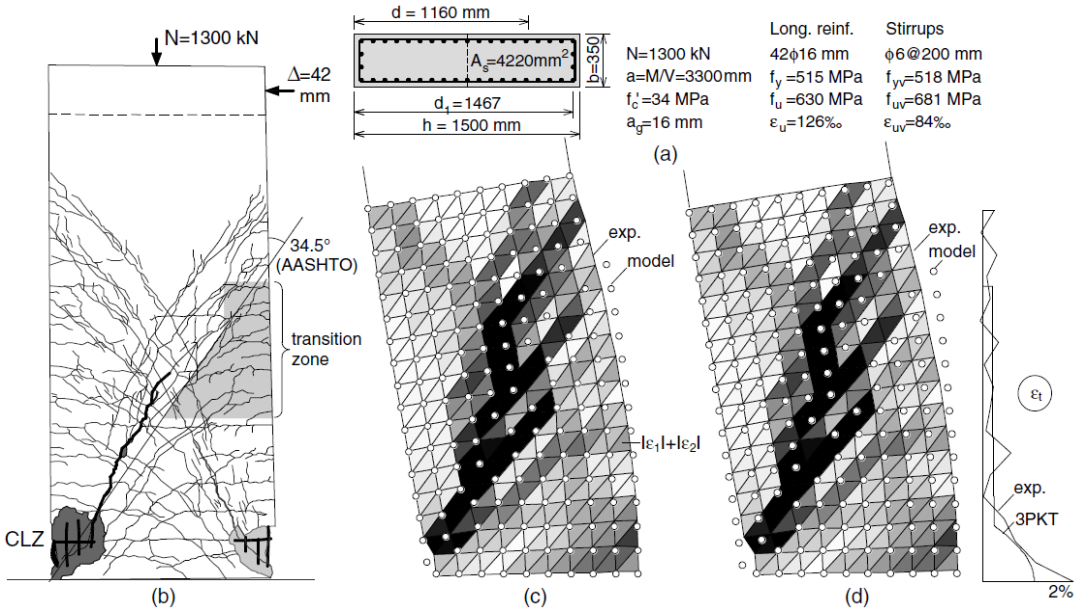

Figure 4.1 Deformation patterns in shear-dominated walls—specimen VK3 (Bimschas 2010): ((a) wall properties; (b) crack pattern at failure; (c) deformations at failure ×15 and 3PK model with fitted DOFs; (d) deformations at failure and 3PK model with predicted DOFs) (Mihaylov et al. 2016)

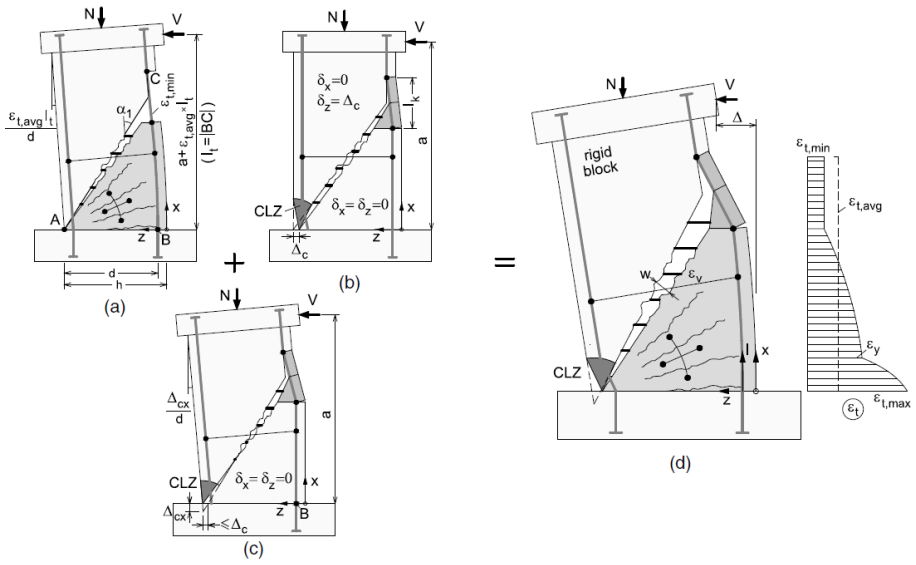

Figure 4.2 Three-parameter kinematic model for shear-dominated walls: (a) DOF $\varepsilon_{t,avg}$, $\Delta_c = \Delta_{cx} = 0$; (b) DOF Δ_c, $\varepsilon_{t,avg} = \Delta_{cx} = 0$; (c) DOF Δ_{cx}, $\Delta_c = \varepsilon_{t,avg} = 0$; (d) combined deformed shape (Mihaylov et al. 2016)

4.2 THREE PARAMETER KINEMATIC THEORY FOR SHEAR DOMINATED WALLS

The 3PKT approach describes the displacements in the diagonal crack of the deformed cantilever wall with aspect ratio equal or smaller than 3 by only three DOFs (Mihaylov et al. 2016). Initially, the theory was limited only to describe deep beams using two DOFs (Mihaylov et al. 2013). The kinematic model describes the deformed shape of the member with linking local and global deformations to address the performance limits during the assessment of existing structures. It is assumed in the model that the critical crack started in the inner edge of the support and then it extends to the far edge of the tributary area where the shear force is applied. The kinematic conditions are combined with equilibrium equations and constitutive relationships to predict the DOFs. The three DOFs are $\varepsilon_{t,avg}$, Δ_c and Δ_{cx} (Figure 4.2) ,where $\varepsilon_{t,avg}$ is the average tensile strain in the flexural reinforcement, Δ_c is the horizontal displacement in the critical zone, and Δ_{cx} is the displacement in the downward direction in the the CLZ .As it was shown elsewhere (Mihaylov et al. 2013), the displacement of the points in the rigid block of the wall in x-z coordinate can be computed by the following equations:

$$\delta_x(x,z) = \frac{\varepsilon_{t,avg} l_t}{d}(h - z) + \frac{\Delta_{cx}}{d}(h - d - z) \quad (1)$$

$$\delta_z(x,z) = \left(\frac{\varepsilon_{t,avg} l_t}{d} + \frac{\Delta_{cx}}{d}\right) x + \Delta_c \quad (2)$$

while the fan displacements are given as below:

$$\delta_x(x,z) = \varepsilon_{t,\mathrm{avg}} x \quad (3)$$

$$\delta_z(x,z) = \frac{\varepsilon_{t,\mathrm{avg}}\, x^2}{h - z} \quad (4)$$

It can be seen that the displacements in the fan depend on $\varepsilon_{t,avg}$ causing the rotation of the radial struts about A. As it can be seen in Figure. 4.2, Δ_{cx} is associated both the rotation of the rigid block about point B with an angle Δ_{cx}/d and the axial load N which pushes the rigid block downwards. The

horizontal displacement Δ_c is associated with the shear deformation while $\varepsilon_{t,avg}$ is based on the rotation of the rigid block about point A with $\varepsilon_{t,avg}$ l_t/d angle and the deformation in the concrete fan. The diagonal shear crack is represented by a straight line with an angle of α_1 with respect to the vertical axis. Figure 4.3 shows the spring model in shear walls where the rigid block is located above the critical diagonal crack while the fan is below the diagonal crack. The free body diagram of the rigid block is shown in Figure 4.3(a). The rigid block is connected to the foundation through forces at CLZ and the fan through forces across the diagonal crack. The load bearing mechanisms are modeled as nonlinear springs representing the aggregate interlock force F_{ci}, the tension in the stirrups F_s, the tension in the flexural reinforcement $F_{t,min}$, and the force due to dowel action of the flexural reinforcement F_d . On the other hand, Figure 4.3(b) shows the forces that are applied to the fan which are F_{ci}, F_s, F_d, *and* $F_{t,min}$ across the critical diagonal crack . These forces are balanced by forces F_b and $F_{t,max}$ at the base section of the wall.

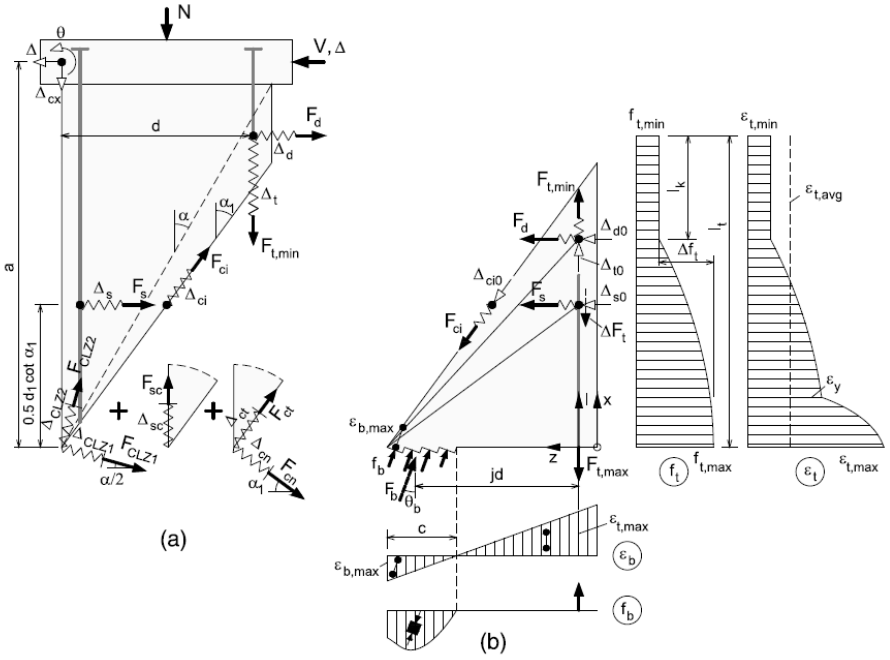

Figure 4.3 Spring model a) rigid block region b) fan region (Mihaylovet al. 2016)

The theory assumes the failure of the member to occur along a single dominant diagonal crack. It should be known that the model has applicability limits which are: cantilever wall with major shear cracks, axial load ratio N/bh$f_c^{'}$ ≤0.2, shar span to depth ratio ≤ 3.0, wall height to thickness ratio ≤ 25, normal strength concrete and no diagonal reinforcement. The 3PKT showed excellent predictions for shear walls when validated using a database of 34 rectangular cross-sections walls with a shear-span-to-depth ratio between 0.33 and 3 (Mihaylov et al. 2016). The ratios of experimental-to-predicted

results for the peak loads had a mean value of 1.03 and a COV of 11.6%, while the ratios for the drift capacity had an average of 0.99 and a COV of 16.4%.

4.3 TEST SERIES BY ABOUTAHA (1994)

In this section, the predicted responses of the specimens using VecTor2 and 3PKT with the measured responses will be discussed. Figure 4.4 shows the load -drift ratio responses of the test series by Aboutaha. The vertical axis is representing the shear force V (kN) while the drift ration $\Delta=(\delta/a)$ % is represented by the horizontal axis. It should be known that these specimens were not subjected to axial forces. The summarized main properties of specimens are mentioned as well on the plots.

It can be seen from Figure. 4.4 that the 3PKT approach captured successfully the responses of the specimens. Moreover, the prediction of 3PKT was more accurate than the VecTor2 prediction. This is because the shear strength and the stiffness results captured by the 3PKT were almost the same as the experimental results. Since the 3PKT modeled the bottom part of the wall with a series of rigid radial struts to account for yielding of the reinforcement, the predicted stiffness by 3PKT was almost the same as the experimental results. In addition, Figure 4.4 clearly shows that the pre-peak and the post-peak were reasonably well predicted by the 3PKT.

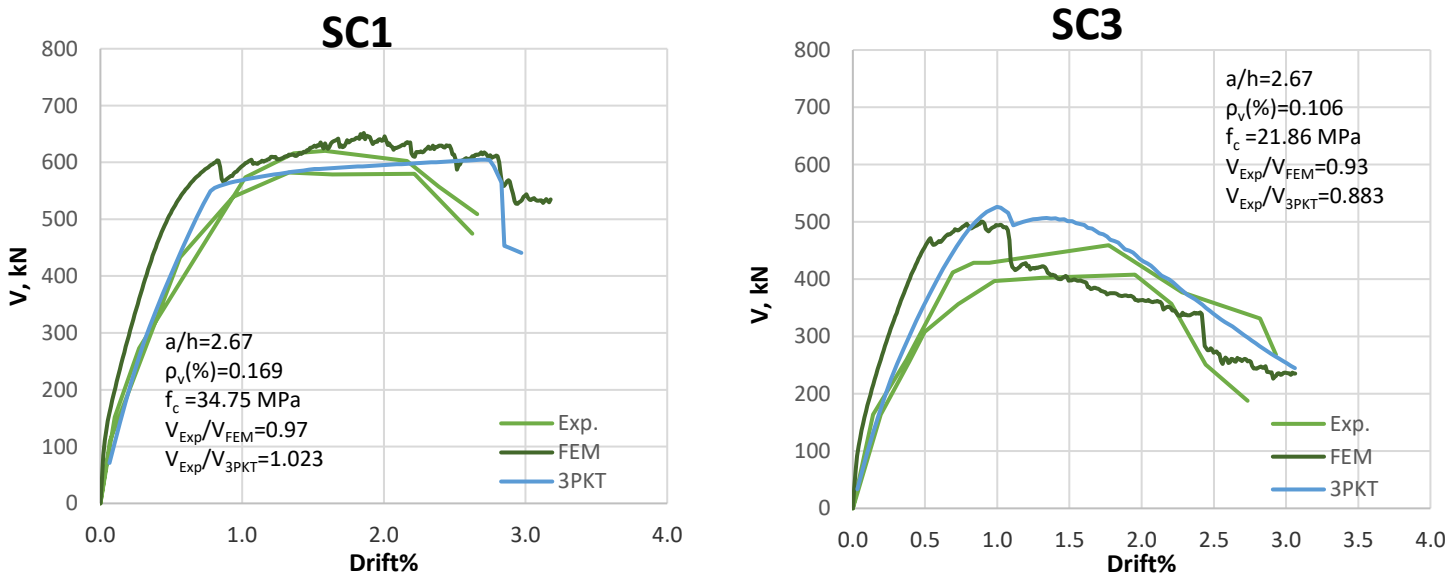

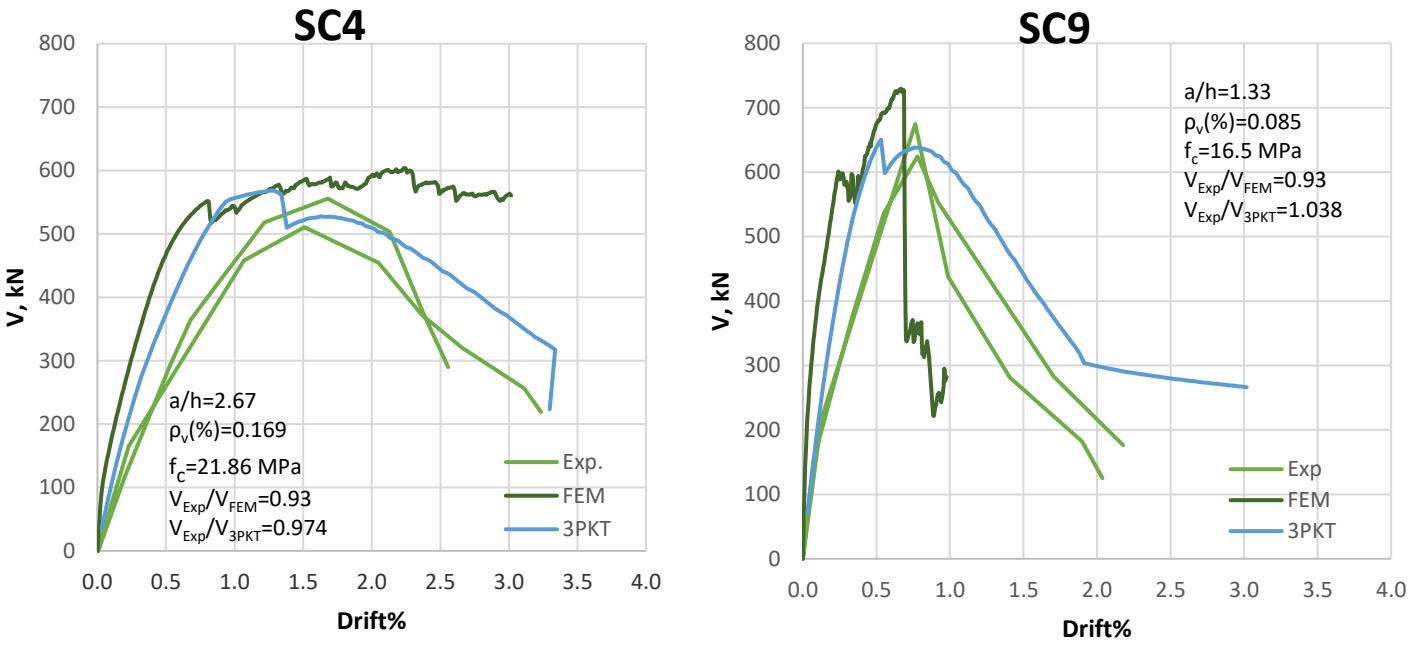

Figure 4.4 Comparison of predicted and measured load-deformation response of Aboutaha series

Figure 4.5 depicts the effect of concrete strength on peak shear force predictions. Generally, the graph shows that for increasing concrete strength the shear strength of a member increases. Similarly, a strong agreement between the peak shear load predictions by 3PKT and FEM methods with the experimental results was clearly shown in Figure 4.5.

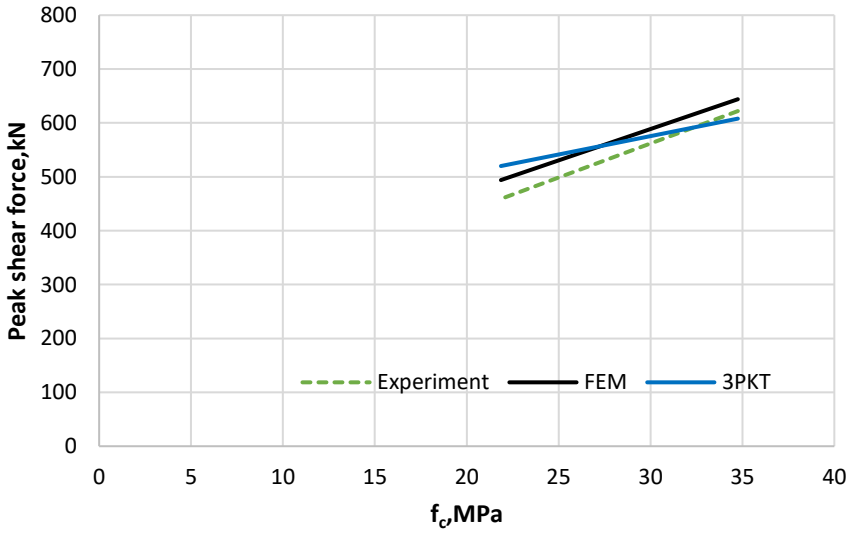

Figure 4.5 Effect of concrete strength on peak shear force predictions (Aboutaha series)

It can be concluded from Figure 4.6 that the shear strength decreases gradually with increasing the shear-span-to-depth ratio, where for the deepest member the shear resistance has the highest value. For the highest a/h ratio the shear strength of the column shows to be the lowest. The 3PKT approach predicted the peak shear force in a better way than FEM as its trend is much closer to the experimental results (Figure 4.6).

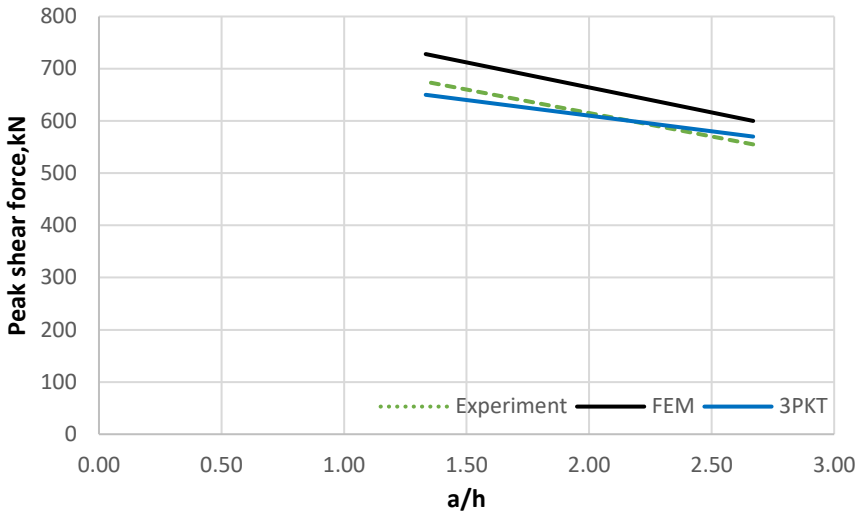

Figure 4.6 Effect of a/h on peak shear force predictions (Aboutaha series)

4.4 TEST SERIES BY TANAKA AND PARK (1990)

Comparison of predicted and measured load-deformation response of Tanaka and Park series is shown in Figure 4.7. As it can be seen that 3PKT reasonably predicted the shear load hysteretic responses of the specimens. The post-peak behaviour was successfully captured by VecTor2 unlike 3PKT prediction. As a matter of fact, the specimens experienced a serious buckling of compression reinforcement with rupture of reinforcements which need a complex model to predict that failure by 3PKT. Both VecTor2 and 3PKT predicted the stiffness to be more than the measured one due to neglecting the block base deformation in the models.

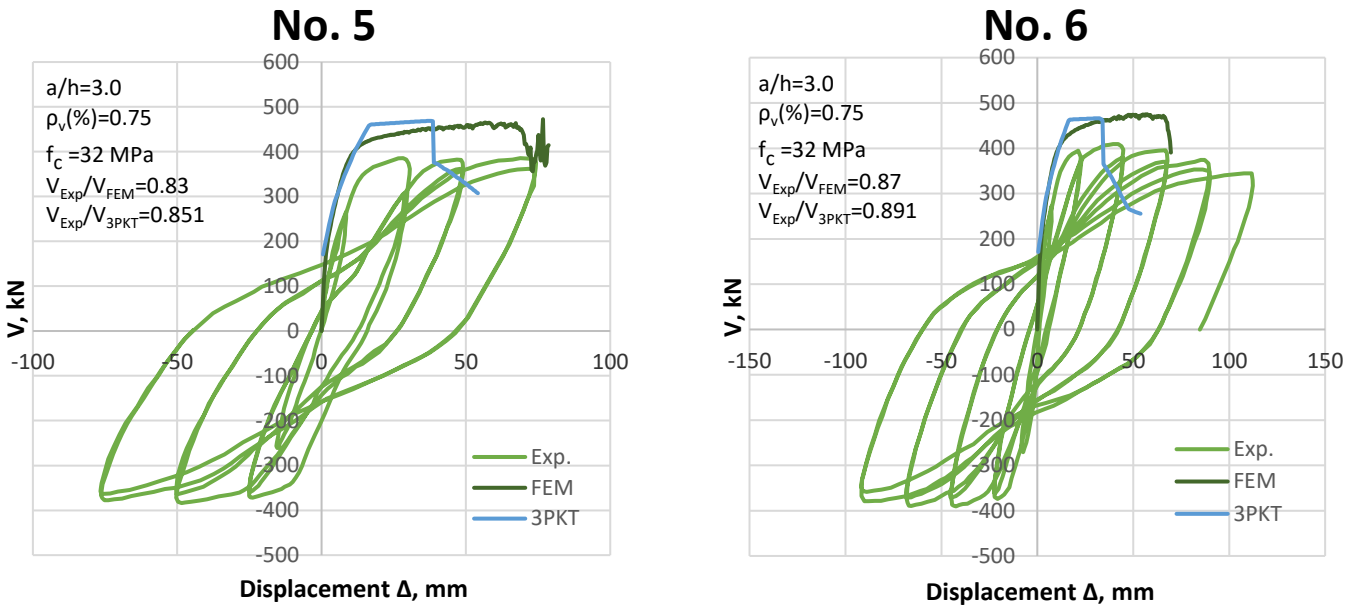

Figure 4.7 Comparison of predicted and measured load-deformation response of Tanaka and Park series

4.5 TEST SERIES BY WIGHT AND SOZEN (1973)

Figure 4.8 shows the comparison of the predicted and the measured load-deformation responses of Wight and Sozen series. The 3PKT reasonably captured the responses of the specimens, however, the experimental stiffness was much lower than the calculated with VecTor2. As shown in Figure 4.8, the VecTor2 predicted the post-peak behaviour of the specimens while the 3PKT could not predict it well. This is due to the fact that the failure of the specimen was due to the crushing of the compression zone and rupture of the reinforcement in the base section. In this case, the 3PKT requires a complex model for such failure mode in order to capture the post-peak behaviour of the specimens.

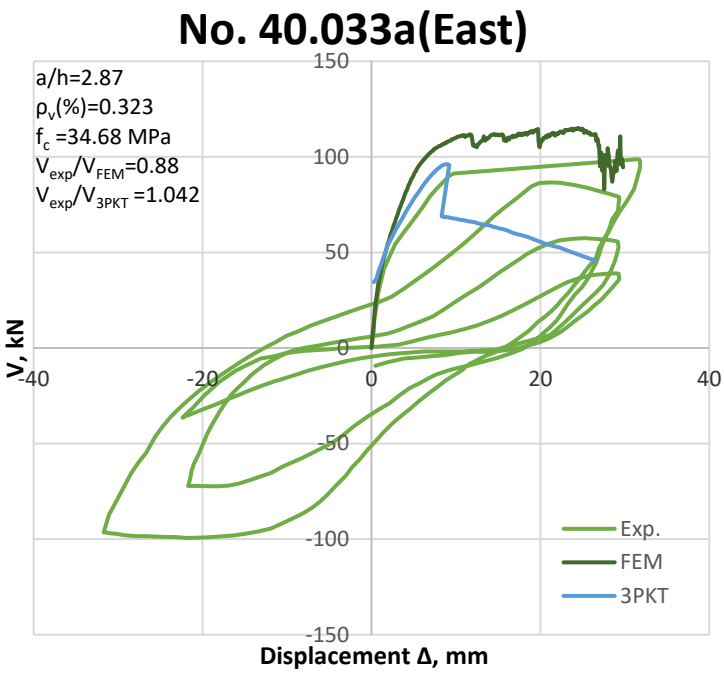
No. 40.033a(East)
a/h=2.87
ρv(%)=0.323
fc =34.68 MPa
Vexp/VFEM=0.88
Vexp/V3PKT =1.042
V, kN
Displacement Δ, mm
Exp.
FEM
3PKT

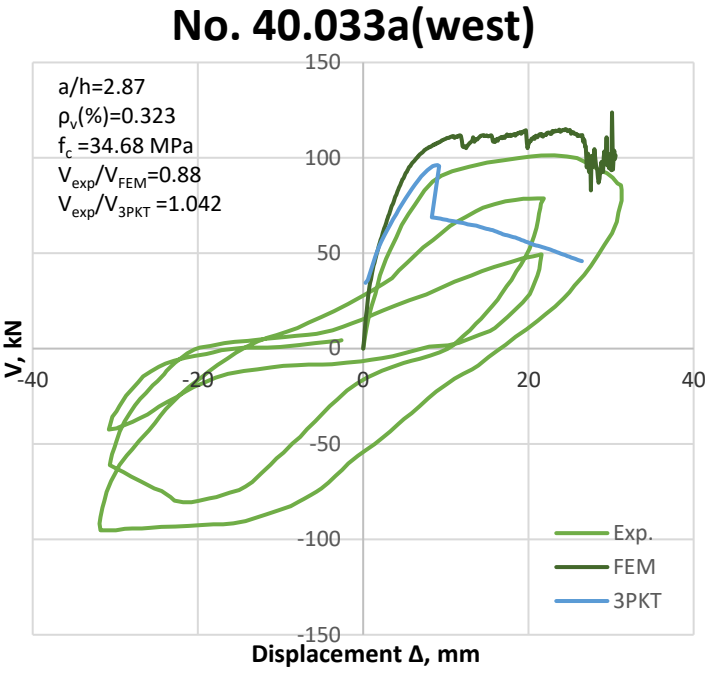
No. 40.033a(west)
a/h=2.87
ρv(%)=0.323
fc =34.68 MPa
Vexp/VFEM=0.88
Vexp/V3PKT =1.042
V, kN
Displacement Δ, mm
Exp.
FEM
3PKT

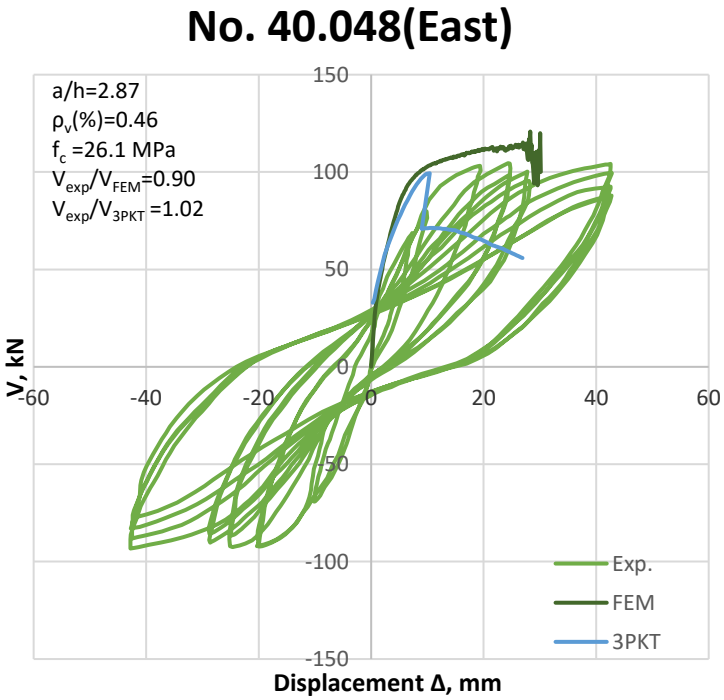
No. 40.048(East)
a/h=2.87
ρv(%)=0.46
fc =26.1 MPa
Vexp/VFEM=0.90
Vexp/V3PKT =1.02
V, kN
Displacement Δ, mm
Exp.
FEM
3PKT

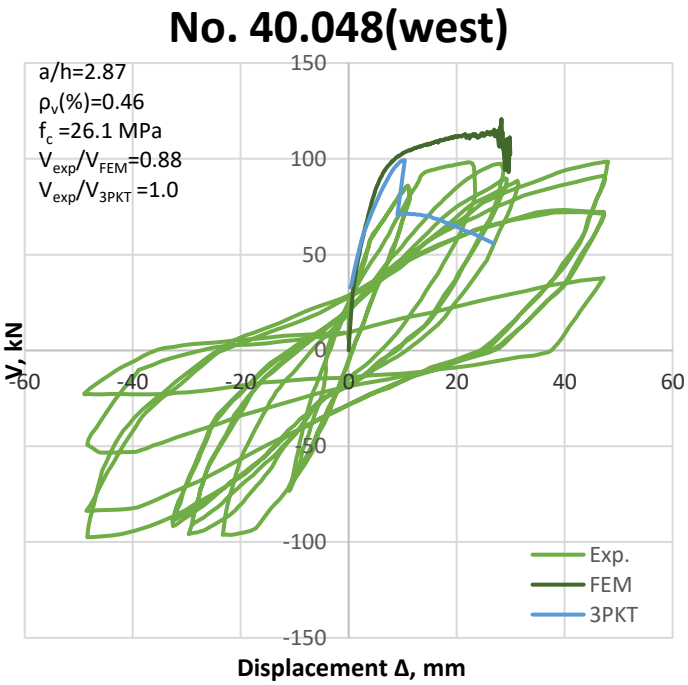
No. 40.048(west)
a/h=2.87
ρv(%)=0.46
fc =26.1 MPa
Vexp/VFEM=0.88
Vexp/V3PKT =1.0
V, kN
Displacement Δ, mm
Exp.
FEM
3PKT

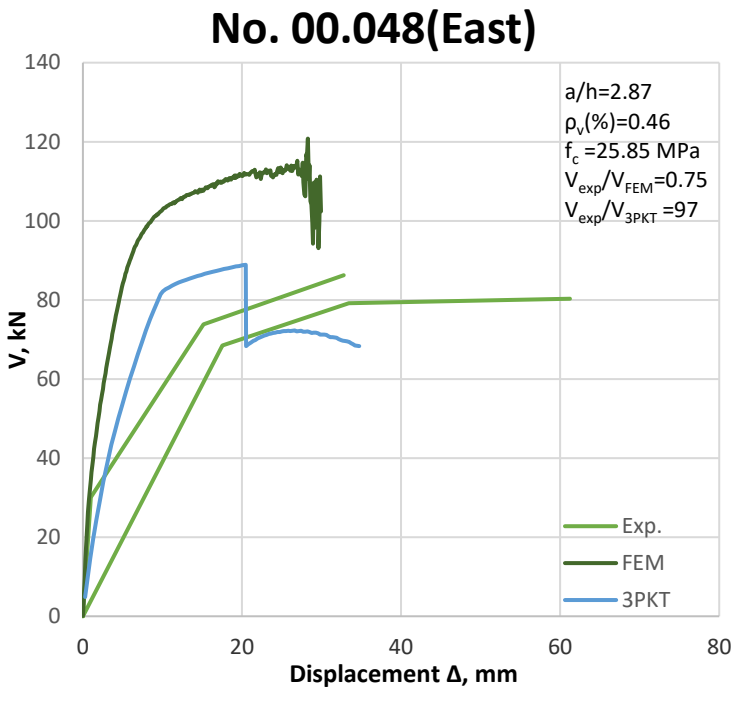
No. 00.048(East)
a/h=2.87
ρv(%)=0.46
fc =25.85 MPa
Vexp/VFEM=0.75
Vexp/V3PKT =97
Exp.
FEM
3PKT
V, kN
Displacement Δ, mm

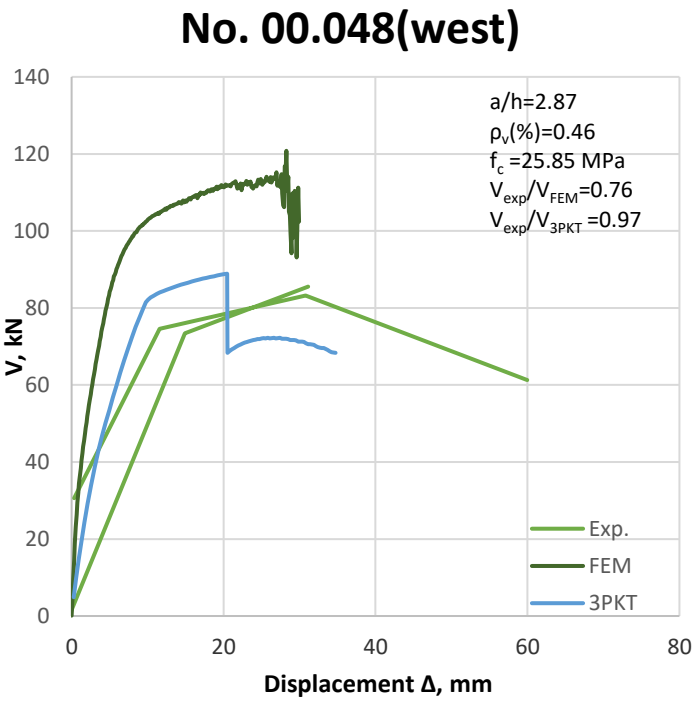
No. 00.048(west)
a/h=2.87
ρv(%)=0.46
fc =25.85 MPa
Vexp/VFEM=0.76
Vexp/V3PKT =0.97
Exp.
FEM
3PKT
V, kN
Displacement Δ, mm

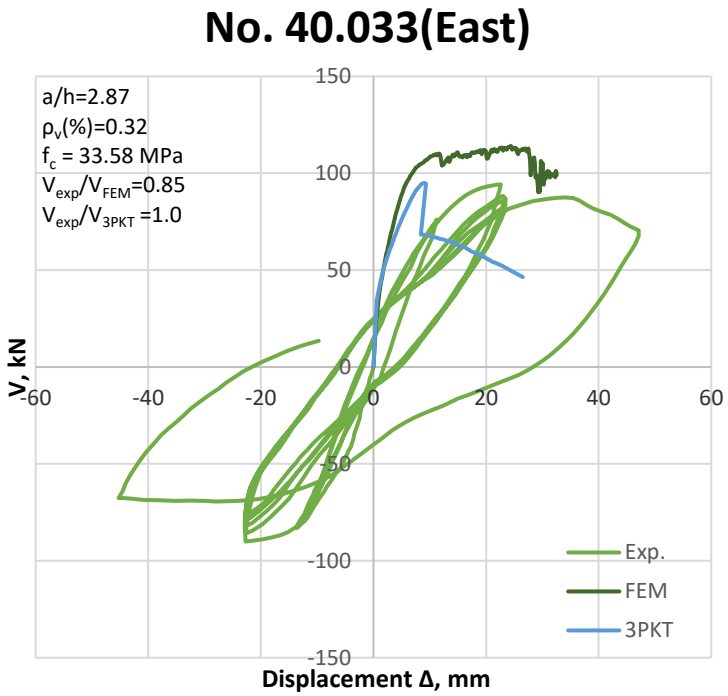
No. 40.033(East)
a/h=2.87
ρv(%)=0.32
fc = 33.58 MPa
Vexp/VFEM=0.85
Vexp/V3PKT =1.0
Exp.
FEM
3PKT
V, kN
Displacement Δ, mm

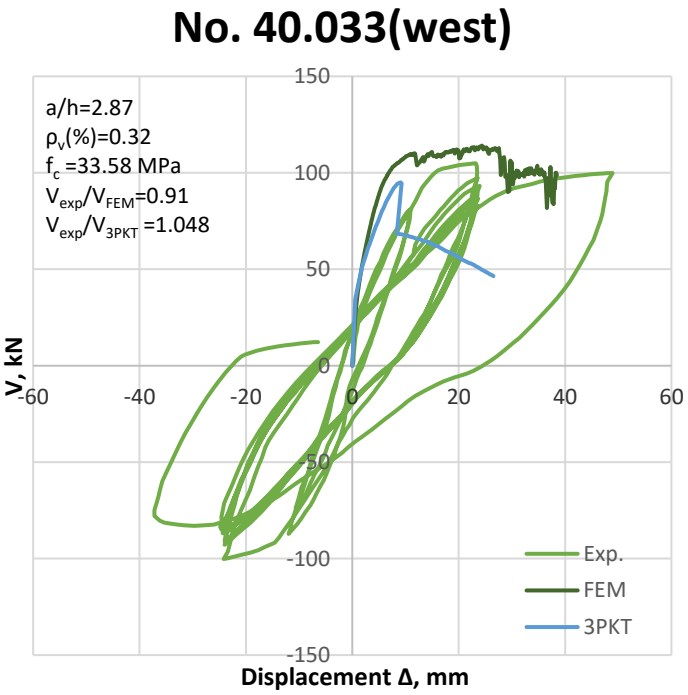
No. 40.033(west)
a/h=2.87
ρv(%)=0.32
fc =33.58 MPa
Vexp/VFEM=0.91
Vexp/V3PKT =1.048
Exp.
FEM
3PKT
V, kN
Displacement Δ, mm

No. 25.033(East)

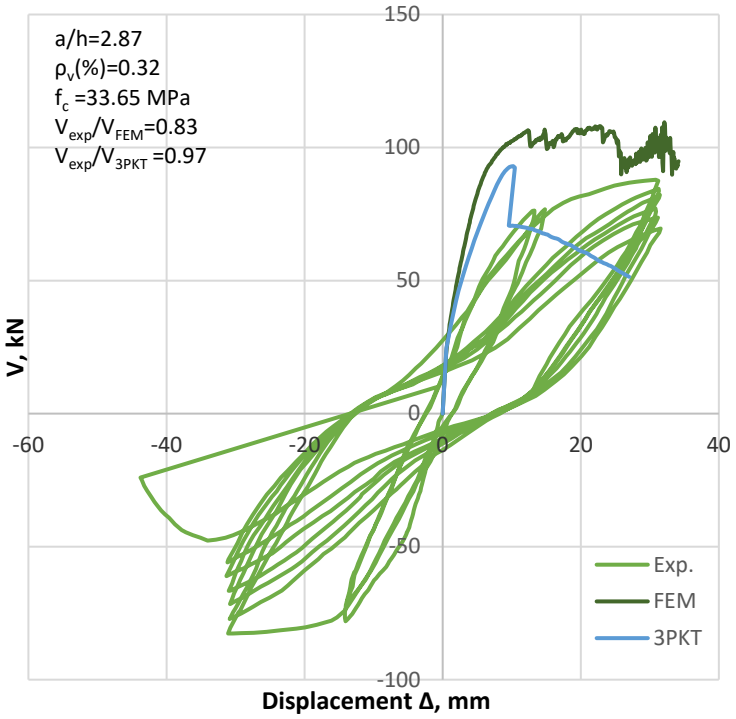

No. 25.033(west)

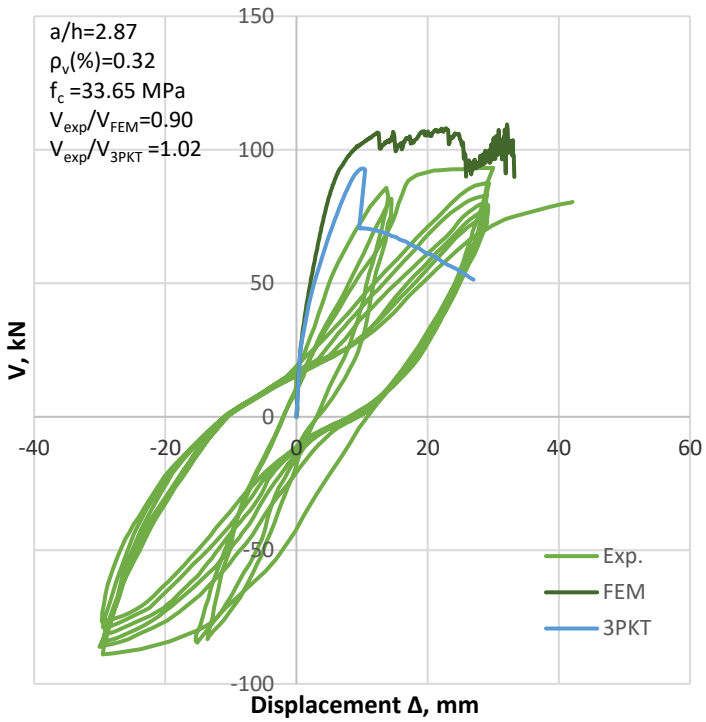

No. 00.033(East)

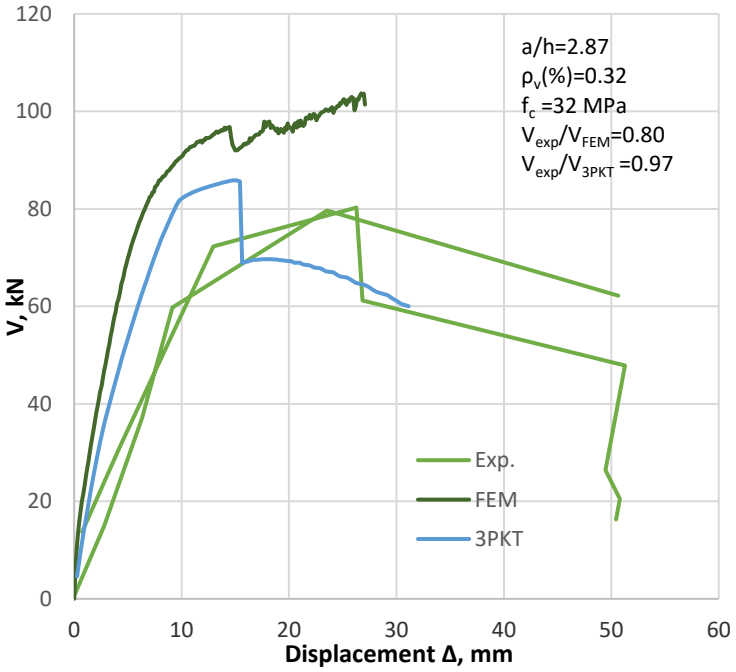

No. 00.033(west)

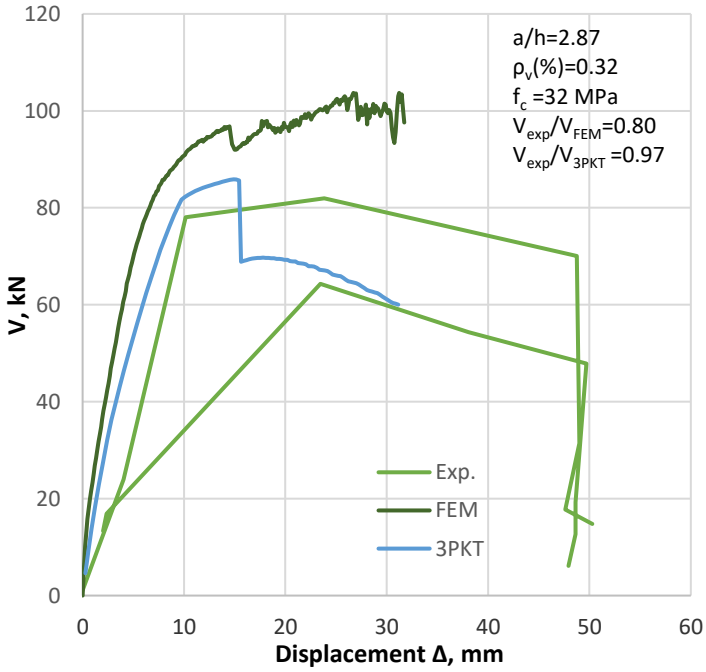

No. 40.067(East)

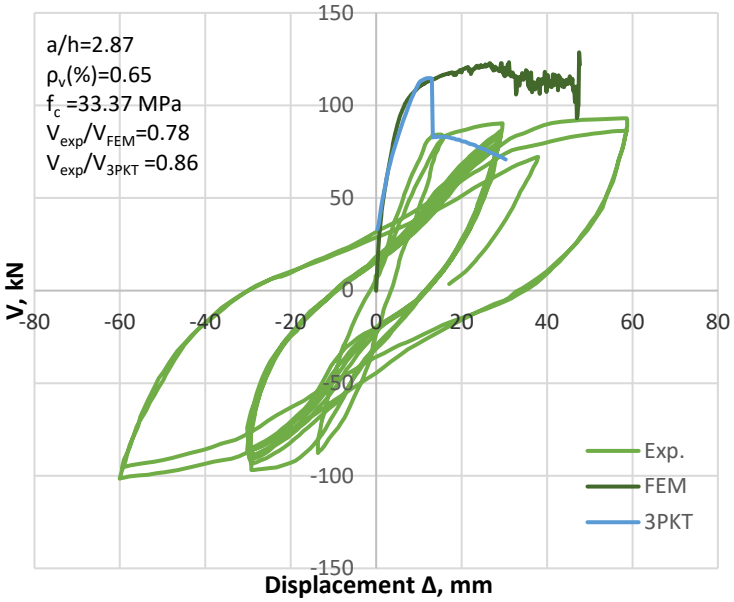

No. 40.067(west)

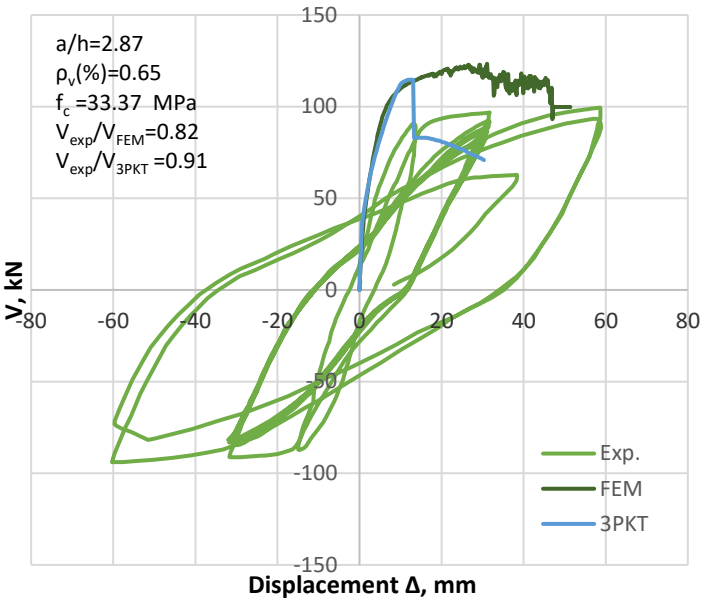

No. 00.067(East)

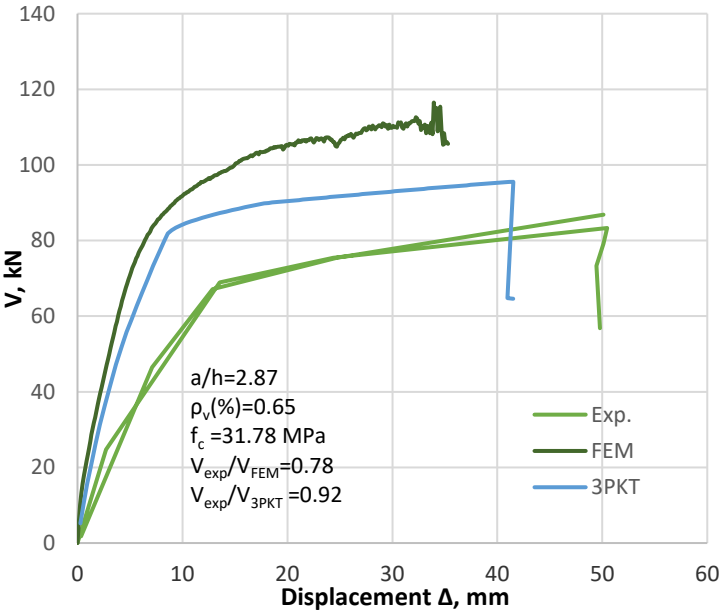

No. 00.067(west)

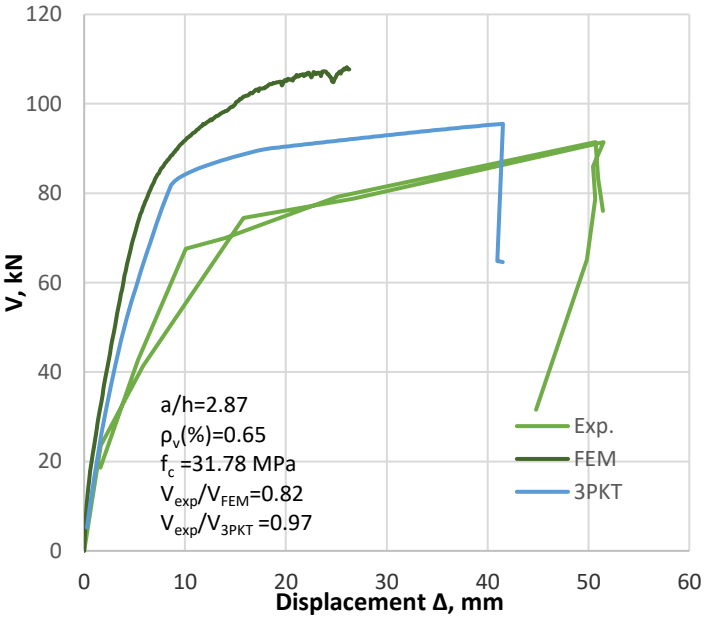

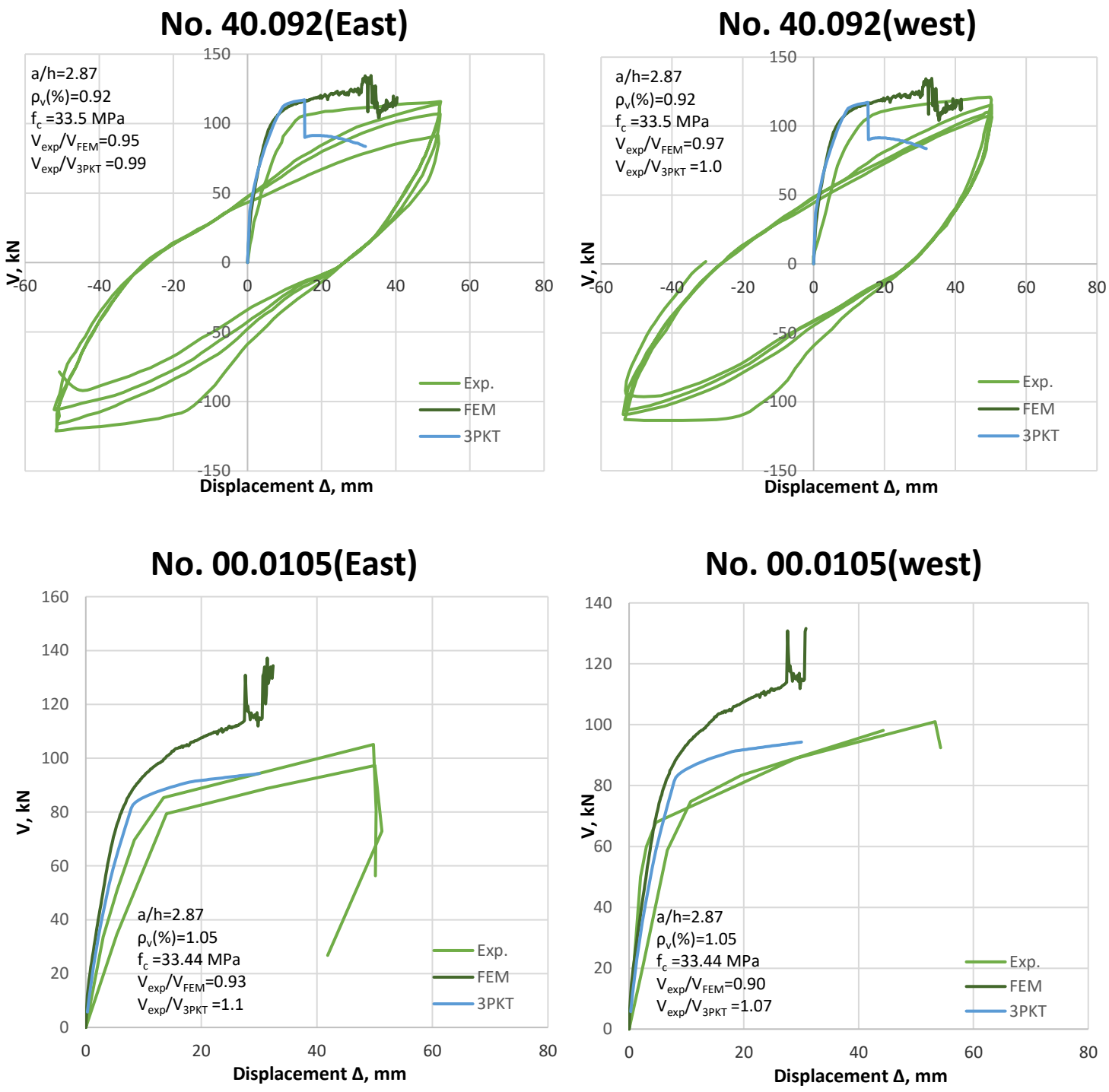

Figure 4.8 Comparison of predicted and measured load-deformation response of Wight and Sozen series

The effect of axial load ratios on the prediction of peak shear forces was evaluated for different transverse reinforcement ratios as Figure 4.9 shows. Horizontal axis describes the values of axial load ratios (N/bhf_C), while the vertical axis represents the peak shear forces. It can be observed that the shear strength increases gradually with increasing axial load ratios. For the highest axial load ratio, the shear strength of the column shows to be the highest as well. The effect of transverse reinforcement ratios on shear strength was investigated in the same figure. The predicted peak shear forces resulted from FEM and 3PKT was compared with the measured ones for different levels of transverse reinforcement ratios as elaborated in Figure 4.9. It can be seen that members with high $\rho_v\%$ resulted in high shear forces. The curves in the level of $\rho_v\% \approx 1.0$ are higher than in the case of $\rho_v\% \approx 0.4$ which shows the significant impact of the transverse reinforcement ratios on the shear forces of the members. Moreover, in comparison with the experimental results, FEM approach shows a higher gap compared to the 3PKT approach. The 3PKT prediction approach for the peak shear force was much closer to the experimental results. As a result, we conclude that the 3PKT approach is more conservative than the FEM approach.

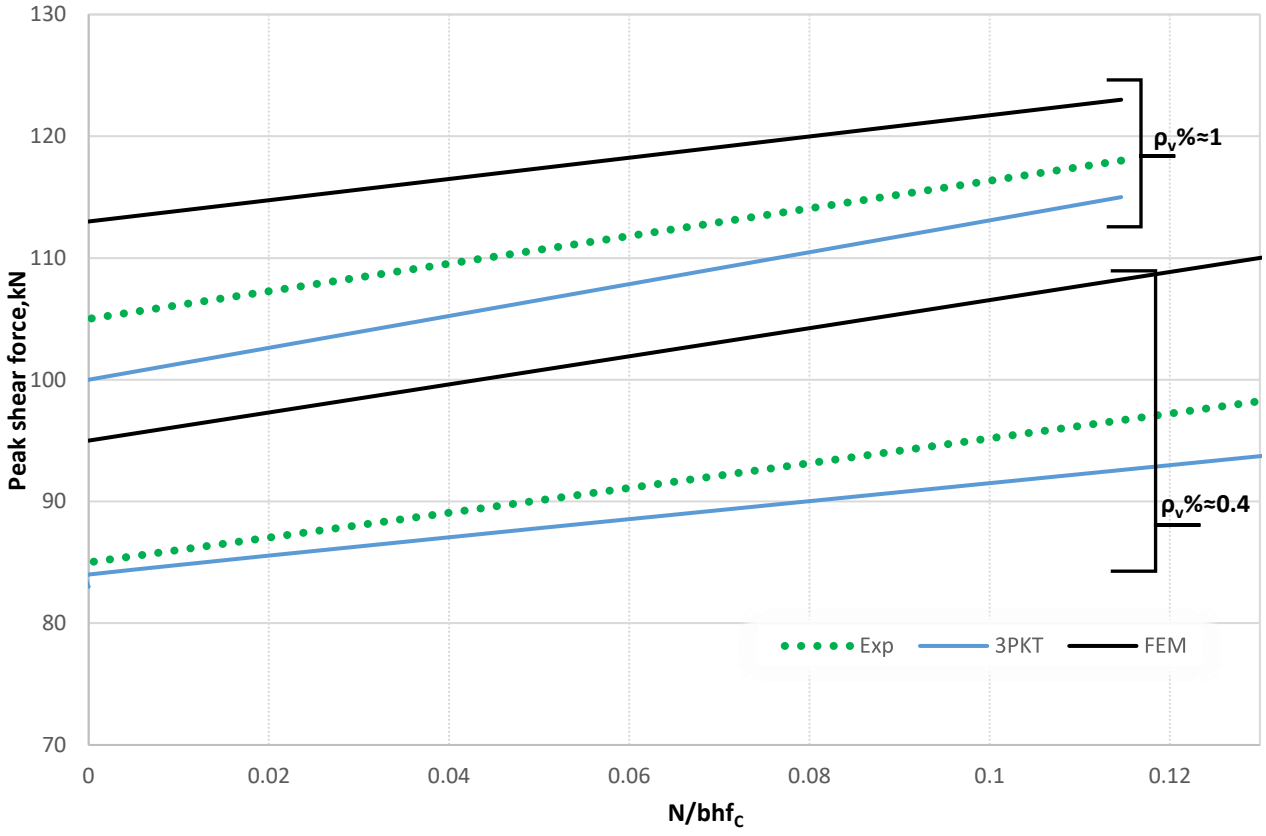

Figure 4.9 Effect of axial load ratios on peak shear force predictions for different transverse reinforcement ratios (Wight and Sozen series)

4.6 SUMMARY OF 3PKT RESULTS

Table 4.1 summarises the main properties of the short column specimens including the comparison of predicted to observed peak shear forces. The mean value of the measured to 3PKT predicted peak shear forces ratio (V_{exp}/V_{3PKT}) was 0.982 with a standard deviation of 0.0666 and a coefficient of variation of 6.78 %. On the other hand, the experimental to predicted peak shear forces using FEM had a mean of 0.866, standard deviation of 0.0658 and a coefficient of variation of 7.59%. It can be said that both modelling tools gave almost the same prediction of the peak shear forces as they have almost the same coefficient of variation. However, FEM is non-conservative compared to 3PKT approach because the 3PKT approach has a better average than FEM.

Table 4.1 Comparison of peak shear forces of all the specimens with 3PKT prediction

Test ID	a (mm)	b (mm)	h(mm)	a/h	ρ_l (%)	ρ_v(%)	f_c(MPa)	N/bhf$_c$	V_{exp}(kN)	V_{3PKT} (kN)	V_{FEM}(kN)	V_{exp}/V_{3PKT}	V_{exp}/V_{FEM}
SC1	1220	915	457	2.67	1.878	0.1691	34.75	0.00	622	608	644	1.023	0.966
SC3	1220	915	457	2.67	1.878	0.1057	21.86	0.00	459	520	494	0.883	0.929
SC4	1220	915	457	2.67	1.878	0.1691	21.86	0.00	555	570	600	0.974	0.925
SC9	1220	457	915	1.333	1.878	0.085	16.50	0.00	675	650	728	1.038	0.927
No. 5	1650	550	550	3.00	1.246	0.748	32.00	0.1000	383	450	465	0.851	0.824
No. 6	1650	550	550	3.00	1.246	0.748	32.00	0.1000	410	460	472	0.891	0.869
No. 40.033a(East)	876	152	305	2.87	2.45	0.323	34.68	0.1176	100	96	114	1.042	0.877
No. 40.033a(west)	876	152	305	2.87	2.45	0.323	34.68	0.1176	100	96	114	1.042	0.877
No. 40.048(East)	876	152	305	2.87	2.45	0.461	26.06	0.1473	102	100	113	1.020	0.903
No. 40.048(west)	876	152	305	2.87	2.45	0.461	26.06	0.1473	100	100	113	1.00	0.885
No. 00.048(East)	876	152	305	2.87	2.45	0.461	25.86	0.00	85	88	114	0.966	0.746
No. 00.048(west)	876	152	305	2.87	2.45	0.461	25.86	0.00	85	88	112	0.966	0.759
No. 40.033(East)	876	152	305	2.87	2.45	0.323	33.58	0.1143	95	95	112	1.00	0.848
No. 40.033(west)	876	152	305	2.87	2.45	0.323	33.58	0.1143	103	95	113	1.084	0.912
No. 25.033(East)	876	152	305	2.87	2.45	0.323	33.65	0.0713	90	93	108	0.968	0.833
No. 25.033(west)	876	152	305	2.87	2.45	0.323	33.65	0.0713	95	93	105	1.022	0.905
No. 00.033(East)	876	152	305	2.87	2.45	0.323	32.00	0.0000	82	85	103	0.965	0.796
No. 00.033(west)	876	152	305	2.87	2.45	0.323	32.00	0.0000	82	85	103	0.965	0.796
No. 40.067(East)	876	152	305	2.87	2.45	0.646	33.37	0.1150	95	110	122	0.864	0.779
No. 40.067(west)	876	152	305	2.87	2.45	0.646	33.37	0.1150	100	110	122	0.909	0.820
No. 00.067(East)	876	152	305	2.87	2.45	0.646	31.78	0.00	87	95	112	0.916	0.777
No. 00.067(west)	876	152	305	2.87	2.45	0.646	31.78	0.00	92.00	95.00	112	0.968	0.821
No. 40.092(East)	876	152	305	2.87	2.45	0.918	33.50	0.1146	116	117	122	0.991	0.951
No. 40.092(west)	876	152	305	2.87	2.45	0.918	33.50	0.1146	118	117	122	1.009	0.967
No. 00.0105(East)	876	152	305	2.87	2.45	1.049	33.44	0.00	105	95	113	1.105	0.929
No. 00.0105(west)	876	152	305	2.87	2.45	1.049	33.44	0.00	102	95	113	1.074	0.903
											Average =	0.982	0.866
											SD =	0.0666	0.0658
											COF =	6.78	7.59

5 CONCLUSIONS

At the first stage, all experimental data on short reinforced concrete columns was collected and placed in a test database. However, the studies by Aboutaha (1994), Tanaka and Park (1990) and Wight and Sozen (1973) were considered in this project as their experimental specimens were within the limitation of the project. A short column is a D-region and predominantly fails in shear pattern which can not be modeled using the beam theory. This thesis introduced an efficient approach for modelling such members, hence the objective of this project was as following:

- To validate the ability of a nonlinear finite element approach (VecTor 2) based on the disturbed stress field model (DSFM) to capture the shear behaviour of short columns and compare it with the experimental results.
- To apply a modified 3PKT to predict the force-deformation behavior of short columns. Knowing that 3PKT was originally developed to predict the behavior of shear-dominated reinforced concrete walls ((Mihaylov et al. 2016).

After modelling the specimens using both the modified 3PKT and VecTor2, it can be concluded that:

- VecTor2 predicted reasonably well the responses of the specimens including their crack deformation and failure modes. As compared with the observed results, the experimental-to-predicted ratios for the peak load had a mean value of 0.866 and a coefficient of variation of 7.59%.
- The 3PKT described well the behavior of the members including a reasonable prediction of the pre-peak and the post- peak responses of the members. The mean value of the measured to 3PKT predicted peak shear force ratios was 0.982 with a coefficient of variation of 6.78 %.

At the end, the 3PKT can achieve better accuracy than non-linear FEM in predicting the shear strength of short columns as the 3PKT approach has a better average than FEM. However, while the FEM uses thousands of DOFs to model a single column, the 3PKT is significantly more efficient because it uses only 3DOFs. Finally, further research is needed to extend the range of applicability of the 3PKT approach.

REFERENCES:

Aboutaha,R.(1994). "Seismic Retrofit of Non-Ductile Reinforced Concrete Columns Using Rectangular Steel Jackets (Thesis)". University of Texas at Austin. 746 pages.

Alqatamin, A., Talpoşi, A. (2009). "The action of short columns at reinforced concrete building constructions". Bulletin of the Transilvania University of Braşov• Vol, 2, 51.

Bimschas, M. (2010). "Displacement-based seismic assessment of existing bridges in regions of moderate seismicity". IBK Rep. 326, Swiss Federal Institute of Technology ETH, Zurich, Switzerland.

Li, Y. A., Huang, Y. T., & Hwang, S. J. (2014). "Seismic response of reinforced concrete short columns failed in shear". *ACI Structural Journal,* 111(4), 945.

Mihaylov, B. I., Bentz, E. C., and Collins, M. P. (2010). "Behavior of large deep beam subjected to monotonic and reversed cyclic shear". *ACI Struct. J.*, 107(6), 726–73.

Mihaylov, B. I., Bentz, E. C., and Collins, M. P. (2013). "Two-parameter kinematic theory for shear behavior of deep beams". *ACI Struct. J.*,110(3), 447–456.

Mihaylov, B. I., Hannewald, P., and Beyer, K. (2015). "Three-parameter kinematic theory for shear-dominated reinforced concrete walls: Implementation". Zenodo, Geneva, Switzerland.

Mihaylov, B. I., Hannewald, P., & Beyer, K. (2016). "Three-parameter kinematic theory for shear-dominated reinforced concrete walls". *Journal of Structural Engineering*, 142(7), 04016041.

Nilson, A., Darwin,D.Dolan,C. (1997). "Design of concrete structures". (No. 12th Edition). McGraw-Hill.

Saatcioglu, M.,Ozcebe, G.(1989). "Response of reinforced concrete columns to simulated seismic loading". *Structural Journal*, 86(1), 3-12.

Schlaich, J., Schäfer, K., & Jennewein, M. (1987). "Toward a consistent design of structural concrete". *PCI journal*, 32(3), 74-150.

Tanaka, H., Park, R.,(1990). "Effect of Lateral Confining Reinforcement on the Ductile Behaviour of Reinforced Concrete Columns". Department of Civil Engineering, University of Canterbury. Report 90-2, 458 pages.

Vecchio, F.J., (2000). "Disturbed Stress Field Model for Reinforced Concrete: Formulation".*ASCE Journal of Structural Engineering,* Vol. 126, No. 9, pp. 1070-1077.

Wight, J. K., Sozen, M. A. (1973). "Shear strength decay in reinforced concrete columns subjected to large deflection reversals". University of Illinois Engineering Experiment Station. College of Engineering. University of Illinois at Urbana-Champaign.

Wong, P. S., Vecchio, F. J., Trommels, H. (2013). "VecTor2 and FormWorks User's Manual". 2nd edition.

Wong, P.S., and Vecchio, F.J. (2002). "VecTor2 and FormWorks User's Manual".Technical Report, Department of Civil Engineering, University of Toronto, 217 p.

Yoshimura, K., Kikuchi, K., Kuroki, M., Wang, J., Ichinose, K. (2004). "Seismic strengthening of rectangular R/C columns confined by circular steel-and CF-jackets". *In 13th World Conference on Earthquake Engineering, Vancouver,* BC Canada, Paper (No. 2036).

APPENDIX

This code is based on a Three-Parameter Kinematic Theory (3PKT) for Shear-Dominated Reinforced Concrete wall presented in the following paper: Mihaylov, B.I., Hannewald, P. & Beyer, K. "Three-Parameter Kinematic Theory for Shear-Dominated Reinforced Concrete Columns "ASCE Journal of Structural Engineering, accepted for publication December 2015. The 3PKT has been then modified to be applied on the short reinforced concrete columns.

%Other applicability checks are performed automatically in the code.

% The user accepts and understands that no warranty is expressed or implied by the developers on the accuracy or the reliability of this code.

clear

clc

% Below is the code that used to read the input of the specimens directly from the excel sheet :

```
ColumnID =' ColumnID '

 path0 = strcat('C:\Users\',getenv('USERNAME'),'\Dropbox\Gamil''s
research\Column database\finalized\');
 [~,~,dumID] = xlsread(strcat(path0,'ColumnDatabase_v0.xltx
'),'MetaData-SI_Units','D1:D100');
% %
% %

strcat('CA',num2str(find(strcmp(ColumnID,dumID))),':','DC',num2str
(find(strcmp(ColumnID,dumID))))
 [dum1,dum2,dum3] = xlsread(strcat(path0,'ColumnDatabase_v0.xltx
'),...
  'MetaData-
SI_Units',strcat('BM',num2str(find(strcmp(ColumnID,dumID))),...
  ':','CO',num2str(find(strcmp(ColumnID,dumID)))));

N = dum3{1}*1000;
a = dum3{2};
acl = dum3{3};
h = dum3{4};
d1 = dum3{5};
b = dum3{6};
ρl,web = dum3{7};
As = dum3{9};
d = dum3{11};
```

```
db = dum3{12};
ρv = dum3{13};
Es = dum3{14};
fyl = dum3{15};
ful = dum3{16};
eul = dum3{17};
fyv = dum3{18};
fuv = dum3{19};
euv = dum3{20};
fc = dum3{21};
ag = dum3{22};
Asc = dum3{23};
sl = dum3{24};
slb = dum3{25};
sv = dum3{26};
bc = dum3{27};
dc = dum3{28};
Ast = dum3{29};

[N,a,acl,h,d1,b,ρl,web,As,d,db,ρv,Es,fyl,ful,eul,fyv,fuv,euv,fc,ag,ecu,lble,
Asc,sl,slb,sv,bc,dc,Ast,L0]=inputdata(ColumnID{1});
 Input (U6)
%% Imposed lateral displacements

D=(0.01:0.01:1)'*0.03*a; % The default maximum imposed
displacement corresponds to a drift of 3%. This value can be
changed if needed.


 %example of a short column input
 % ColumnID = 'No. 40.033a(west)'
% % N=189050; % axial compression load [N]
% % a=876.0; % Column height from the base to the applied lateral
load [mm]
% % acl=876; % clear Column height [mm]
% % h=305.0; % depth of Column section [mm]
% % d1=254.2; % distance from compressive edge of section to furthest
tension longitudinal bar [mm]
% % b=152.0; % width of Column cross section [mm]
% % ρl,web =0; % ratio of longitudinal web reinforcement [%]
% % As=567.057474; % area of longitudinal reinforcement located in
the flexural-tension one-half of the section [mm^2]
% % d=254.2; % effective depth of section from the compression edge
of the section to the centroid of As [mm]
% % db=19; % diameter of main longitudinal reinforcement [mm]
% % ρv =0.323; % ratio of transverse reinforcement [%]
% % Es=200000; % modulus of elasticity of longitudinal reinforcement
[MPa]
% % fyl=496.42; % yield strength of main longitudinal reinforcement
[MPa]
```

```
% % ful=835.00; % breaking stress of main longitudinal reinforcement
[MPa]
% % eul= 100/1000; % breaking strain of main longitudinal
reinforcement [-]
% % fyv=344.00; % yield strength of transverse reinforcement [MPa]
% % fuv=551.00; % breaking stress of transverse reinforcement [MPa]
% % euv= 1/10; % breaking strain of transverse reinforcement [-]
% % fc=34.68; % concrete cylinder strength [MPa]
% % ag=20; % concrete maximum aggregate size [mm]
% % Asc=567.057474; % area of longitudinal reinforcement in the
critical loading zone or confined edge zone [mm^2]
% % sl=203.4; % axial distance between the longitudinal bars in the
web measured parallel to the long side of the section [mm]
% % slb=203.4; % clear distance between the longitudinal bars in the
confined edge zones of the section measured parallel to the long
side of the section [mm]
% % sv=127.0; % clear distance between the confining hoops/ties in
the edge zones of the section measured parallel to the height of the
Column [mm]
% % bc=101.1; % axial distance between the external legs of the
confining hoops/ties measured parallel to the short side of the
section [mm]
% % dc=235; % axial distance between the external legs of the
confining hoops/ties plus one hoop/tie diameter measured parallel to
the long side of the section [mm]
% % Ast=0; % cross-sectional area of the legs of the hoops/ties in
the edge zones perpendicular to the plane of the Column [mm^2];
use 0 if the edge zones are not confined


%% Applicability check
% ------------------------------------------------------------------
------------------------------------------------------------------
---------------------------
FM=[];
if N/b/h/fc>=0.2 || a/h>3 || a/b>25 || fc>60
    FM='3PKT not applicable'

%     return
end

%% Concrete
% ------------------------------------------------------------------
------------------------------------------------------------------
---------------------------
Ec=(3320*fc^0.5+6900)/1;
n=0.8+fc/17;
ec=-fc/Ec*n/(n-1);
kk=0.67+fc/62;

%% Confinement of the CLZ (Mander and Priestley model)
```

```
% ------------------------------------------------------------------
------------------------------------------------------------------
---------------------------
rhocc=Asc/bc/dc;
ke=(1-(2*bc^2+2*round(dc/slb)*slb^2)/6/bc/dc)*max(1-
sv/2/bc,0)*max(1-sv/2/dc,0)/(1-rhocc); % ratio of effective
confined area to actual area (bc*dc-Asc)
% The effective area is calculated halfway between the hoops
taking into account the arch action in the three planes.
% Conservatively it is assumed that only one arch forms across the
thickness of the Column.
% The number of arches in the other direction is calculated as
round(dc/slb).
fltp=ke*(Ast/dc/sv)*fyv; % confining pressure perpendicular to the
Column; the pressure parallel to the Column is not calculated
fcclz=fc*(-1.254+2.254*(1+7.94*fltp/fc)^0.5-2*fltp/fc); % This
equation applies when the confinement pressures in the two
directions are equal.
% It is assumed that the pressure perpendicular to the Column is
always the smaller of the two pressures. Then, conservatively, it
is assumed that the pressure parallel to the Column is equal to
that perpendicular to the Column.
ecclz=ec*(1+5*(fcclz/fc-1));
if fltp==0
    nclz=n;
    kkclz=kk;
else
    nclz=5000*fc^0.5/(5000*fc^0.5-abs(fcclz/ecclz));
    kkclz=1;
end
%% Geometry
% ------------------------------------------------------------------
------------------------------------------------------------------
---------------------------
lb1e=min(0.11*(a^2+h^2)^0.5,370);
[Vsect Qsect]=AASHTOsect(N,a,h,b, ρl,web,As,d, ρv,fyv,fc,ag,sl); %
performs shear strength calculation according to the AASHTO code
alfa=atan(h/acl);
alfa1=max(alfa,Qsect);
alfa3=atan(d1/(d1/2/tan(alfa1))); % angle of the strut connected
to the stirrups spring

nb=As/(pi*db^2/4);
Id=nb*pi*db^4/64;

smax=0.28*db/(As/b/min(2.5*(h-d),h/2));  % crack spacing MC90
model code

l0=min(max(min(1.5*(h-d),d-h/2)/tan(alfa1),smax),d/tan(alfa1));
lk=l0+min(d*(1/tan(alfa)-1/tan(alfa1)),smax);
```

```
lt=d/tan(alfa1)-l0+lk;
Av= ρv /100*b*max((d1/tan(alfa1)-1.5*lb1e-
l0/d*d1),0.5*d1/tan(alfa1));

if ρl,web >=0.2
    kw=max(lk/smax,1); % Crack control factor
else
    kw=1;
end

lv=0.9*d1;
xv=d/tan(alfa3);

if (lt-lk)>0
    x=[(0:1/200:1)'*(lt-lk); lt];
else  % can occur in the case of very short Columns
    x=[(0:1/200:1)'*0.9*lt; lt];
end

%% Distribution of the concrete and steel stresses in the
compression zone of the fan as a function of the maximum strain in
the zone
% -----------------------------------------------------------------
-----------------------------------------------------------------
---------------------------
ecarray=-(0:0.001:1)'*(0:0.001:1)*0.1;
ecmax=-ecarray(:,1001);

fconc=fc*n*ecarray/ec./(n-1+(ecarray/ec).^(n*kk));
freinf=min(-Es*ecarray,fyl+(ful-fyl)/(eul-fyl/Es)*(-ecarray-
fyl/Es))*(As/b/(h/2));
ftot=fconc+freinf*cos(alfa);

ftavg=sum((ftot(:,1:1000)+ftot(:,2:1001))/2*0.001/1,2);

centr=1-
(ftot(:,1:1000)+ftot(:,2:1001))/2*0.001*(0.0005:0.001:0.9995)'./ft
avg; % distance from the compressed edge to the center of the
stress block
centr(1)=1/3;

%% Initial stiffness of the springs
% -----------------------------------------------------------------
-----------------------------------------------------------------
---------------------------
kclz10=Ec*b*tan(alfa); % 1
kclz20=Ec*b*tan(alfa); % 2
kd0=12*Es*Id/lk^3; % 4
ks0=Es*Av/lv; % 5
kl0=Es*As/lt; % 6
kcn0=Ec*b*tan(alfa1); %7
```

```
kct0=0; %8
ksc0=Es*Asc/lb1e; % 9

[nci0,vci0]=CDM(fc,ag,0.1,0.1);
vci0=0.18*vci0;
Fci0=b*(d1/sin(alfa1))*vci0;
kci0=Fci0/0.1; % 3

kclz1j=kclz10;
kclz2j=kclz20;
kcij=kci0;
kdj=kd0;
ksj=ks0;
klj=kl0;
kcnj=kcn0;
kctj=kct0;
kscj=ksc0;

%% Initial stiffness matrix
% ------------------------------------------------------------------
------------------------------------------------------------------
----------------------------
K(1,1)=kclz1j*cos(alfa/2)^2+kclz2j*sin(alfa/2)^2+kcij*sin(alfa1)^2
+kdj+ksj+kcnj*cos(alfa1)^2+kctj*sin(alfa1)^2; % x u1
K(2,2)=kclz1j*sin(alfa/2)^2+kclz2j*cos(alfa/2)^2+kcij*cos(alfa1)^2
+klj+kcnj*sin(alfa1)^2+kctj*cos(alfa1)^2+kscj; % x u2
K(3,3)=kclz1j*(a*cos(alfa/2))^2+kclz2j*(a*sin(alfa/2))^2+kcij*(a*s
in(alfa1))^2+kdj*(a-lt)^2+ksj*(a-
d1/tan(alfa3))^2+klj*d^2+kcnj*(a*cos(alfa1))^2+kctj*(a*sin(alfa1))
^2; % x u3
K(2,1)=-
kclz1j*cos(alfa/2)*sin(alfa/2)+kclz2j*sin(alfa/2)*cos(alfa/2)+kcij
*sin(alfa1)*cos(alfa1)-
kcnj*cos(alfa1)*sin(alfa1)+kctj*sin(alfa1)*cos(alfa1); % x u1
K(3,1)=-kclz1j*cos(alfa/2)*(a*cos(alfa/2))-
kclz2j*sin(alfa/2)*(a*sin(alfa/2))-kcij*sin(alfa1)*(a*sin(alfa1))-
kdj*(a-lt)-ksj*(a-d1/tan(alfa3))-kcnj*cos(alfa1)*(a*cos(alfa1))-
kctj*sin(alfa1)*(a*sin(alfa1)); % x u1
K(3,2)=kclz1j*sin(alfa/2)*(a*cos(alfa/2))-
kclz2j*cos(alfa/2)*(a*sin(alfa/2))-kcij*cos(alfa1)*(a*sin(alfa1))-
klj*d+kcnj*sin(alfa1)*(a*cos(alfa1))-
kctj*cos(alfa1)*(a*sin(alfa1)); % x u2
K(1,2)=K(2,1); % x u2
K(1,3)=K(3,1); % x u3
K(2,3)=K(3,2); % x u3
Kr=K(2:3,2:3);
K0=K;
Kr0=Kr;
```

```
%% Transformation matrix that links the displacements in the
springs to the 3 DOFs u of the rigid block (T*u = displacements of
individual springs)
% -------------------------------------------------------------------
-------------------------------------------------------------------
----------------------------
T=[cos(alfa/2) -sin(alfa/2) -(a*cos(alfa/2));...
    sin(alfa/2) cos(alfa/2) -a*sin(alfa/2);...
    sin(alfa1) cos(alfa1) -a*sin(alfa1);...
    1 0 -(a-lt);...
    1 0 -(a-d1/tan(alfa3));...
    0 -1 d;...
    cos(alfa1) -sin(alfa1) -a*cos(alfa1);...
    sin(alfa1) cos(alfa1) -a*sin(alfa1);...
    0 1 0];

%% Initial values of various quantities
% -------------------------------------------------------------------
-------------------------------------------------------------------
----------------------------
Dy=0;
Du=0;
m=0; % counts the converged load steps
UC=0; % counts the unconverged load steps
Dcipj=0;
Ddpj=0;
Dspj=0;
Dlpj=0;
kdfj=1;
esj=0;
flj=0;
wj=0.1;
sj=0.1;
epi=zeros(200+2,1);
mm1=0;
mm2=0;

%% Iterative solution
% -------------------------------------------------------------------
-------------------------------------------------------------------
----------------------------
LS=size(D,1);
for i=1:1:LS % Goes through the load steps (LS)
    100*i/LS

    kdfj=1;

    for j=1:1:400 % iterations to calculate the 3 DOFs taking into
account the non-linearity of the springs and the deformations in
the fan
```

```
        % Solution to the linear equations based on the secant
stiffness of the springs and taking into account the movement of
the "supports" of the springs due to the deformations in the fan
        % -------------------------------------------------------
-------------------------------------------------------------------
-----------------------------------
        Aj=Kr\[N-K(2,1)*D(i)+kcij*Dcipj*cos(alfa1)-klj*Dlpj...
            -N*h/2-K(3,1)*D(i)-kcij*Dcipj*a*sin(alfa1)-
kdj*Ddpj*(a-lt)-ksj*Dspj*(a-d1/tan(alfa3))+klj*Dlpj*d]';
        uj(1,1)=D(i);
        uj(2:3,1)=Aj;

        % Stores the current secant stiffness of the springs
        kclz1jprev=kclz1j;
        kclz2jprev=kclz2j;
        kcijprev=kcij;
        kdjprev=kdj;
        ksjprev=ksj;
        kljprev=klj;
        kcnjprev=kcnj;
        kctjprev=kctj;
        kscjprev=kscj;

        % Critical loading zone calculations (CLZ)
        % -------------------------------------------------------
-------------------------------------------------------------------
-----------------------------------
        Dclz1j=T(1,:)*uj;
        Dclz2j=T(2,:)*uj;

        if Dclz2j>=Dclz1j*tan(alfa/2) && Dclz2j>=-
Dclz1j*tan(alfa/2)
            gammaj=atan(abs(Dclz1j)/Dclz2j); % angle between Dclz
and the axis of symmetry of the CLZ
            alfa2j=alfa/2-atan(tan(alfa/2)-
2*sin(alfa/2)^2*(tan(alfa/2)+tan(gammaj-alfa/2))); % angle between
Fb and the axis of symmetry of the CLZ
            eFj=(abs(Dclz1j)*cos(pi/2-
alfa2j)+Dclz2j*cos(alfa2j))/(3*lb1e*cos(alfa));
            fcavgj=sum((fcclz*nclz*(-
(0.001:0.001:1)'*eFj)/ecclz./(nclz-1+((-
(0.001:0.001:1)'*eFj)/ecclz).^(nclz*kkclz))+...
                        fcclz*nclz*(-
(0:0.001:0.999)'*eFj)/ecclz./(nclz-1+((-
(0:0.001:0.999)'*eFj)/ecclz).^(nclz*kkclz)))/2*0.001*eFj)/eFj;
            Fej=fcavgj*b*lb1e*alfa;
            F1j=sign(Dclz1j)*Fej*cos(pi/2-alfa2j);
            F2j=Fej*cos(alfa2j);
            kclz1j=F1j/Dclz1j; % updated secant stiffness
            kclz2j=F2j/Dclz2j; % updated secant stiffness
        else
```

```
            kclz1j=Ec*b*tan(alfa);
            kclz2j=Ec*b*tan(alfa);
        end

        % Contact spring
        % ------------------------------------------------------------
------------------------------------------------------------------
-----------------------------------
        Dcnj=T(7,:)*uj;
        if Dcnj>0
            kcnj=0;
        else
            kcnj=kcn0;
        end
        Fcnj=kcnj*Dcnj;

        % Friction spring
        % ------------------------------------------------------------
------------------------------------------------------------------
-----------------------------------
        Dctj=T(8,:)*uj;
        Fctmaxj=0.7*abs(Fcnj);
        kctj=Fctmaxj/max(abs(Dctj),0.1);
        Fctj=kctj*Dctj;

        % Reinforcement in the CLZ
        % ------------------------------------------------------------
------------------------------------------------------------------
-----------------------------------
        Dscj=T(9,:)*uj;
        Fscj=Asc*min(Es*Dscj/lb1e,fyl);
        kscj=Fscj/Dscj;

        % Aggregate interlock
        % ------------------------------------------------------------
------------------------------------------------------------------
-----------------------------------
        Dcij=max(T(3,:)*uj-Dcipj,0);

        wj=(wj+((uj(1)-
uj(3)*a)*cos(alfa1)+esj(end)*lk*(d1/d)/2/sin(alfa1)+uj(2)/d*(d1/2/
sin(alfa1)-d*sin(alfa1)))/kw)/2;
        sj=(sj+Dcij)/2;

        [ncij,vcij]=CDM(fc,ag,sj,wj); % calculates the stresses on
the crack for given crack width and slip according to a contact
density model
                                        %(Li, B., Maekawa, K.
and Okamura, H. (1989) "Contact density model for stress transfer
across cracks in concrete,"
```

```
                                                % J. Faculty Eng., The
University of Tokyo (B), 40(1), 9-52.
        vcij=0.18*vcij;
        Fcij=b*(d1/sin(alfa1))*vcij;
        if abs(Dcij)>0
            kcij=Fcij/Dcij;
        else
            kcij=0;
        end

        % Stirrups
        % ------------------------------------------------------------
------------------------------------------------------------------------
-----------------------------------
        Dsj=T(5,:)*uj-Dspj;
        evj=Dsj/lv;
        fvj=min(Es*evj,fyv+(fuv-fyv)/(euv-fyv/Es)*(evj-fyv/Es));
        Fsj=Av*fvj;
        if Dsj>0
            ksj=Fsj/Dsj;
        else
            ksj=0;
        end

        % Dowel action
        % ------------------------------------------------------------
------------------------------------------------------------------------
-----------------------------------
        Ddj=max(T(4,:)*uj-Ddpj,0);
        fyej=fyl*(1-min(flj/fyl,1)^2);
        Fdj=min(kd0*Ddj,nb*fyej*db^3/3/lk);
        if Ddj>0
            kdj=Fdj/Ddj;
        else
            kdj=0;
        end

        % Longitudinal reinforcement
        % ------------------------------------------------------------
------------------------------------------------------------------------
-----------------------------------
        Dlj=T(6,:)*uj;

        dfj=(d1/tan(alfa3)*Fsj+(1-kdfj)*d*cos(alfa1)*Fcij+(lt-
lk)*Fdj)/(kdfj*d)/As;

        [fsj esj Dlactj Dlpj
k]=LongReinf(lt,lk,Dlj,dfj,Es,fyl,ful,eul,epi,x); % calculates the
stress and strain distribution along the longitudinal
reinforcement for a given elongation
```

```
% of the reinforcement and a known stress difference between the
top and bottom end of the reinforcement
        flj=fsj(end);
        Flj=As*flj;
        if Dlj>Dlpj
            klj=Flj/(Dlj-Dlpj);
        else
            klj=0;
        end
        ebasej=esj(1);

        % Displacements of the "supports" of the springs due to
the deformations in the fan
        % -------------------------------------------------------
-------------------------------------------------------------------
-----------------------------------
        Dlcij=Dlactj-esj(end)*lk; % elongation of the longitudinal
reinforcement at distance (lt-lk) from the base
        Dlsj=sum(esj(1:200).*max(sign(xv-
x(1:200)),0)+esj(2:(200+1)).*max(sign(xv-
x(2:(200+1))),0))/2*(1/200)*(lt-lk); % elongation of the
longitudinal reinforcement at distance xv from the base
        Ddpj=Dlcij/d*(lt-lk);
        Dspj=(Dspj+Dlsj/d*d1/tan(alfa3))/2;

        % Base section of the fan
        % -------------------------------------------------------
-------------------------------------------------------------------
-----------------------------------

Qbj=atan((As*dfj+Fcij*cos(alfa1))/(Fcij*sin(alfa1)+Fdj+Fsj));

Fbdj=((As*dfj+Fcij*cos(alfa1))^2+(Fcij*sin(alfa1)+Fdj+Fsj)^2)^0.5;

        eedgevector=(0:0.001:1)'*0.1; % possible strains at the
compression edge of the section

cbdasevector=eedgevector./((eedgevector+ebasej)/d1)*sin(Qbj); %
depth of compression zone
        if ebasej==0
            cbdasevector(1)=d1*sin(Qbj);
        end

Fbdvector=interp1(ecmax,ftavg,eedgevector).*cbdasevector*b;
        [Fbdmax row]=max(Fbdvector);
        if row<1001
            Fbdvector((row+1):1001)=[];
            eedgevector((row+1):1001)=[];
            cbdasevector((row+1):1001)=[];
        end
```

```
        if Fbdmax>=Fbdj
            eedgej=interp1(Fbdvector,eedgevector,Fbdj);
        else
            eedgej=max(eedgevector);
        end

        cbasej=eedgej/((eedgej+ebasej)/d1);
        kdfj=(d-interp1(ecmax,centr,eedgej)*cbasej)/d;

        % Displacements of the "supports" of the springs due to
the deformations in the fan
        % -------------------------------------------------------
-------------------------------------------------------------------
-----------------------------------
        Dcipj=(Dcipj+eedgej*d1/2/sin(alfa1))/2;

        % Error check for the convergence of the secant stiffness
of the springs
        % -------------------------------------------------------
-------------------------------------------------------------------
-----------------------------------
        errorj(j,1)=(kclz1jprev-kclz1j)^2+(kclz2jprev-
kclz2j)^2+(kcijprev-kcij)^2+(kdjprev-kdj)^2+(ksjprev-
ksj)^2+(kljprev-klj)^2+...
            (kcnjprev-kcnj)^2+(kctjprev-kctj)^2+(kscjprev-kscj)^2;
        if errorj(j)<0.01
            break
        end

        % Updated secant stiffness matrix
        % -------------------------------------------------------
-------------------------------------------------------------------
-----------------------------------

K(1,1)=kclz1j*cos(alfa/2)^2+kclz2j*sin(alfa/2)^2+kcij*sin(alfa1)^2
+kdj+ksj+kcnj*cos(alfa1)^2+kctj*sin(alfa1)^2; % x u1

K(2,2)=kclz1j*sin(alfa/2)^2+kclz2j*cos(alfa/2)^2+kcij*cos(alfa1)^2
+klj+kcnj*sin(alfa1)^2+kctj*cos(alfa1)^2+kscj; % x u2

K(3,3)=kclz1j*(a*cos(alfa/2))^2+kclz2j*(a*sin(alfa/2))^2+kcij*(a*s
in(alfa1))^2+kdj*(a-lt)^2+ksj*(a-
d1/tan(alfa3))^2+klj*d^2+kcnj*(a*cos(alfa1))^2+kctj*(a*sin(alfa1))
^2; % x u3
        K(2,1)=-
kclz1j*cos(alfa/2)*sin(alfa/2)+kclz2j*sin(alfa/2)*cos(alfa/2)+kcij
*sin(alfa1)*cos(alfa1)-
kcnj*cos(alfa1)*sin(alfa1)+kctj*sin(alfa1)*cos(alfa1); % x u1
        K(3,1)=-kclz1j*cos(alfa/2)*(a*cos(alfa/2))-
kclz2j*sin(alfa/2)*(a*sin(alfa/2))-kcij*sin(alfa1)*(a*sin(alfa1))-
```

```
kdj*(a-lt)-ksj*(a-d1/tan(alfa3))-kcnj*cos(alfa1)*(a*cos(alfa1))-
kctj*sin(alfa1)*(a*sin(alfa1)); % x u1
        K(3,2)=kclz1j*sin(alfa/2)*(a*cos(alfa/2))-
kclz2j*cos(alfa/2)*(a*sin(alfa/2))-kcij*cos(alfa1)*(a*sin(alfa1))-
klj*d+kcnj*sin(alfa1)*(a*cos(alfa1))-
kctj*cos(alfa1)*(a*sin(alfa1)); % x u2
        K(1,2)=K(2,1); % x u2
        K(1,3)=K(3,1); % x u3
        K(2,3)=K(3,2); % x u3
        Kr=K(2:3,2:3);

    end

    % Stores the errors at each load step
    % ------------------------------------------------------------
------------------------------------------------------------------
--------------------------------
    error(i,1)=D(i);
    error(i,2)=errorj(j);
    error(i,3)=k;
    error(i,4)=sign(uj(3));

    % Sets the stiffness to initial values if the error is larger
than the limit, if the stiffness matrix is singular, or if the
rotation of the rigid block is negative
    % ------------------------------------------------------------
------------------------------------------------------------------
--------------------------------
    if errorj(j)>=0.01 || isnan(rcond(Kr))==1 || uj(3)<0
        UC=UC+1;

        K=K0;
        Kr=Kr0;
        kclz1j=kclz10;
        kclz2j=kclz20;
        kcij=kci0;
        kdj=kd0;
        ksj=ks0;
        klj=kl0;
        kcnj=kcn0;
        kctj=kct0;
        kscj=ksc0;

        Dcipj=0;
        Ddpj=0;
        Dspj=0;
        Dlpj=0;
        kdfj=1;
        Fcij=0;
        Fdj=0;
        wj=0;
```

```
        sj=0;

        if UC<100
            continue
        else
            break % stops the analysis if the unconverged load
steps are >=100
        end
    end

    % Check for bar buckling
    % ------------------------------------------------------------
------------------------------------------------------------------
-------------------------------
    if abs(eFj)>max(abs(ecclz),0.004) && mm1==0 % buckling of bars
in the CLZ
        Asc=0;
        mm1=1;
    end
    if eedgej>max(abs(ecclz),0.004) && mm2==0 % buckling of bars
in the compression zone of the fan
        ftot=fconc;
        ftavg=sum((ftot(:,1:1000)+ftot(:,2:1001))/2*0.001/1,2);
        centr=1-
(ftot(:,1:1000)+ftot(:,2:1001))/2*0.001*(0.0005:0.001:0.9995)'./ft
avg;
        centr(1)=1/3;
        mm2=1;
    end

    % Check for crushing of the concrete in the compression zone
of the fan
    % ------------------------------------------------------------
------------------------------------------------------------------
-------------------------------
    if Fbdmax<Fbdj
        FM='Flexural Crushing';
        break
    end

    % Check for rupture of the flexural reinforcement
    % ------------------------------------------------------------
------------------------------------------------------------------
-------------------------------
    if ebasej>0.6*eul
        FM='Steel Rupture at the base';
        break
    end

    epi=max(epi,esj-fsj/Es); % plastic strains in the flexural
reinforcement
```

```
    % Check whether the shear reinforcement yields before the
flexural reinforcement; if not, the 3PKT is not applicable
    % -------------------------------------------------------------
-------------------------------------------------------------------
--------------------------------
    if esj(1)>fyl/Es && evj<fyv/Es
        FM='3PKT not applicable';
%         return
    end

    m=m+1; % number of converged load steps

    % Stores results
    % -------------------------------------------------------------
-------------------------------------------------------------------
--------------------------------
    u(m,1:3)=uj(1:3)';

    Dl(m,1)=Dlj;
    Dlact(m,1)=Dlactj;
    Fl(m,1)=Flj;
    fl(m,1)=flj;
    df(m,1)=dfj;
    Dlp(m,1)=Dlpj;
    fs(:,m)=fsj;
    es(:,m)=esj;
    Dls(m,1)=Dlsj;
    ep(:,m)=epi;

    Dclz1(m,1)=Dclz1j;
    Fclz1(m,1)=kclz1j*Dclz1j;
    Dclz2(m,1)=Dclz2j;
    Fclz2(m,1)=kclz2j*Dclz2j;
    alfa2(m,1)=alfa2j;
    eF(m,1)=eFj;
    alfa2(m,1)=alfa2j-alfa/2;

    Dcn(m,1)=Dcnj;
    Fcn(m,1)=kcnj*Dcnj;
    Dct(m,1)=Dctj;
    Fct(m,1)=Fctj;

    Fsc(m,1)=Fscj;

    w(m,1)=wj;
    s(m,1)=sj;
    vci(m,1)=vcij;
    Dci(m,1)=Dcij;
    Fci(m,1)=Fcij;
    Dcip(m,1)=Dcipj;
```

```
    Dd(m,1)=Ddj;
    Fd(m,1)=Fdj;

    Ds(m,1)=Dsj;
    Fs(m,1)=Fsj;
    ev(m,1)=evj;
    fv(m,1)=fvj;
    Dsp(m,1)=Dspj;

    kdf(m,1)=kdfj;
    eedge(m,1)=eedgej;
    cbase(m,1)=cbasej;
    Ncbase(m,1)=As*dfj+Fcij*cos(alfa1);
    Qb(m,1)=Qbj;

    kclz1(m,1)=kclz1j;
    kclz2(m,1)=kclz2j;
    kci(m,1)=kcij;
    kd(m,1)=kdj;
    ks(m,1)=ksj;
    kl(m,1)=klj;
    kcn(m,1)=kcnj;
    kct(m,1)=kctj;
    ksc(m,1)=kscj;

    V(m,1)=K(1,:)*uj-kcij*Dcipj*sin(alfa1)-kdj*Ddpj-ksj*Dspj; %
lateral load = shear force

end

%% Indicators shown after the analysis
% -----------------------------------------------------------------
-----------------------------------------------------------------
----------------------------
max(error(:,2))
UC
FM

%% Shear strength components
% -----------------------------------------------------------------
-----------------------------------------------------------------
----------------------------
Vclz=Fclz1*cos(alfa/2)+Fclz2*sin(alfa/2);
Vc=Fcn*cos(alfa1)+Fct*sin(alfa1);
Vci=Fci*sin(alfa1);
Vd=Fd;
Vs=Fs;

%% Moment equilibrium of the rigid block
```

```
% ------------------------------------------------------------------
------------------------------------------------------------------
--------------------------
M=V*a-N*h/2-Fd*d/tan(alfa1)-Fs*d1/2/tan(alfa1)-Fl*d; % should be 0

%% Crack width at the base
% ------------------------------------------------------------------
------------------------------------------------------------------
--------------------------
wbase=es(1,:)'.*smax/2;

%% Calculates the initial linear response and the intersection
with the non-linear response curve
Dleft=0;
Dright=u(end,1);
Dvector=[0; u(:,1)];
Vpl=[V(1); V];
while 100*abs(Dleft-Dright)/Dright>0.00001
    Dmid=(Dleft+Dright)/2;
    if
interp1(Dvector,Vpl,Dmid)>1/(a^3/3/Ec/(b*h^3/12)+1.2*a/(0.4*Ec)/(b
*h))*Dmid
        Dleft=Dmid;
    else
        Dright=Dmid;
    end
end
Dplot=[];
Vplot=[];
j=0;
for i=1:size(V,1)
    if u(i,1)>Dmid
        j=j+1;
        Dplot(j,1)=u(i,1);
        Vplot(j,1)=V(i,1);
    end
end
Dplot=[0; Dmid; Dplot];
Vplot=[0; 1/(a^3/3/Ec/(b*h^3/12)+1.2*a/(0.4*Ec)/(b*h))*Dmid/1000;
Vplot/1000];

%% Rotation at the base
Dpo=(min(es(1,:)',(fyl/Es)).*(2 + 3500*min(es(1,:)',(fyl/Es))) +
max((0.047*(ful-fyl)*(es(1,:)'-fyl/Es)),0)) * db/(fc/20)^(2/3)
./(d-cbase)*a;

% db=16;% !!!!!!!!!!!1
fct=0.33*fc^0.5;
k0=2*fct*pi*db;
k1=k0/2;
Ss=min(Es*es(1,:)',fyl+(ful-fyl)/(eul-fyl/Es)*(es(1,:)'-fyl/Es));
```

```
L0=min(Ss,fyl)*pi*db^2/4/k0;
L1=max(Ss-fyl,0)*pi*db^2/4/k1;
Dpo=((es(1,:)'+fyl/Es)/2.*L1+min(es(1,:)',fyl/Es).*L0/2)./(d-
cbase)*a;

%% Plots
% ------------------------------------------------------------------
------------------------------------------------------------------
--------------------------
%% Deformed shape of the Column
coord1=[[(0:0.01:1)'; ones(101,1)]*h [(0:0.01:1)'; (1:-
0.01:0)']*h/tan(alfa1)*0.99999999];
coord1(1,1)=0.00001;
coord2=[[0 h h 0 0]' [0 h/tan(alfa1) a a 0]'];
coord3=[[d1/2 d1/1.999999]' ones(2,1)*d1/tan(alfa3)];
coord4=[[d d d]' [0 lt-lk lt]'];
SCF=a*20/100/max(u(:,1));
SCFf=200/max((max(V)^2+N^2).^0.5);
Ab=[];
uh1=[];
uv1=[];
uh2=[];
uv2=[];
uh3=[];
uv3=[];
uh4=[];
uv4=[];
ebasemax=max(es(1,:));
for i=1:m
    Ab(1,1)=0;
    for j=2:size(x,1)
        Ab(j,1)=Ab(j-1)+(es(j,i)+es(j-1,i))/2*(x(j)-x(j-1));
    end
    for jj=1:size(coord1,1)
        if coord1(jj,2)<coord1(jj,1)/tan(alfa1)

uv1(jj,1)=interp1(x,Ab,min(coord1(jj,2)/coord1(jj,1)*d,lt-
lk))/d*coord1(jj,1);
            uh1(jj,1)=-uv1(jj)*coord1(jj,2)/coord1(jj,1);
        else
            uv1(jj,1)=-u(i,2)+u(i,3)*coord1(jj,1);
            uh1(jj,1)=-u(i,1)+u(i,3)*(a-coord1(jj,2));
        end
    end
    for jj=1:size(coord2,1)
        if coord2(jj,2)<coord2(jj,1)/tan(alfa1)

uv2(jj,1)=interp1(x,Ab,min(coord2(jj,2)/coord2(jj,1)*d,lt-
lk))/d*coord2(jj,1);
            uh2(jj,1)=-uv2(jj)*coord2(jj,2)/coord2(jj,1);
```

```
        else
            uv2(jj,1)=-u(i,2)+u(i,3)*coord2(jj,1);
            uh2(jj,1)=-u(i,1)+u(i,3)*(a-coord2(jj,2));
        end
    end
    for jj=1:size(coord3,1)
        if coord3(jj,2)<coord3(jj,1)/tan(alfa1)

uv3(jj,1)=interp1(x,Ab,min(coord3(jj,2)/coord3(jj,1)*d,lt-
lk))/d*coord3(jj,1);
            uh3(jj,1)=-uv3(jj)*coord3(jj,2)/coord3(jj,1);
        else
            uv3(jj,1)=-u(i,2)+u(i,3)*coord3(jj,1);
            uh3(jj,1)=-u(i,1)+u(i,3)*(a-coord3(jj,2));
        end
    end
    for jj=1:size(coord4,1)
        if coord4(jj,2)<coord4(jj,1)/tan(alfa1)

uv4(jj,1)=interp1(x,Ab,min(coord4(jj,2)/coord4(jj,1)*d,lt-
lk))/d*coord4(jj,1);
            uh4(jj,1)=-uv4(jj)*coord4(jj,2)/coord4(jj,1);
        else
            uv4(jj,1)=-u(i,2)+u(i,3)*coord4(jj,1);
            uh4(jj,1)=-u(i,1)+u(i,3)*(a-coord4(jj,2));
        end
    end
    figure(1)
    plot([-1500 3500],[-1000 4000],'ok')
    hold on
    plot([0; (0:0.01:1)'*cbase(i)],[0; -interp1(ecmax,ftavg,(1:-
0.01:0)'*eedge(i))]/max(interp1(ecmax,ftavg,(1:-
0.01:0)'*eedge(i)))*h/6,'Color',[0.5 0.5 0.5]);
    hold on
    plot(coord1(:,1)+SCF*uh1,coord1(:,2)+SCF*uv1,'Color',[0 0
0.7],'LineWidth',2.5)
    hold on
    plot(coord2(:,1)+SCF*uh2,coord2(:,2)+SCF*uv2,'Color',[0 0
0.7],'LineWidth',2.5)
    hold on
    if ev(i)/(fyv/Es)<1
        plot(coord3(:,1)+SCF*uh3,coord3(:,2)+SCF*uv3,'Color',[0.5
0.5 0.5],'LineWidth',2.5)
    else
        plot(coord3(:,1)+SCF*uh3,coord3(:,2)+SCF*uv3,'Color',[0.7
0 0],'LineWidth',2.5)
    end
    hold on
```

```
    plot(coord4(:,1)+SCF*uh4,coord4(:,2)+SCF*uv4,'-o','Color',[0.5
0.5 0.5],'LineWidth',2.5,'MarkerFaceColor',[0.5 0.5
0.5],'MarkerSize',3)
    hold on
    plot([0 h],[0 0],'Color',[0 0 0.7],'LineWidth',2.5)
    hold on

hh=quiver(coord2(3,1)+SCF*uh2(3)+3*SCFf*V(i),coord2(3,2)+SCF*uv2(3
),-3*SCFf*V(i),0,'Color',[0.7 0
0],'LineWidth',2,'MaxHeadSize',0.8,'AutoScale','off');
    hold on

hh=quiver((coord2(3,1)+coord2(4,1))/2+SCF*(uh2(3)+uh2(4))/2,(coord
2(3,2)+coord2(4,2))/2+SCF*(uv2(3)+uv2(4))/2+3*SCFf*N,0,-
3*SCFf*N,'Color',[0.7 0
0],'LineWidth',2,'MaxHeadSize',0.8,'AutoScale','off');
    hold on
    plot([0; -u(1:i,1)]/max(u(:,1))*1000+3200,[0;
V(1:i)]/max(V)*1000+2700,'Color',[0 0.7 0],'LineWidth',2.5);
    hold on
    plot([-1200 0 0]+3200,[0 0 1200]+2700,'Color',[0.5 0.5 0.5]);
    hold on
    plot(es(:,i)/ebasemax*1200+h+200,x,'-o','Color',[0.5 0.5
0.5],'MarkerSize',3)
    hold on
    plot([es(1,i)/ebasemax*1200 0 0 0
es(200+2,i)/ebasemax*1200]+h+200,[0 0 a lt lt],'Color',[0.5 0.5
0.5]);
    hold on
    plot([0 -500*eF(i)/max(eF) -500*eF(i)/max(eF) 0 0]-
500,[3*lb1e*cos(alfa) 3*lb1e*cos(alfa) 0 0 a],'Color',[0.5 0.5
0.5]);
    hold on

text(1.1*h/2,h/2/tan(alfa1),0,mat2str(w(i),2),'HorizontalAlignment
','left','FontSize',12);
    hold on
    text(3/4*h,-
100,0,mat2str(wbase(i),2),'HorizontalAlignment','left','FontSize',
12);
    hold on
    text(-750,-
100,0,mat2str(1000*eF(i),3),'HorizontalAlignment','center','FontSi
ze',12);
    hold on
    text(es(1,i)/ebasemax*1200+h+200,-
100,0,mat2str(1000*es(1,i),3),'HorizontalAlignment','center','Font
Size',12);
    hold off
    grid off
```

```
    set(gca,'PlotBoxAspectRatio',[4500 4500 1])
    view(0,90);
    pause(0.01)
end
%%
figure(11)
plot(u(:,1),min(es(1,:)/(fyl/Es),1),'-ob')
hold on
plot(u(:,1),min(ev/(fyv/Es),1),'-or')
hold off
legend('long','trans')
%% Load-displacement curves
figure(2)
% plot(Exp1(:,1),Exp1(:,2),'-b','LineWidth',1,'MarkerSize',2)
hold on
plot(u(:,1),V(:,1)/1000,'-o','Color',[0.7 0
0],'LineWidth',2.5,'MarkerSize',2)
hold on
plot(u(:,1)+Dpo,V(:,1)/1000,':o','Color',[0.7 0
0],'LineWidth',2.5,'MarkerSize',2)
hold on
plot(u(:,1),Vclz/1000,'-o','Color',[0 0
0],'LineWidth',1,'MarkerSize',2)
hold on
plot(u(:,1),Vc/1000,'-o','Color',[0.7 0
0],'LineWidth',1,'MarkerSize',2)
hold on
plot(u(:,1),Vci/1000,'-o','Color',[0 0.7
0],'LineWidth',1,'MarkerSize',2)
hold on
plot(u(:,1),Vs/1000,'-o','Color',[0 0
0.7],'LineWidth',1,'MarkerSize',2)
hold on
plot(u(:,1),Vd/1000,'-o','Color',[0.5 0.5
0.5],'LineWidth',1,'MarkerSize',2)
hold on
legend('\Delta 3PKT','\Delta + \Delta_p_o
3PKT','Vclz','Vcf','Vci','Vs','Vd','Location','NorthWest')
xlabel('\Delta ,  mm');
ylabel('V ,  kN');
print -dmeta -painters


%%
RESULTS = [u(:,1) u(:,1)+Dpo V(:,1)/1000 ];
FM;
```